INSTITUTO SUPERIOR DE ENGENHARIA DE LISBOA
ÁREA DEPARTAMENTAL DE ENGENHARIA MECÂNICA

Design and Development of a Modular Windshield Wiper System for Helicopters

JOÃO DO NASCIMENTO AMARAL

Bachelor in Mechanical Engineering

Submitted to the Graduate School of the Instituto Superior de Engenharia de Lisboa in partial fulfilment of the requirements for the degree of Masters of Science in Mechanical Engineering

Supervisor:
PhD João Filipe de Almeida Milho

Co-Supervisor:
MSc Afonso de Sousa Leite
MSc Ingo Rohacek-Costa

Jury:

Chairperson:	PhD Silvério João Crespo Marques
Members of the Committee:	PhD Ricardo José Fontes Portal
	PhD João Filipe de Almeida Milho

June 2019

THIS PAGE IS INTENTIONALLY LEFT IN BLANK

INSTITUTO SUPERIOR DE ENGENHARIA DE LISBOA
ÁREA DEPARTAMENTAL DE ENGENHARIA MECÂNICA

Design and Development of a Modular Windshield Wiper System for Helicopters

JOÃO DO NASCIMENTO AMARAL

Bachelor in Mechanical Engineering

Submitted to the Graduate School of the Instituto Superior de Engenharia de Lisboa in partial fulfilment of the requirements for the degree of Masters of Science in Mechanical Engineering

Supervisor:
PhD João Filipe de Almeida Milho

Co-Supervisor:
MSc Afonso de Sousa Leite
MSc Ingo Rohacek-Costa

Jury:

Chairperson:	PhD Silvério João Crespo Marques
Members of the Committee:	PhD Ricardo José Fontes Portal
	PhD João Filipe de Almeida Milho

June 2019

THIS PAGE IS INTENTIONALLY LEFT IN BLANK

A toda a família pelo apoio incondicional e suporte na busca de melhores oportunidades,
aos amigos pelos momentos de descontracção,
aos colegas pelo saudável incentivo em busca do conhecimento

THIS PAGE IS INTENTIONALLY LEFT IN BLANK

Resumo

Este trabalho aborda o desenvolvimento e adaptação de um sistema limpa pára-brisas já existente de forma a torná-lo modular para que possa ser adaptado a outros tipos de aeronaves com diferentes tipos de geometrias e ligações. Foi realizado em parceria com a Airbus Helicopters Deutschland GmbH para o Trabalho Final de Mestrado. Esta obra corresponde à fase inicial de desenvolvimento do projecto com vista à aprovação e certificação aeronáutica para que seja levada a cabo a sua produção e implementação nos diversos modelos de helicopteros da empresa.

Numa fase inicial foi feita uma pesquisa quanto a sistemas similares existentes no mercado, não só da aeronáutica como de outras áreas de negócio, antes do modelo da Airbus ser alvo de análises cinemáticas. Após ter sido entendido o propósito e funcionamento básico de sistemas idênticos procedeu-se às análises computacionais do sistema da Airbus e, posteriormente, à sua adaptação a uma aeronave com um diferente tipo de conecção e de geometria.

Todos os estudos foram desenvolvido com recurso a tecnologia CAD através do software SolidWorks com o objectivo de obter um modelo não apenas resistente aos carregamentos externos aplicados, mas principalmente resistente a esforços cíclicos. Isto foi relevante acima de tudo para a nova peça de adaptação que foi projectada.

Os estudos cinemáticos, estáticos e de fadiga foram levados a cabo com sucesso culminando na validação da peça projectada, os correspondentes elementos de ligação e a chumaceira seca.

Abstract

This work addresses the development and adaptation of an existing windshield wiper system in order to make it modular so that it can be adapted to other aircraft types, with different kinds of geometries and connections. It was carried out in partnership with Airbus Helicopters Deutschland GmbH for the Master of Science Thesis. This work corresponds to the initial development phase of the project for the aeronautical approval and certification, to see its production and implementation in the company's helicopters being carried.

At an early stage, research was carried out on similar systems in the market, not only in aeronautics but also in other business areas, before the Airbus model was subjected to kinematic analysis. After having understood the purpose and basic operation of identical systems, the computational analysis of Airbus' system was carried out and, after that, its adaptation to an aircraft with a different type of connection and geometry.

All studies were developed using CAD technology through the software SolidWorks in order to obtain a model not only resistant to the applied external loads, but mainly resistant to cyclic forces. This was relevant especially for the new adaptation part that was designed.

Kinematic, static and fatigue studies were successfully completed, culminating in the validation of the projected part, the corresponding connecting elements and the dry bearing.

THIS PAGE IS INTENTIONALLY LEFT IN BLANK

Palavras-Chave

Sistema limpa pára-brisas, Design, Helicóptero, Modelação 3D, Concepção Assistida por Computador, Método de Elementos Finitos, Estudo Cinemático, Estudo Estático, Estudo de Fadiga

Keywords

Windshield Wiper System, Design, Helicopter, 3D Modelling, Computer-Aided Design, Finite Element Method, Kinematic Study, Static Study, Fatigue Study

THIS PAGE IS INTENTIONALLY LEFT IN BLANK

Glossary

2D Bidimensional

3D Tridimensional

AHD Airbus Helicopters Deutschland GmbH

BR Basic Regulation

CAD Computer-aided Design

CS Certification Specification

EASA European Aviation Safety Agency

FEA Finite Element Analysis

FEM Finite Element Method

FLF Fatigue Load Factor

FoS Factor of Safety

JAA Joint Aviation Authorities

JAR Joint Aviation Requirements

PTFE Polytetrafluoroethylene

SW SolidWorks

WWS Windshield Wiper Sistem

Symbols

$\boldsymbol{\sigma_{ys}}$ Yield Stress
$\boldsymbol{\sigma_1, \sigma_2, \sigma_3}$ Principal Stresses
$\boldsymbol{\sigma_{12}, \sigma_{23}, \sigma_{31}}$ Shear Stresses
$\boldsymbol{\sigma_{vm}}$ von Mises Equivelent Stress
$\boldsymbol{\sigma_{Tys}}$ Tensile Yield Stress
$\boldsymbol{\tau_{ys}}$ Shear Yield Stress
$\boldsymbol{\sigma_{Cys}}$ Compressive Yield Stress
$\boldsymbol{\sigma_a}$, **S** Alternating Stress
N Number of Cycles
$\boldsymbol{\sigma_{max}}$ Maximum Stress
$\boldsymbol{\sigma_{min}}$ Minimum Stress
$\boldsymbol{\sigma_{fl}}$ Endurance Limit or Fatigue Limit
$\boldsymbol{\sigma_u}$ Ultimate Stress
$\boldsymbol{k}$ Spring Constant Factor
$\boldsymbol{x_{sp}}$ Spring's relaxed length
$\boldsymbol{h_{min}}$ Minimum distance between the Arms and the Windshield
γ Windshield Cleaning Angle
$\boldsymbol{\sigma_{al}}$ Allowable Stress
Fx, **Rx** x axis reaction
Fy, **Ry** y axis reaction
Fz, **Rz** z axis reaction
Mx Torque around x axis
My Torque around y axis
Mz Torque around z axis
G Gravitational Acceleration
Fi Bolt's Pre load Stress
$\boldsymbol{v_s}$ Service Velocity
$\boldsymbol{v_{max}}$ Maximum Velocity
$\boldsymbol{n}$ Angular Velocity
$\boldsymbol{r}$ Radius
$\boldsymbol{\sigma_s}$ Service Stress
$\boldsymbol{F}$ Applied Force
$\boldsymbol{A}$ Projected Area

T_s Service Temperature
T_{max} Maximum Temperature
T_a Ambient Temperature
f Friction Coefficient
P Pressure
v Velocity
Fybolt Reaction Force at the bolt
Mybolt Torque Reaction at the bolt
d WWS Bottom Connection Height
e WWS Structure Height

THIS PAGE IS INTENTIONALLY LEFT IN BLANK

Contents

List of Figures

List of Tables

Chapter 1

Introduction

The report herein presented is the result of the development of a theme in partnership with Airbus Helicopters Deutschland GmbH (AHD) for the Master of Science Thesis, consisting in the design and development of a modular Windshield Wiper Sistem (WWS) for Airbus helicopters.

The need for a well functioning WWS to, in such occasions, protect and improve the line of sight of the pilots during the flight is an important part of the aircraft safe performance. At first, this system may seem secondary and not as important as some other vital mechanisms of the helicopters, which are crucial for its operation without life threatening situations, but in a perspective of availability of the aircraft it is. In the case of malfunction or damage of the WWS the aircraft will be prevented from taking off due to its incapability of assuring a good line of sight to the pilots against aggressive environmental conditions like rain, dust, mud or snow.

AHD presented a problem with the current WWS used in the H130 aircraft, and also with some other helicopter models that use similarly unreliable systems. Besides, they stated that they would be interested in having a study about the possibility of implementing the same pantographic system in the biggest number of aircrafts possible. This way, the proposed theme to be developed in this document was an adaptation of the current best WWS model of Airbus helicopters to the H130 and to other models, making it a modular wiping system that could be adapted to any aircraft of the company, if possible.

1.1 Objectives

It's in this project scope to provide to AHD a substantiated report for a working product with the goal of a future production of a modular WWS.

It should be carried out the motion and kinematic analysis to the system, the study of adaptation of it to other helicopter models and the design, static, and fatigue studies of new parts using Tridimensional (3D) modelling software, if needed. All studies should be guided by European Aviation Safety Agency (EASA)'s Certification Specification (CS) 27 & 29 and also Joint Aviation Requirements (JAR) 27 & 29 documents where they are found to be covered by it.

All additional parts must be designed taking into consideration mainly its weight and cost reduction to keep the aircraft as lightweight as possible without raising the WWS price.

The aircraft modifications must be a ultimate resource, and kept to the absolute minimum, since it would involve further tests, requirements and certifications to the affected parts, by the company.

The applicable connecting parts will also be subjected to validation according to their final purpose.

1.2 Structural Framework and Organization

The developed document presents the following structure:

⇒ In Chapter 2 the theoretical framework is described with focus on the regulations and specifications applicable to this project. The basis for the methodology employed in this document are also described in it, specially the processing of the Computer-aided Design (CAD) data used by the 3D modelling and simulation software.

⇒ Chapter 3 is dedicated to the conceptual framework, where the research of the existing systems in use, in the different industries, are presented. A simple model os WWS is also kinematically analysed with the goal of knowledge gathering about a more basic process of operation of the WWS, before moving to a more complex model.

⇒ In Chapter 4 a detailed kinematic analysis of the H135's WWS is carried out with the aim of attaining a reliable digital CAD model that could be compared to the real life WWS of the mentioned helicopter and accessing its applicability. Some iterations are made from the free movement of just the wiper model connected to a motor, to the adaptation of it into the H135's windshield surface, and its analysis by resorting to SolidWorks (SW)'s Motion Studies. This Add-In carries graphical simulations of the motion in assembly models, producing data to be compared with the existing system.

⇒ In Chapter 5 the adaptation of the pantographic WWS is implemented in a different surface geometry and, contrasting with the previous chapter, into a different type of connection. Here the design of a new part with the purpose of accommodating the WWS is performed. This is necessary due to the particularity of the introduced helicopter model with one axis wiper system only, which needs to be accounted for in the pantographic WWS.

⇒ Chapter 6 shows the validation of the bolts and the bearing of the new designed fixation part, for the applied forces involved during the wiper system operation and to its flight conditions. The torque reactions that were not previously considered are also added to the static and fatigue studies and the results are presented.

⇒ At last, in Chapter 7 are discussed the main conclusions of this report and future works are also regarded.

Chapter 2

Theoretical Framework

This chapter presents the theoretical basis in which this project will be developed.

2.1 Applicable regulations

2.1.1 CS and JAR specifications

Some regulations are necessary being followed when the operations, maintenance, licensing and certification/design standards of all classes of aircraft are regarded. From 2003 until this day, EASA is the aviation regulatory authority responsible for publishing the mentioned certifications of aircraft, not only in the EU but also for some non-EU Countries in Europe. It's important for a project to conform with EASA's specifications because this certificate testifies that the aircraft meets the safety requirements set by the European Union [1].

EASA's technical standards are the CS, which are non-binding, and are adopted in order to meet the essential requirements of the Basic Regulation (BR). They are composed by the Airworthiness Code and the Acceptable Means of Compliance which shall be used to indite this project.

Even thought the CS's are the current valid technical standards, they supervene the existence of the JAR. These were specifications created by the Joint Aviation Authorities (JAA), a group of regulatory authorities from countries that worked together to develop and implement common safety regulatory standards and procedures, in order to produce common certification codes for aircraft production and use. In the current days, any amendment done to the JAR specs is included in the CS published amendments. This shows that, although the JAR are not the documents that regulate the industry any more, they are not obsolete for they include some important aspects [2].

The following paragraphs of the mentioned regulations were indicated by AHD as possibly important to this project, and should be taken into account if applicable in the work that will be developed:

- CS 27.303
- CS 27.601
- CS 27.603
- CS 27.609
- CS 27.611
- CS 27.1301
- CS 27.1309
- CS 27.1559
- JAR 29.303
- JAR 27.305
- JAR 27.561
- JAR 27.603

In CS 27.303 is indicated specifically that when needed, the use of a factor of safety should be of 1.5, unless otherwise any other value is provided. Most of the paragraphs, however, are generalities, as for instance, the CS 27.601 refers that no previous features who are shown to be unreliable should be used and that test should establish the suitability of the design. The CS 27.603 is about the materials, indicating that the they should be chosen in the basis of experience or tests, meet specifications to ensure its properties and take into account the environmental conditions. Other paragraphs mention inspection previsions, function and installation, etc., that are not used in the present document but should be taken into consideration on the next steps towards production of the system [3].

Table 2.1: JAR 27.603 (a) Investigation load cases

Load case No.	Notation
1	Emergency Landing; 8g forward
2	Emergency Landing; 6g rearward
3	Emergency Landing; 8g downward
4	Emergency Landing; 4g upward
5	Emergency Landing; 6g lateral
6	Maximal available motor torque. (Ultimate Load)

The same happens with the JAR specs, in which it was found most relevant and useful for the studies presented in this project, the JAR 27.603. This paragraph points out the investigation load cases, also mentioned as emergency landing cases, shown in in Table 2.1. This cases should be considered to find out which situation represents the overall worst case scenario, allowing to design parts that are fit for use in the most extreme conditions [4].

2.2 Computer-Aided Design

The CAD technology is used in the conception and design stage of a product, before having a prototype or even considering if it goes into production. This technology allows the creation of detailed engineering designs (3D and Bidimensional (2D)), defined by geometrical parameters and representing the physical components. The CAD programs also afford a rendering display of the developed products, allowing a life-like representation of the concepts. With these virtual objects, it's possible for the designer/engineer to, after having created the conceptual design, manipulate it, present a product layout, strength and dynamic analysis of a part or the assembly, and even determine the manufacturing processes. These technologies show to be positive and a good investment to a company since it reduces the prototyping and experimental analysis stage to what is only strictly necessary.

2.2.1 Finite Element Method

CAD software resorts to Finite Element Method (FEM) to compute and solve problems such as stress analysis, heat transfer, fluid flow and electromagnetics, by computer simulation. FEM is a numerical approach by which these partial differential equations can be solved approximately, being able to present a solution to complex problems where an exact solution is not practical to be pursued [5].

In an engineering perspective, by using simulation software in a computer, there's always limitations on the amount of processing power that the machine is capable of providing. In this case, an exact solution is not practicable to go after, so the use of estimations are the most suitable outcome.

In a first analysis, the subject that's being studied is divided in a finite number of smaller line segments, areas or volumes, which are designated finite elements. This process is called discretization, and is illustrated in Figure 2.1. In a linear elastic analysis, when employing the FEM, usually there is the need of determining, in a first place, the displacement field of a finite number of points in the system. To those points is given the name of nodes, being usually located in the vertex of the elements, as seen in the mentioned figure.

There are commonly 3 main phases of the FEM analysis: the pre-processing, the analysis and the post-processing. Inside the pre and the post-processing there are also two steps to be taken in each, the concept definition and model, and the interpretation and results representation, respectively. Those steps are described in more detailed next [6]:

1. Pre-processing: Where the geometric model is built, and the geometrical parameters and other imposed conditions are defined. Usually simplifications are able to be made which will influence the quality of the final results (eg. the kind of finite elements and mesh).

    (a) Concept definition: Here are made considerations about the influences of the environment on the system, and how it can be represented in a digital model in a faithfully equivalent manner.

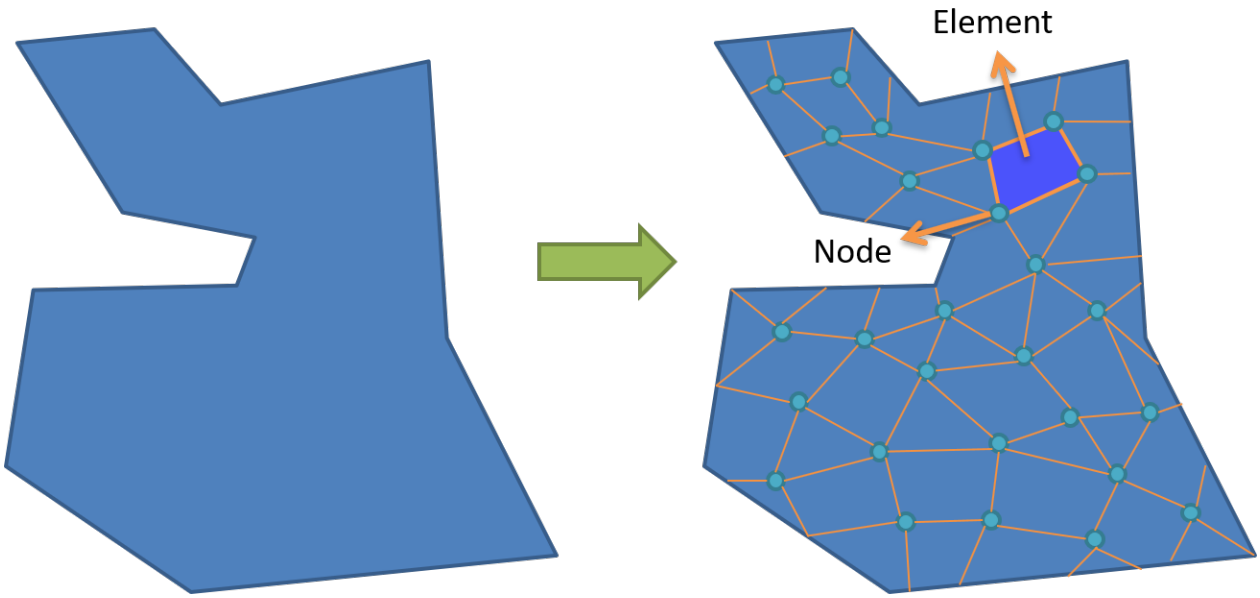

Figure 2.1: Schematic representation of the discretization process

(b) Modelling: Stage where the geometry, nodes, elements, boundary conditions, materials and loadings are defined. At this point, also the analysis control parameters are defined. The problem's domain is subdivided into finite elements.

2. Analysis: The model is verified and if no errors are identified, the numerical analysis is conducted. The equations for the elements are then developed and, in the case of an assembly, the equations of the entire system from the equations of individual elements.

3. Post-processing: In this phase the output information is presented in a schematic way, like graphic or in a tabular form.

   (a) Interpretation: It's where the results are evaluated – displacement, forces, stress, deformation, temperature, pressure, etc.

   (b) Results Representation: The results are represented in the form of isovalues, contours, value variation with time, animations, etc.

2.2.2 Nodes vs Elements

The result values calculated in the Finite Element Analysis (FEA) initially are in reference to points in the elements called Gauss points (Or Quadrature points), represented in orange in Figure 2.2. The process of presenting the values relative to the node is a series of iterations: from the Gauss points; to the node values inside each element; to then the average value in the element nodes (represented in blue in the same Figure) or to the average value of the node. This last step allows the FEA to present the results either the results in the element or the node, which will most likely produce distinct plot results across the body.

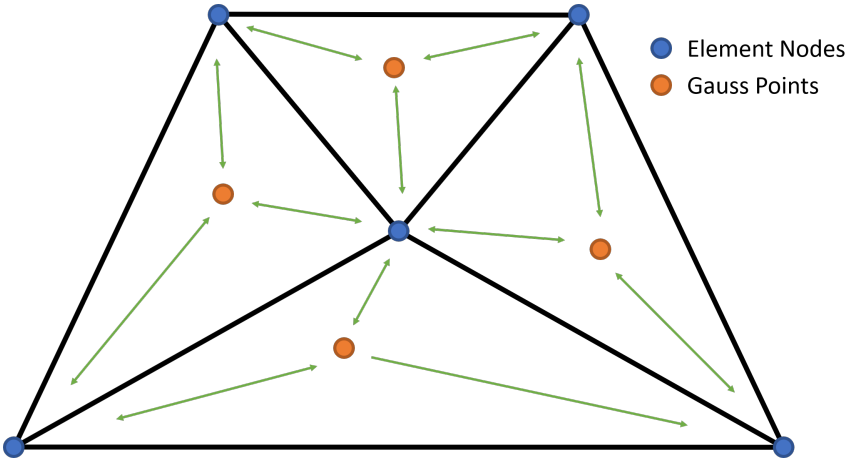

Figure 2.2: Schematic representation of the nodes and Gauss points on elements

The process, illustrated in Figure 2.3, shows that the nodes with elements in common have different values; one referent to each element. The average value of the node from the neighbour elements is then computed by the simulation software, where values are given to the nodes themselves as shown on the top right of the Figure. This method produces what is called averaged (or nodal) results.

Element values, alternately, can be averaged to report a single elemental result within each element from extrapolation of the Gaussian points. Although these are averaged between Gauss points, they are called non-averaged because the averaging is done internally within the same element, as shown in the bottom right of the same Figure.

With that in mind, it is preferable to have the results being presented in the nodes, because one node is most often shared by several elements, and each element reports different values at the shared node. Reported values from all adjacent elements are then averaged to obtain a single value.

In comparison, it can be said that the average in the nodes are influenced by the neighbour element values, being that the element average doesn't weight the adjacent elements, justifying have the results being presented in the nodes by having a higher consistency across the studied body [7].

2.2.3 Static Study

One of the studies in which the FEM analysis can be applied to spare processing time, especially when having 3D geometries or complex systems, is the static study. In the previously mentioned post-processing phase, the axial, shear, torsional and bending stresses are calculated in the system by resourcing to its nodes/elements equations. That way it's possible to attain the displacement field of each node, having in a grater scale, the schematic or tabular representation of the system's results, such as deformation, stress, etc.

In the FEA one can differentiate between the linear and non-linear analysis. In short, a non-linear analysis is more suitable to be carried in the case of having an alteration of the material's behaviour, changing from elastic domain to plastic (even though some materials may be elastic

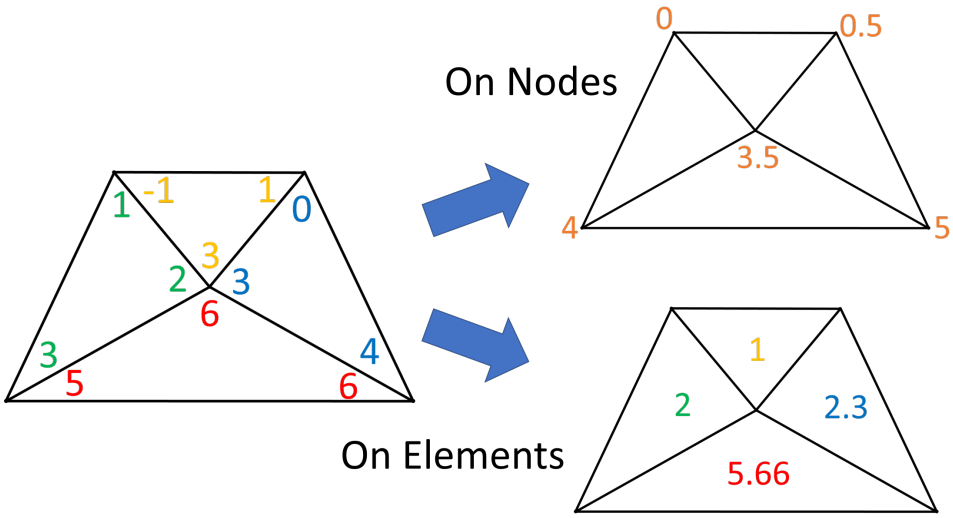

Figure 2.3: Step to average results on the nodes and on the elements

and non-linear, if presenting great displacement values, such as rubbers). In FEA, if the stiffness of the simulated object is not constant the mentioned analysis should be considered instead. This happens in case there's a geometric, a material or a boundary condition non-linearity, which should not be the case in the current project. All simulations will be carried in the elastic domain, with constant geometries and boundary conditions, which means that only the linear analysis are going to be regarded in this thesis [6].

That's usually done by resorting to one of the CAD software available in the market. In this project the one that will be used is the Dassault Systèmes' SolidWorks 2017. This programs offers the possibility of making dynamic and static studies (among others), to the parts designed using the mentioned software, or even to imported parts.

By activating the SW's Simulation Add-In it's possible to create various studies, as some of them are shown in Figure 2.4. In the static study the external conditions applied to the part are defined, the material is chosen and the quality of the mesh is designated. The program also allows connectors to be created instead, which provide already predefined boundary conditions adequate to the type of connections (like pins, bolts and screws), but also have mechanical properties associated to them as if they were extra parts. This should be taken into account if the part or assembly has those connections but it also adds additional intermediary processing that needs to be done, summing more time to conclude the simulation.

The product results of the FEM analysis are possible to be presented graphically in plots, but also the result equations can be accessed, providing informations about the result loads in the fixtures.

Those plots are gradients of colour which correspond to different values. It can be chosen to present, as seen in the last menu of Figure 2.4, the stress, displacement and strain. From the stress plot it's possible to produce the Factor of Safety (FoS) plot which takes into account the yield stress and presents the ratio of the node's equivalent stress and the material's yield stress, giving information that allow the user to identify any weak areas of the design in case of low values. In the opposite case, if the values are too high, it might be the case that some material

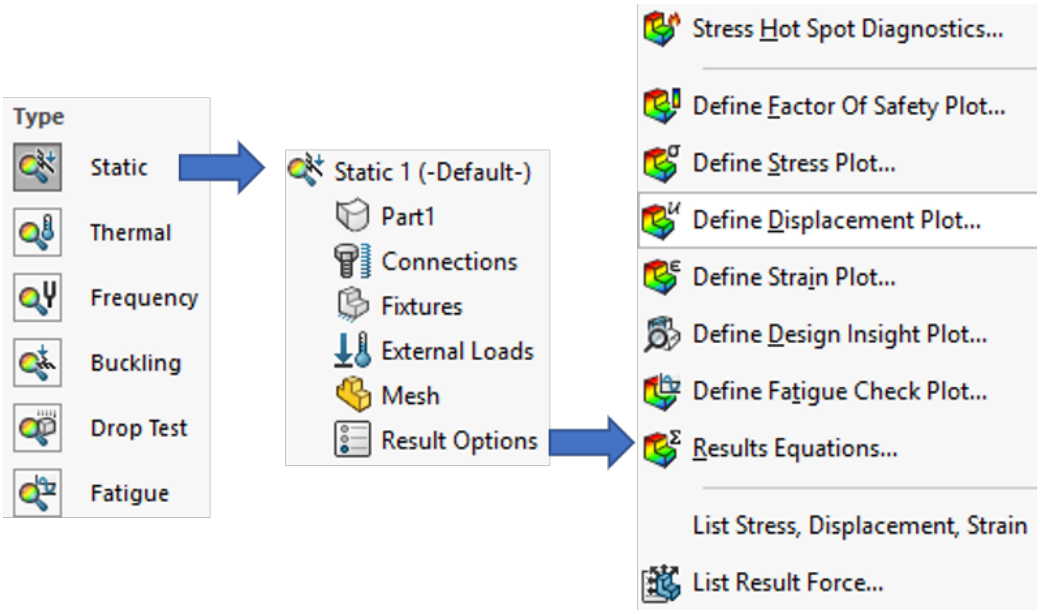

Figure 2.4: Static study sequence

can be saved in that particular area.

Hot Spot Diagnostics

A secondary analysis that can be done in this study is the Hot Spot Diagnostics, being also useful in cases where there are points or small areas of stress concentration, as in the fixture areas shown in Figure 2.5. This tool takes into account the stress results and evaluates the neighbour nodes in order to decide if there is a sudden increase on the stress values. It filters the elements based on the magnitude of the equivalent strain relative to the maximum equivalent strain for each node [7]. The Hot Spot Diagnostics plot then presents the stress plot without the identified hot spots. There can be attested in Figure 2.6 the mentioned elements that the values are identified as hotspots. In the plot legend, on the right of the picture, it can be noted that the maximum values are now in grey, corresponding to the range of values of the hotspot elements.

Besides the graphic schematic presentation of values, it's also possible to assess the results in the form of tables (lists) which sometimes is more convenient, especially if the data is to be exported and treated in a different software.

This analysis, however, is a sub-product of the stress results from the simulation, which means that will not change the values previously obtain. This could be a problem in further simulations that use stress result values (as it is the case of fatigue analysis). Ideally, if hotspots are identified, it's desirable not to regard them in additional studies that will use those values.

If the maximum stress elements are still being considered in the those further analysis, it means that the failure will happen sooner than in the ideal case in those elements, making the part or the system not withstand the load that it should.

This is a limitation of the FEA that has to be taken into consideration.

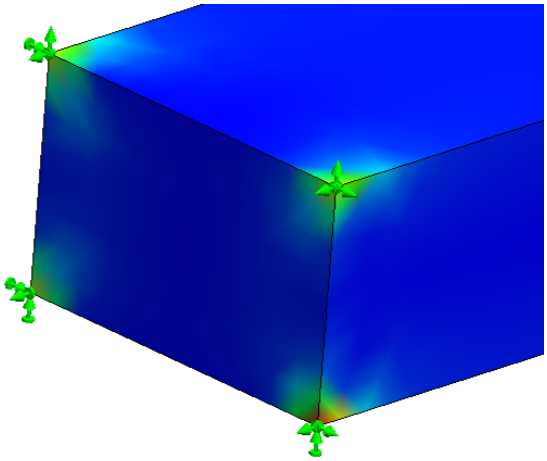

Figure 2.5: Hot spot example located in the fixtures

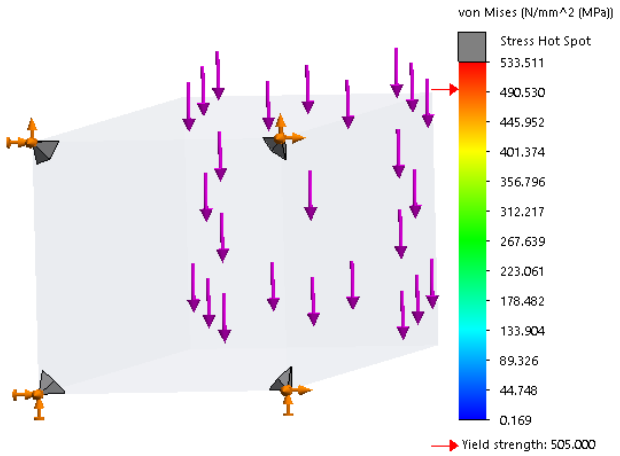

Figure 2.6: Hot spot elements isolated

2.3 Maximum-Distortion-Energy Criterion (von Mises Criterion)

The Maximum-Distortion-Energy Criterion, more commonly known as the von Mises Criterion is one of the most frequently used yield criteria for ductile materials, in order to assert the mechanism of failure of a determined material.

These criteria were created from the need to design parts with materials that could withstand expected load conditions without yield. The need for such criteria happened after it was found that if none of the main stress values were greater than the yield stress, the combination of the mentioned stresses may still result in yielding [8].

Unlike an uniaxial loading, where the results can be extracted from a tensile test of a sample from the same material, and then calculated for the given area, in the case of having a bi or multiaxial stress load, the failure calculation needs to consider the combination of stresses applied to it. A multiaxial situation is not possible to be related to a test due to the high variability of internal stress cases in similar loads. Hence the need to having a broader method of including several components of stress [9].

The Maximum-Distortion-Energy Criterion, or von Mises criterion, essentially stated that yielding occurs when the distortion strain energy per unit volume reaches or exceeds the distortion strain energy per unit volume for yield in simple tension or compression of the same material [10]. This can be translated to a general expression with all stresses taken into account as in Equation 2.1 It can also be simplified for the principal stresses as in Figure 2.7, analytical corresponding to the Equation 2.2. A further simplification is generally preferred, representing the equivalent von Mises stress in the principal plane stress with $\sigma_3 = \sigma_{12} = \sigma_{23} = \sigma_{31} = 0$, as shown graphically in Figure 2.8 and analytically in Equation 2.3.

$$\sigma_{vm} = \sqrt{\frac{(\sigma_1 - \sigma_2)^2 + (\sigma_2 - \sigma_3)^2 + (\sigma_3 - \sigma_1)^2 + 6 \cdot (\sigma_{12}^2 + \sigma_{23}^2 + \sigma_{31}^2)}{2}} \tag{2.1}$$

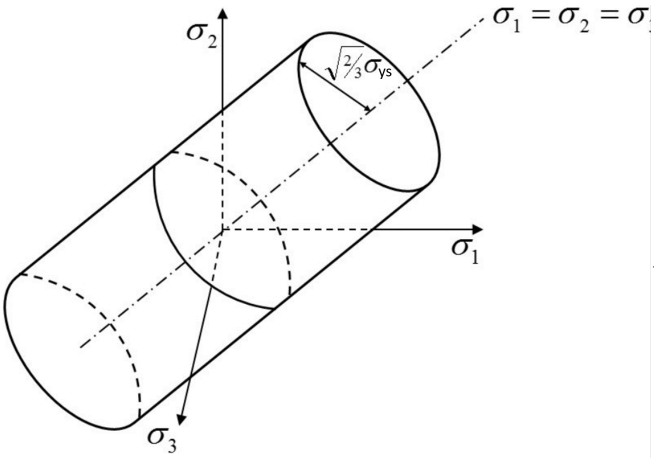

Figure 2.7: von Mises yield surface in 3D space

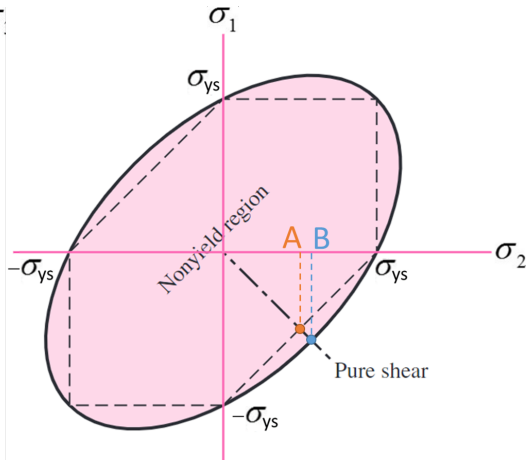

Figure 2.8: von Mises yield surface in the principal plane stress

$$\sigma_{vm} = \sqrt{\frac{(\sigma_1 - \sigma_2)^2 + (\sigma_2 - \sigma_3)^2 + (\sigma_3 - \sigma_1)^2}{2}} \tag{2.2}$$

$$\sigma_{vm} = \sqrt{\sigma_1^2 - \sigma_1\sigma_2 + \sigma_2^2} \tag{2.3}$$

The von Mises criteria also predicts that the tensile yield stress σ_{Tys}, shear yield stress τ_{ys}, and compressive yield stress σ_{Cys} are related by: $\sigma_{Tys} = \sigma_{Cys} = 3\tau_{ys}$.

2.3.1 Maximum-Shear-Stress Criterion (Tresca)

Knowing that the yielding occurs in ductile materials due to slippage along oblique surfaces and happens due primarily to shearing stresses, as can be seen in deformed tensile-test specimens, this criterion is formulated based on that observation. Slip lines in those cases can be seen appearing at 45° since the shear stress is maximum in that orientation, developing the mechanism of failure from the mentioned shear stress.

Since the shear stress is maximum at 45° from the axis of tension, it makes sense to think that this is the mechanism of failure, so it can be noted that the oblique plane has half the stress at yield from the centric axial load.

Knowing this, if the principal stresses have the same sign, the criterion gives us $|\sigma_1| < \sigma_{ys}$, if the principal stresses have oposite signs, the criterion gives us $|\sigma_1 - \sigma_2| < \sigma_{ys}$. This can be seen graphically in the interior hexagon in Figure 2.8.

2.3.2 Comparison

On the intersection of the bisector of the second and fourth quadrants with the von Mises ellipse and the Tresca hexagon, there can be observed a difference of coordinates, corresponding to different yield stress results. The point A from Tresca's criterion corresponds to $0.5\sigma_{ys}$, being that the point B from von Mises criterion corresponds to $0.577\sigma_{ys}$.

When observing the ratio between the results obtained from a torsion test for the yield strength (τ_{ys}) with the yield strength obtained for tension (σ_{ys}), it can be attested values from 0.55 to 0.60 back to the values of the yield stress in a pure shear situation, the obtained values with the von Mises criterion are between the range of the stresses ratio [11].

Although the Tresca criterion can be more conservative, the von Mises can be more accurate in its results when it comes to torsion, as proved before. In the cases of having any of the principal plane stresses equal to the yield stress, or $\sigma_1 = \sigma_2 = \sigma_{ys}$, the values given by both are the same (seen as the coincident vertices of Figure 2.8). Therefore, in this project the von Mises criterion will be preferred over Tresca.

2.4 Fracture mechanics

With the increased use of metal in structures, largely irons and steels, many unforeseen accidents began to occur due to the failure of this structures. This was a worrying problem, especially in passenger vehicles or factory equipment, where a catastrophic failure would end up with the loss of human lives.

There are mainly two characteristics of fracture failures: Progressive development of crack (ductile behaviour) or sudden fracture without any warning since yielding is practically absent (brittle behaviour). This types of failures are influenced by: Nature and magnitude of the stress cycle, endurance limit, stress concentration points and surface characteristics.

The materials used in parts designed to withstand expected static loads greater than they were subjected to were observed to still fail. It was discovered that it was happening due to pre-existing flaws in the materials that could initiate cracking and fracture. The carried investigations revealed that the fractures were brittle and that flaws and stress concentrations were responsible for the failure.

It was also discovered that low temperatures promoted the brittle behaviour of steel, being that the energy required for fracture decreases abruptly under a certain value, as seen in Charpy's impact Energy for steel, in the graph of Figure 2.9, where the absorbed impact energy from the Charpy hammer, after hitting the notched specimen are indicated in vertical axis and the test temperature in the abscissa axis, getting from ductile to brittle behaviour. This can be prevented by using material with low transition temperatures (especially in welding) [12].

as seen in Charpy's impact Energy (fig. 2.9) , where the absorbed impact energy from the Charpy hammer, after hitting the notched specimen are indicated in vertical axis and the test temperature in abscissa axis

2.4.1 Fatigue

Fatigue is is a failure mechanism that occurs in structural applications that are subjected to cyclical and dynamic stresses. In this situations it is possible that the failure will happen at stress levels well under the tensile or yield strength values for static loads. Fatigue is important inasmuch as it is the single largest cause of failure in metals, estimated to comprise approximately 90% of all metallic failures [13]. Polymers and ceramics, generally speaking, are also

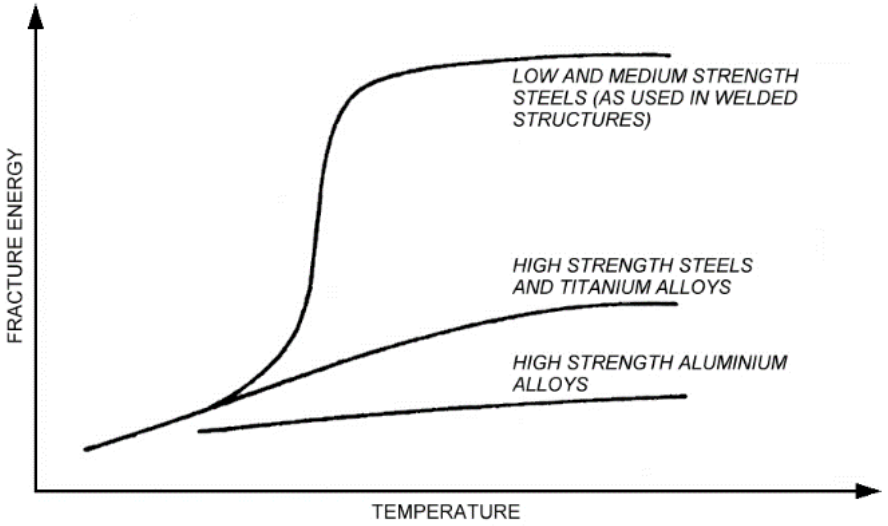

Figure 2.9: Scheme of the effect of temperature on the fracture energy of some metals [12]

susceptible to this fatigue, but harder to predict for having plastic behaviour, in the case of the polymer, or being too brittle, in the case of the ceramics. This type of failure is catastrophic and insidious, occurring very suddenly and without warning.

Even in ductile type materials, the fatigue failure takes a brittle-like behaviour due to crack propagation in a perpendicular direction to the applied tensile stress, showing almost no plastic deformation. This way, fatigue must be considered in the design of all structural components subjected to repeated or fluctuating loads.

If the example of a rotating shaft is taken, it can be ensured to work at a certain static load without failure, but while rotating, one point on the surface of the shaft changes from tension to compression once every revolution. If it's working at $1500rpm$, for instance, that means that the rotating shaft changes from tension to compression 1500 times each minute, which can be intuitively foreseen to lead to a different form of failure other than yield [10].

2.4.2 Strength and Endurance Limit

A S-N Curve is a plot of the magnitude of an alternating stress (σ_a or S) versus the number of cycles (N) for a given material. Typically both the stress and number of cycles are displayed on logarithmic scales and the curve is used to predict the fatigue strength and life when stress cycle is completely reversible.

These values are obtained from experience, by performing tests to specimens in order to get the two readings (S-N) used to then plot the results from the repeated tests with different stresses. If a series of tests is conducted using different maximum stress levels, the resulting data is plotted as a S-N curve. For each test, the alternating stress is plotted as an ordinate and the number of cycles as an abscissa. Because of the large number of cycles required rupture, the cycles are plotted on logarithmic scale.

The test specimen of a material or an engineering component is subjected to a sufficiently severe cyclic stress, a fatigue crack or other damage may be developed, leading to complete

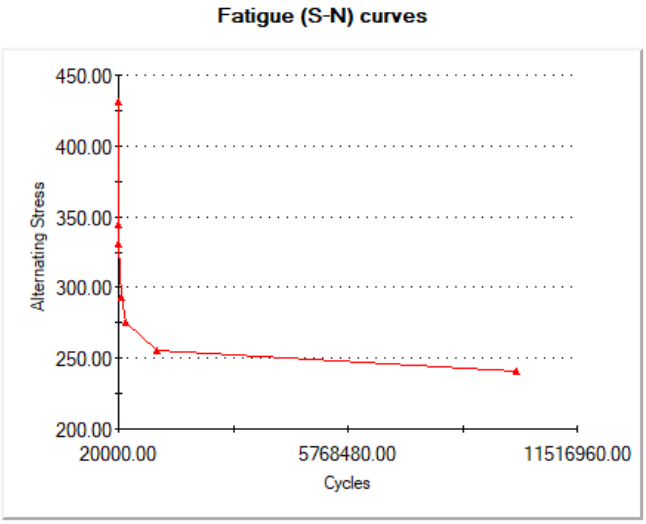

Figure 2.10: S-N curve for the Aluminium 7075-T6 from SolidWorks

failure of the member. If the test is repeated at a higher stress level, the number of cycles to failure will be smaller [14].

As the alternating stress is reduced, the number of cycles required to cause rupture increases, until the endurance limit is reached. The endurance limit, or fatigue limit (σ_{fl}) is the stress for which failure does not occur, even for an indefinitely large number of loading cycles. For a low-carbon steel, such as structural steel, the endurance limit is about one-half of the ultimate strength (σ_u) of the steel [11].

2.4.3 Fatigue Failure Criteria

The cyclical loads are characterized as shown in Figure 2.11. There can a different range of typical alternated loads, but generally it can be characterized by 4 variables. The mean stress (σ_m) is the distance between the mean value of the sinusoidal wave to the horizontal axis. The maximum (σ_{max}) and minimum stress (σ_{min}) are the distance between the horizontal axis and the crest and trough of the sinusoidal wave, respectively. The alternating stress is the distance between the maximum and the minimum stress, which can also be described as the amplitude.

The relation between this stresses is given by: $\sigma_m = (\sigma_{max} + \sigma_{min})/2$ and $\sigma_a = (\sigma_{max} - \sigma_{min})/2$.

Usually, the criteria is chosen depending on the material's behaviour, this is, if it's brittle, the ultimate stress should be taken into account because the failure is catastrophic, presenting no deformation; if the material is ductile the yield stress is more adequate to be used.

This means that the Goodman and Gerber criteria is more directed to brittle behaviour structures and the Soderberg to ductile ones.

The structures or parts are to be designed for their values of stress to be under the chosen criterion's line, meaning that it will not be in the failure area.

The Gerber parabolic line predicts the failure of the materials by fatigue, which correspond

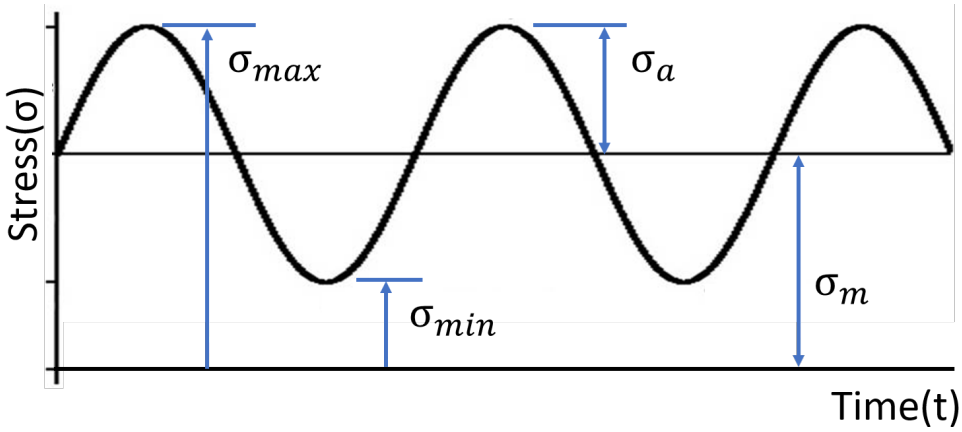

Figure 2.11: Examples of a cyclical load and its variables

to results from fatigue tests. Generally speaking, this is the criteria that relates better to experimental values, fiting the failure points on the best possible way, for if they are marked on the graphic they follow that parabolic line. The Gerber's expression is given by the Equation 2.4 and can be used for brittle materials.

$$1 = \left(\frac{\sigma_m}{\sigma_u}\right)^2 + \frac{\sigma_a}{\sigma_{fl}} \tag{2.4}$$

The Goodman line is also used for brittle materials, and is given by the Equation 2.5. It was proposed by Goodman a linear variation instead of a parabolic one, being safer for design, although still based on the ultimate stress (σ_u) it's completely located inside Gerber's parabola.

$$\frac{1}{FoS} = \frac{\sigma_m}{\sigma_u} + \frac{\sigma_a}{\sigma_{fl}} \tag{2.5}$$

The Soderberg line given by Equation 2.6 provides a very conservative single check of both fatigue and yielding, being the safest of the three failure criteria.

$$\frac{1}{FoS} = \frac{\sigma_m}{\sigma_{ys}} + \frac{\sigma_a}{\sigma_{fl}} \tag{2.6}$$

In the mentioned equations' FoS represents the factor of safety for infinite fatigue life (generally considered at a million cycles).

Following what was previously stated, in this project, the Soderberg criterion will always be preferred due to its conservative nature, but also due to the use of ductile materials.

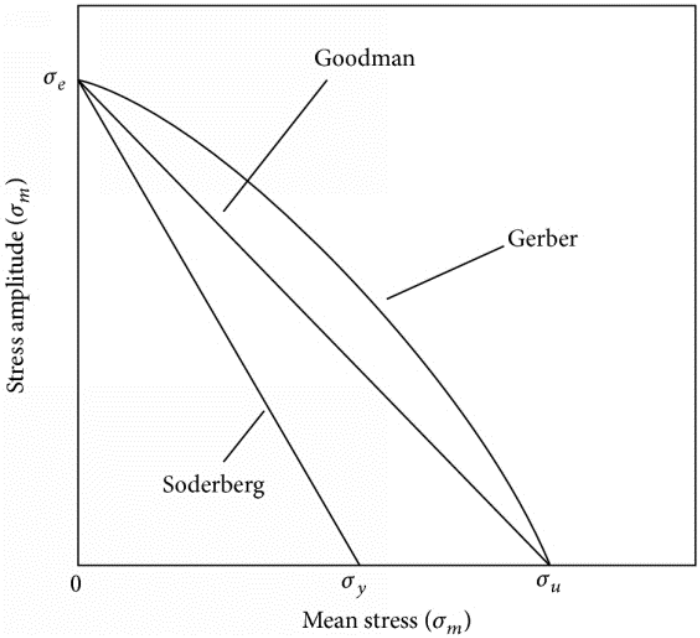

Figure 2.12: Fatigue theory methods graphics [12]

Chapter 3

Conceptual Framework

In this chapter the process of know-how gathering on the WWS' kinematics will be addressed.

3.1 General Windshield Wiper System considerations

The WWS is a system that tries to maximize the vehicle operators' line of sight by removing dust in the windscreen or cleaning it under aggressive weather conditions, such as rain, ice, snow, mud and debris. In this project, it was only studied the parts shown in Figure 3.1, which are essentially the wiper components, the ones acting between the motor axis and the windshield.

Represented by the number 1 is the wiper system's blade, which is usually composed by some kind of rubber, being responsible for dragging of the particles or substances in the windshield out of the line of sight of the operators.

Next there can be seen the small curved arms of the blade's structure with the number 2, which are there to push the blade against the windscreen. These curved arms are presented in various levels (3 in the shown example), being that the highest level has a big curved arm, the second level 2 and the last level 4. This allows the contact force between the windshield and the blade to be distributed by 8 points of contact with the structure, bending the blade and ensuring that the contact is kept at all times with the blade adapting its curvature to the windshield. All curved arms have an hinge in the middle of them, being connected with each other but allowing rotation over themselves.

In the number 3 there's the connector that has an hinge linked to the first level curved arm of the structure (the top one), transmitting translation movement from the arms' rotation to the blade. This part is also linked with two hinges onto the top connector (number 4) of the WWS' arms (number 5), staying in an horizontal position during its motion. This because the example is a pantographic WWS, which will later be described the implications of having a system like this.

In order to transfer the rotational action of the motor inside the vehicle to the blade there are two axes connections, represented by the number 6. They may both be motorized, meaning that the two of them are liked to the motor, or one of them is motorized and the other one is a

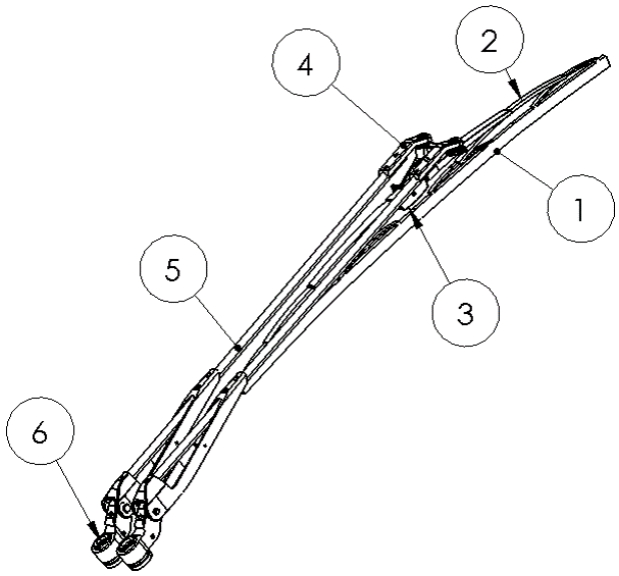

1. Blade
2. Blade structure's small curved arms
3. Blade structure's connector
4. Top arms connector
5. Arms
6. Motor axes

Figure 3.1: WWS scheme

driving axis connection.

These are the main parts present in the wiping system that are important to the studies carried in this work, but there are many more smaller parts that were not mentioned such as pins, screws and spring, that apply force granting the contact.

3.2 Research

After the initial meetings with AHD it was decided that before starting to work with the company's models a broader research about the functioning of WWSs, in different industries, ought to be done.

It was possible to surmise from this research that there are four main types of WWS: tandem system, opposed system, single system and pantographic system.

This systems are extensively used, mainly in the aeronautical, aircraft, railway and automotive industries wherein they all have some pros and cons.

In the following sections of this chapter each system will be described and the positives and negatives aspects of using that particular type of WWS will be elucidated.

3.2.1 Single arm

The classical and simplest way to clean the windshield, producing a cleaning area almost equivalent to a portion of a circle (excluding the small circular area on the inferior of the glass), as seen in the bottom right corner of Figure 3.2. This is a system widely used in small and mostly (or almost) flat windshields, in vehicles such as boats, air-planes, trains and motorbikes.

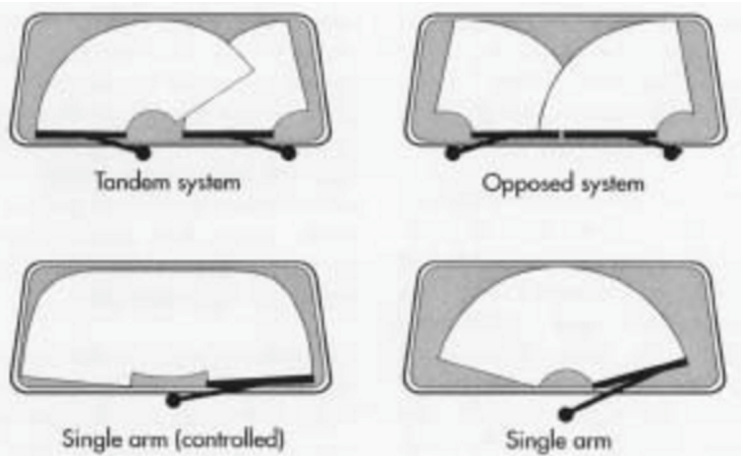

Figure 3.2: Different types of WWS
Source: http://www.madehow.com/images/hpm_0000_0007_0_img0131.jpg

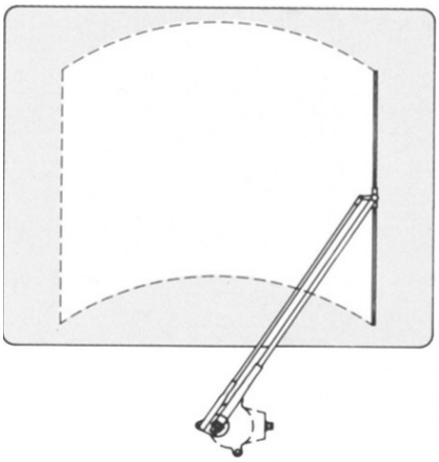

Figure 3.3: Pantographic WWS
Source: https://www.absolutemarine.co.nz/image/cache/catalog/products/Wipers/pantograph_swing-800x800.jpg

Pros

The simplest and, thus, the most reliable system of them all. Not much maintenance needed. One arm only. A lot less space required for the mechanism.

Cons

Small cleaning area. The corners are left unswept, which is not ideal for the driver's best sight.

3.2.2 Single arm (controlled)

Also called eccentric sweep, or Mercedes mono-wiper, it's a complex mechanism that adds a crank slider to the rotational axis of the arm, in comparison with the single arm mechanism. This results in a maximum extension of the arm at 45° and 135°, as seen in the left bottom corner of Figure 3.2.

Pros

Bigger area covered. The upper corners of the windshield surface are much better swept. One arm only.

Cons

Complex and more expensive mechanism. The maintenance is more often needed, so, not as reliable as a simpler model. Cannot operate at high speed as good as models with two arms.

3.2.3 Tandem system

This is a system that uses pretty much the same principles as the single arm system but with two arms, in order to cover a greater area. The motion is transmitted to both axis by a bar that unites them, moving horizontally. On the top left corner of Figure 3.2 it's possible to see that the focus of this mechanism is to clean a bigger area on the driver's side, leaving the top unswept area in the passenger's side.

Pros

Bigger area covered in comparison with the simplest system in Section 3.2.1. Focus on the driver.

Cons

More parts but not a complex system like the simple arm (controlled) mechanism. Not ideal for the passenger. Two blades instead of one.

3.2.4 Opposed system

This system seen, in the top right corner of the Figure 3.2, has pretty much the same working principles as the system in the Section 3.2.3, with the difference of both arms moving in opposite directions instead of the same. This adds usually two bars to the mechanism (or a bigger one), in order to establish an opposing movement while maintaining only one motor.

Pros

Both the driver and the passenger have the same clean view. The overall focus area may be greater due to the possibility of overlapping the blades.

Cons

The top middle area is left unswept (which affects the driver's clean view). The mechanism has slightly more parts than the Tandem. Not as fast as the previous systems because the lower arm can only start moving after the upper arm moves a considerable amount. Two blades.

3.2.5 Pantographic

As seen in Figure 3.3, this system's principle is exactly the same as the simple arm (Chapter 3.2.1) with the addition of a moving head on the top of the arm, that allows the rotation of the blade. This rotation is driven and limited by the second (usually more slender) arm, making it work like a 4-bar mechanism, which keeps the blade vertical during its operation.

Pros

The system that provides the sweeping area most similar to the windshield's projected geometry (almost rectangular). Simple and compact mechanism. One blade only.

Cons

Can't be as easily hidden when not in operation.

3.2.6 Research Conclusions

It's important to notice that some of the mentioned types of WWS are more often used in some specific surfaces than others.

The single arm is widely used in more flat and small surfaces (e.g. trains and planes windows), or secondary windows of the vehicles (like the car rear window). When the glass surface is wider, as in cars and buses front windows, it's more commonly used the the tandem or the opposed system in order to clean a bigger area. In some buses with a more pronounced curvature or complex surfaces like on helicopters, it's more indicated to use the pantographic type of WWS.

After the research was done, some parameters were found to be important to have in mind, if a new model was to be made, such as:

- Blade size
- Blade's structure height
- Arms size
- Axis position

3.3 Simple model

3.3.1 Database search

In order to understand the mechanical operation behind the WWS a search for a simple CAD model was done in an on-line CAD file database. As seen in Figure 3.4, a 4-bar mechanism with a rotating gear was found and imported to the CAD and simulation software SW 2017. Under the red bars is the hidden mechanism, in the vehicles, that allows the cyclical movement of the arms. This is not exactly how most tandem systems' mechanism work, but is a simpler (and still accurate) one.

[1] https://grabcad.com/library/windshield-wiper-mechanism-2

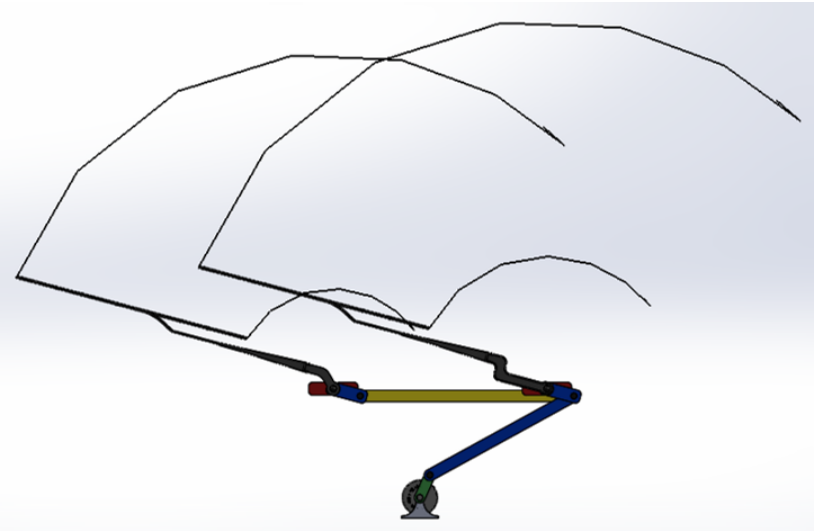

Figure 3.4: Simplified WWS
Source: Model from GrabCad [1]

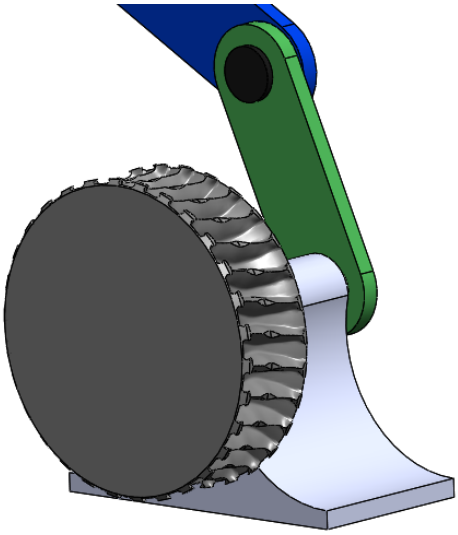

Figure 3.5: Detail of the base and shaft of the simple model

3.3.2 Building the CAD model

It was necessary to redo all the mates and also to remake some parts, maintaining its geometry and sizes, since not all of them were compatible with the software used.

This particular model was a tandem WWS, working as described in Section 3.2.3. The main goal obtaining this design was to start with a simpler working model (it didn't have an hinge in the lower part of the arms and also didn't require springs) in order to progress to a more complex model as the one used by AHD.

In order to establish all mates and relations between the parts, the first red bar was fixed in the assembly's origin. After measuring the distance on the original model, the second red bar was placed at that noted distance horizontally. A new part was designed to place the drive shaft from the motor, as seen in Figure 3.5, and fixed the motor's shaft in its original place.

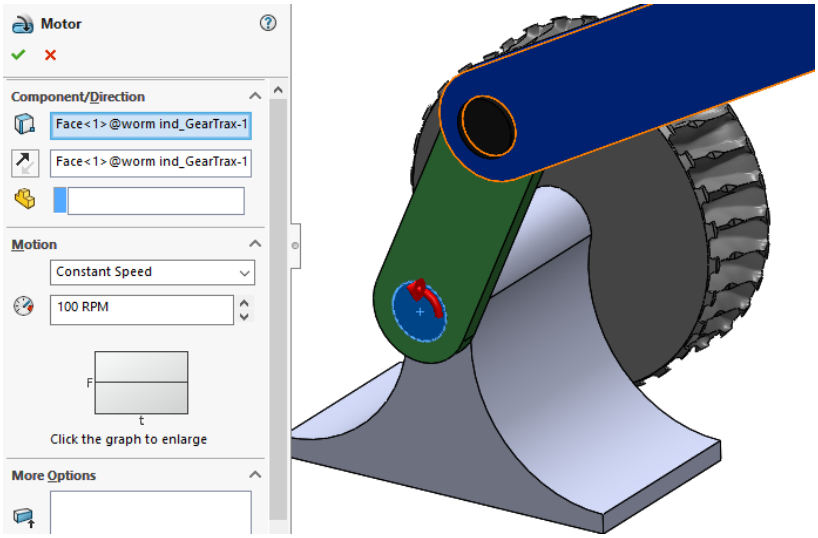

Figure 3.6: Rotary Motor characterization

3.3.3 Animation and Outcome

After all parts placed and mates completed, the kinematic study was done using the Animation type of study, in the Motion Study Add-In. To the Animation study was only needed to add a simple rotary motor as seen in Figure 3.6, in the drive shaft at a constant speed of $100rpm$ (this speed was chosen as the rotation of the arms seemed to be as in a real situation).

The animation result was then produced and the path of the tips of the blades was mapped during its motion, as seen in Figure 3.4.

This was a good learning method of the working mechanism behind the WWS, to understand the transmission of movement from the rotary motor to the bars and, ultimately, to the cyclical rotation of the arms and blades. It was also a useful introduction for a more complex model as the ones used by AHD in their helicopters.

Chapter 4

Kinematic Analysis in the H135

In this chapter the kinematic analysis will further be developed and addressed, this time with the Airbus' state of the art WWS. Some fundamental key issues were faced upon and solved with the support and consulting of Airbus' engineering crew that had already work on the conception of the original WWS.

4.1 Airbus' wiper model

After the conceptual research was done and the kinematic analysis on the simple tandem model completed, a CAD model was then provided by AHD (Figure 4.1). This was a pantographic model that wiped from the center position to both sides, the co-pilot's and the pilot's windshield. The provided model, however, had to be imported from CATIA V5 Simulation Software (the software used originally to design and develop this model by AHD) to SW. Since these are both products from the same company, Dassault Systèmes, it reviled no compatibility issues.

This model was referred by AHD as a well designed and well functioning system. The company stated that the project's goal should be to adapt this specific model to any helicopter's means of connection and its surface curvature. They also added that, having this WWS CAD model, the first approach should be trying to replicate the existing conditions of functioning before advancing to the design and development of new parts to adapt to other helicopters models.

4.1.1 Catia to SolidWorks implementation

In order to study this WWS' kinematics and its motion operation, the shaft from the simple CAD model was availed in order to transmit motion from the motor's one way rotation to the alternative (almost) linear displacement of the bar connected to the base of the arms of the WWS', that rotates by itself. Not only was the shaft added but also was the previously designed support, staying fixed, thus allowing the shaft's rotation.

A new part was also designed to be the static part of the WWS' assembly, which was connected to the base of the arms, as observed in the Figure 4.2. This allowed for the part to

Figure 4.1: Pantographic model used in the H135

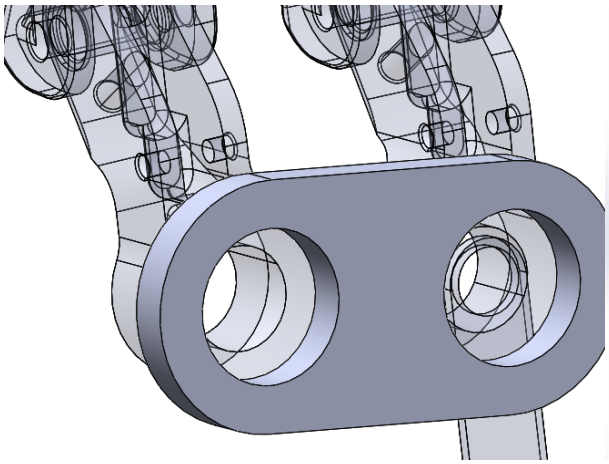

Figure 4.2: Arms static base

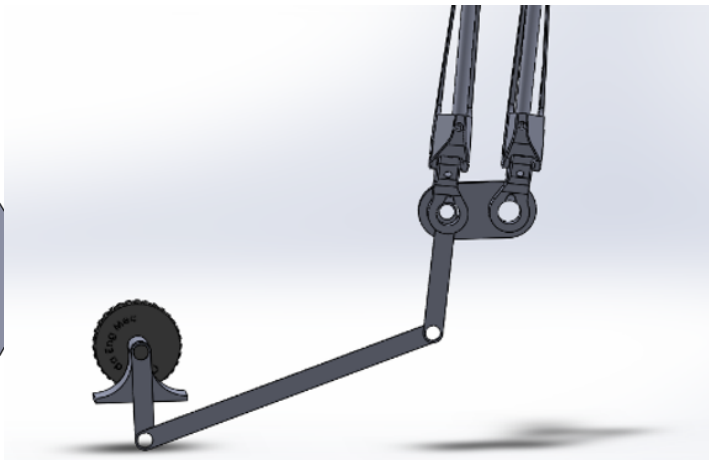

Figure 4.3: H135 WWS' model with shaft

stay fixed while the WWS' components can be moved inside their degrees of freedom, even though without yet taking into account the existing hinge in the lower part of the arms, and also the springs.

As seen in the Figures 4.1 and 4.3, not all parts from the original CAD model produced by AHD were used in this model, primarily due to the complexity of the system, which would overload the simulations, and secondly because it was not necessary: the generic parts were ignored and replaced with geometrical mates like pins, hinges, screws, etc., using the corresponding mechanical mates as the ones seen in Figure 4.4.

No springs were added due to the absence of a surface to push against the blade, in order to create a reaction force to achieve the systems' static equilibrium. Because of this, and since this model, unlike the simple model in 3.3, can rotate by its arms base, as seen in Figure 4.5, it was required to add another mate to restrict the arms rotation.

Because of the above mentioned, an angle mate of 4° (Figure 4.6) was added to keep the

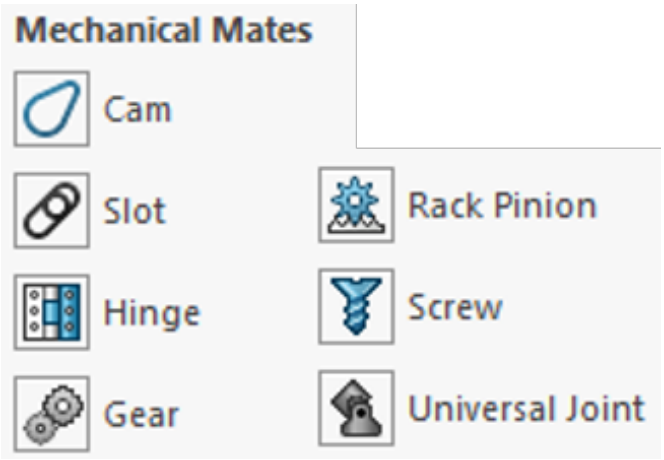

Figure 4.4: SW's mechanical mates

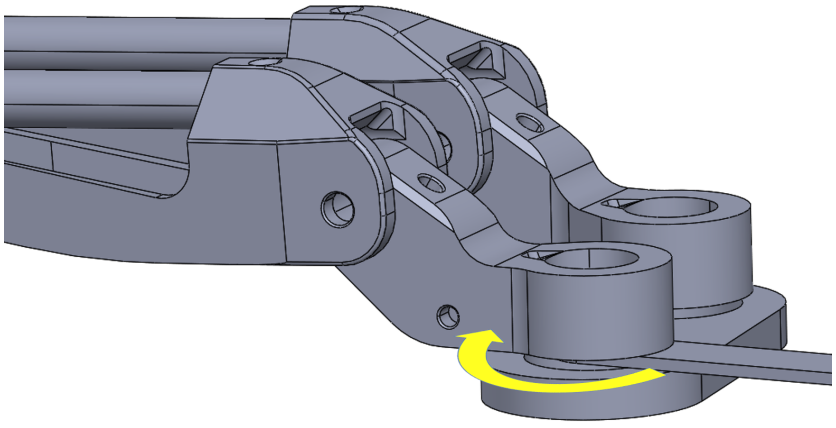

Figure 4.5: Arms rotating base

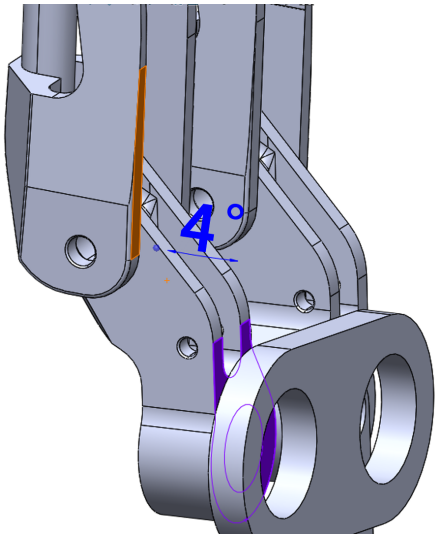

Figure 4.6: Arm's base angle

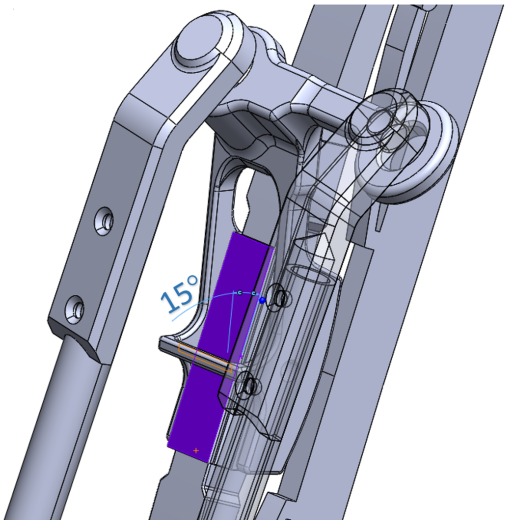

Figure 4.7: Blade's structure angle

arms inclination the same as the middle position in the H135 helicopter. This prevented the arms from straying when its base rotated with the motor's action.

In the same way, an angle mate had to be added to the blade's structure, in this case the only difference was that the angle had a 15° value (Figure 4.7) in order for the blade to be pointing inward during all operation's time.

4.1.2 Kinematic analysis and problems

This, though, was not a viable solution because, when was necessary to animate the model, it was found that the WWS was locked in the centre position, as seen in the Figure 4.1. After redoing each mate much more carefully a few times, and doing it again in a meeting with the advisors, the result was always a complete lock of the model in the center position. The only way that was possible to move the system was by suppressing one of the mates, like a pin or a bolt, which would make the movement unnatural and unlike the real model.

In order to clarify the working method of the wiper, two elementary models with bars were designed, shown in Figure 4.8, following an advisor's counselling. It was deduced that, when the top connector was on the same plan as the others, there was no locking problem, but as the top of the vertical bars (arms) started to flex (angle bigger than 0) it was impossible to move them once all mates were assigned. In the model on the right of the mentioned Figure it was of intuitive understanding that it could not move because, when both arms tried to rotate, the faces on the top of the bars would stop being on coincident planes to start being parallels. The top horizontal bar could never be coincident with both arms on the top, at the same time, besides in the middle position.

Some meetings took place to review the connections on the top of the WWS arms, as they join to the part attached to the blade's structure. It was firstly thought that the problem was some existing clearance that was not being considered, or a plastic/rubber ring that allowed some twisting of the top part that connects the arms to the blade, conceding a few more degrees

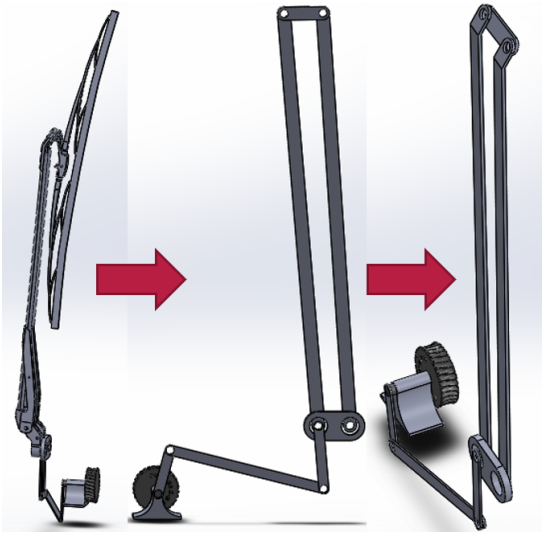

Figure 4.8: Elementary models

of freedom that were not accounted for, which resulted in the model locking.

In a meetings it was ascertained by AHD that there were no such parts nor clearances that allowed any twisting on the top of the arms. It was proposed by the student, in that meeting, that the lock of the model might be due to the stiffness ascribed to its parts that were not verified in the real life WWS model. For example, the arm bars were very slender, so it could be that this physical property of the arms allowed a slight twist that can not be considered in an motion analysis in the software.

Some weeks later, however, in another meeting the initial assumption was confirmed. An AHD's collaborator, who had previously worked on this model's development, affirmed that the model operated perfectly fine in real life but there were limitations, as the described ones above, in he CAD model that was developed by them.

At that point there was not yet a surface present in the assembly because, again, the goal was to, in a first approach, understand each small part's role in the system operation free from the aircraft. Although the goal was to analyse it apart from the helicopter, and its surface, it was proposed by the AHD and the advisors that in the next step a animation with the H135's windshield surface was carried out in order to possibly relieve some restrictions imposed by additional mates, which could be compensated by the contact itself, such as angles.

4.2 H135 surface addition

Due to the previously justified impossibility of carrying out the simulation, the H135's surface was added, resulting in the model seen in Figure 4.9. The WWS connection in the helicopter was kept, such as the wire protection, just to correctly situate the base of the WWS on the model.

Two points of the blade, one in the top and one in the bottom, were made coincident with the window's surface, as shown on top of the Figure 4.16, and the angle mates deleted. Contrary to what was thought, the elimination of the angles and its replacement with the blade's coincidence

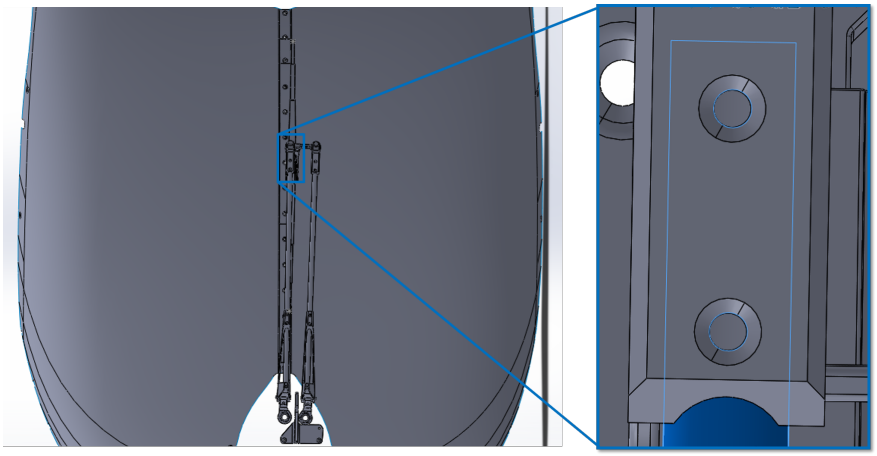

Figure 4.9: WWS with H135's surface and holes detail

with the surface did not solve the locking problem. The WWS was still getting locked in the middle position, unable to move.

4.2.1 Arm holes concentricity

Some modifications on the mates were made in order to relieve the restrictions and one that seemed to work to some extent was the suppression of the concentricity between the holes in the top of the arm and the arm's head, as shown in detail in Figure 4.9.

Validation

However, this couldn't be the optimal solution since the blade, when the arms were moved, tilted away from the windshield. In the real model the blade follows the glass curvature as the arms rotate. Also, as expected and seen in Figure 4.10, the head of the arm without the concentricity on the holes was making an unnatural movement with a noticeable torsion and misalignment.

Besides the mentioned problems, when the interference detection evaluation was run it detected an early penetration (Figure 4.11), at about 17°, which wasn't even near the admissible maximum cleaning angle (γ).

4.2.2 Ball joint

After much thinking about the mates, it was decided to try to simulate a ball joint instead of an hinge, in one of the hinge connections between the arm's head and the part that connects to the blade's structure. This would allow two more degrees of freedom, instead of only a rotation along the z axis, a ball joint would allow a rotation in all three axis, which would again relieve the imposed restrictions.

As shown in Figure 4.12, the ball joint was simulated by two coincident points, each drawn in a midplane in each part and align with the hole axis. Then the points were placed coincident in the assembly.

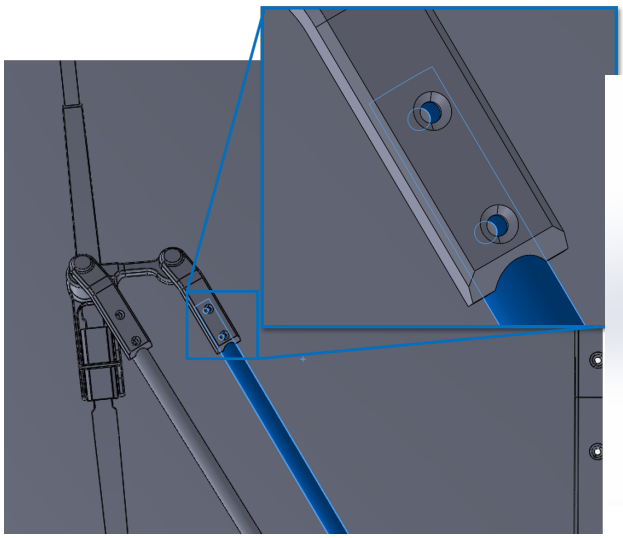

Figure 4.10: Alignment detail view after moving

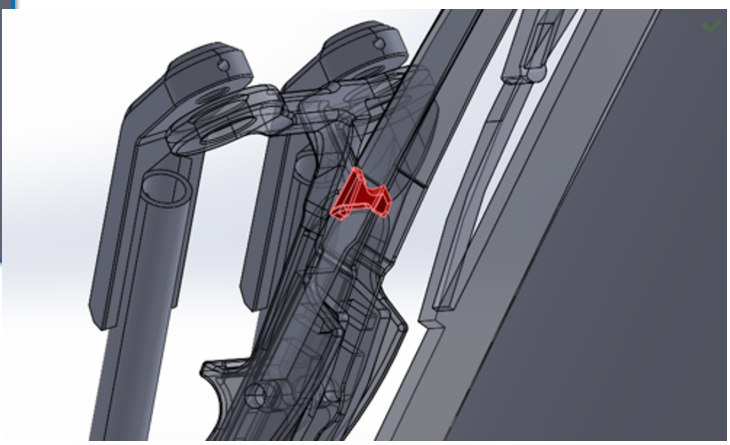

Figure 4.11: Interference detection

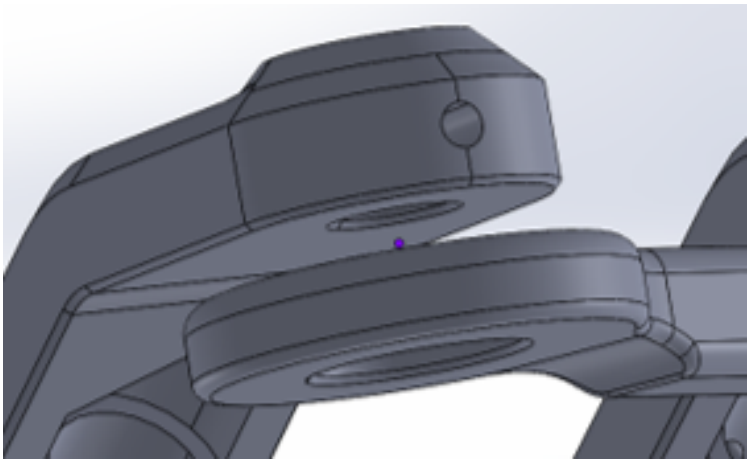

Figure 4.12: Midpoint coincidence

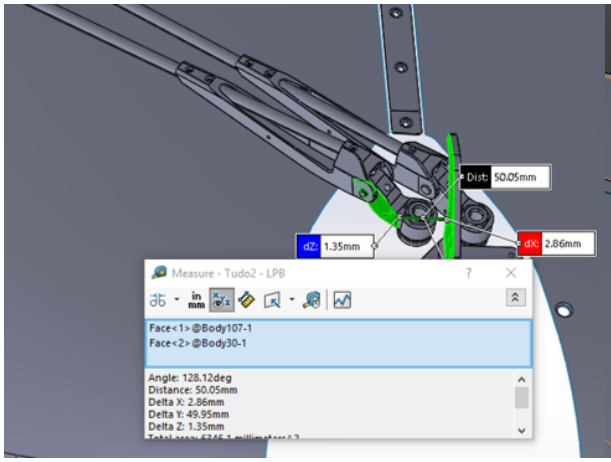

Figure 4.13: Left angle

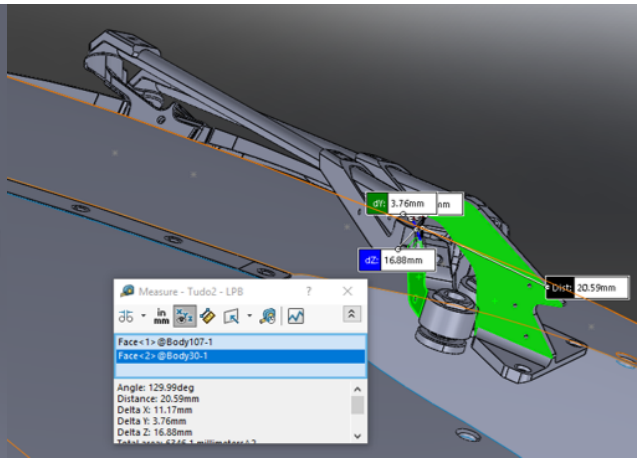

Figure 4.14: Right angle

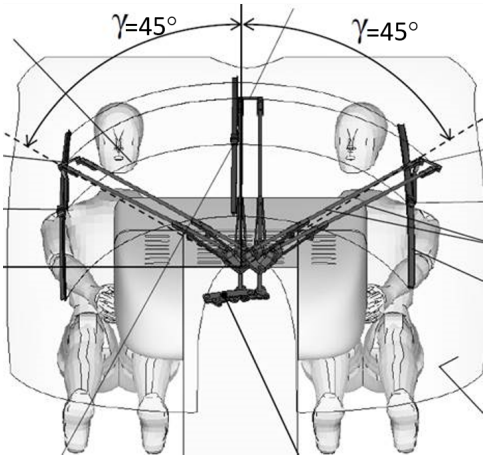

Figure 4.15: AHD's model cleaning angle [15]

Validation

Still before any animation was done, the blade was dragged with the two points coincident to the surface in order to attest the proper functioning of the model. As in Figure 4.13 and Figure 4.14, the maximum cleaning angles (γ) were recorded and compared to the ones in the H135's WWS real model (Figure 4.15).

The maximum cleaning angle was registered when the arms were at a minimum distance of 20 mm from the window [15]. This value is referred in the AHD's internal specification as the minimum distance between the WWS' arms and the windshield for a safe performance.

Both values of the AHD's cleaning angles were 45°, whereas the computational models had a left angle value of 51,8° and right of 49,9°. The of minimum distance between the windshield and the arms was one of the limitations that the WWS should have in order to ensure clearance and no interference in the kinematics of the system [15].

The values when presented to AHD were regarded as quite satisfactory.

There was also no presence of interferences before the maximum cleaning angle, and the blade was correctly going along with the windshield, staying close to a perpendicular position during the movement (what had not happened before).

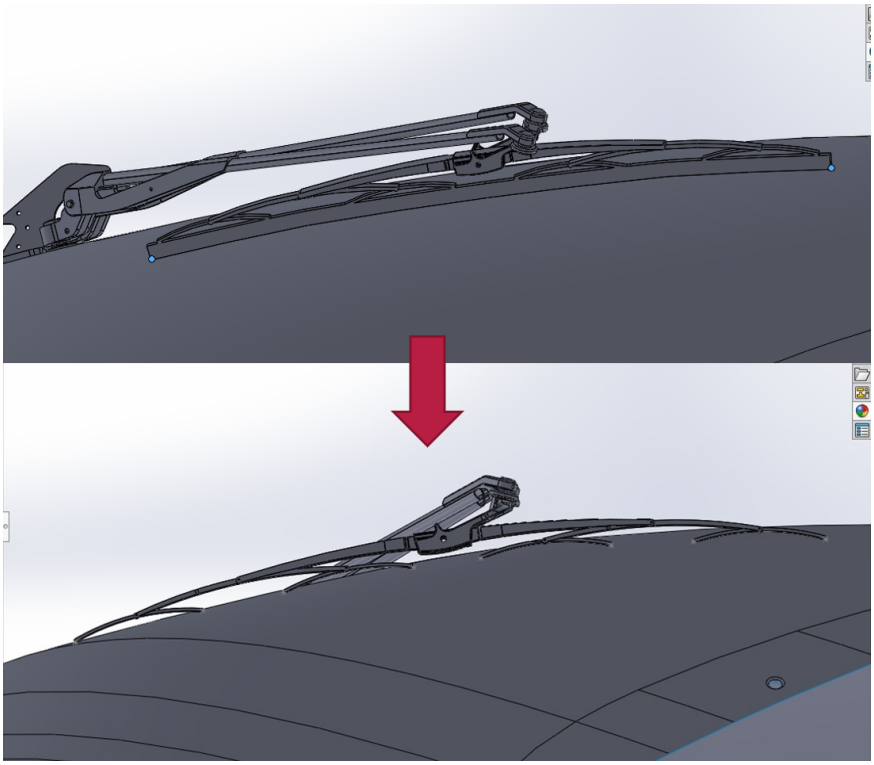

Figure 4.16: Transition to modular structure

The angle between the top and bottom faces of the joint, seen in Figure 4.12, was also measured and it was never greater than 2°, which implied that only a little relief of the restrictions was needed. This could also mean that, since the real model and its materials are not completely stiff, effectively, with some flexibility added to this model, it would work with both the joints as hinges, as stated by AHD. This explains why the real life model works as intended using hinges but that's not possible in the CAD model.

4.2.3 Modular blade structure

It was agreed jointly with AHD that, at this point, the next step should be to make the blade structure modular in order to flex along with windshield.

It was not possible to do so with this blade and the way around it was found was to use the little rotational arms as contact points. As shown in Figure 4.16, this was achieved by redoing each rotational arm independently and then assembly by the rotational connection as hinges. A big, two medium and four small curved arms were designed with the same measurements as the original blade structure.

By allowing the rotation of the arms by themselves it was possible to have a more accurate model which would resemble the blade action by following up the windshield geometry.

As seen in Figure 4.17, the small curved arms that contacts the surface was rounded in the contact area and designed with a 17 mm hight, corresponding to the blade, in order to stay as close to the original model as possible.

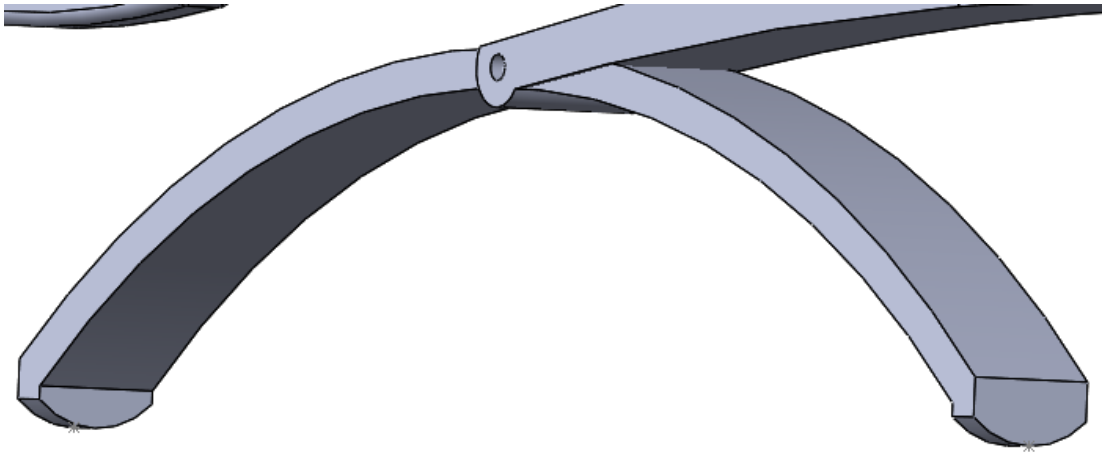

Figure 4.17: Small curved contact arm

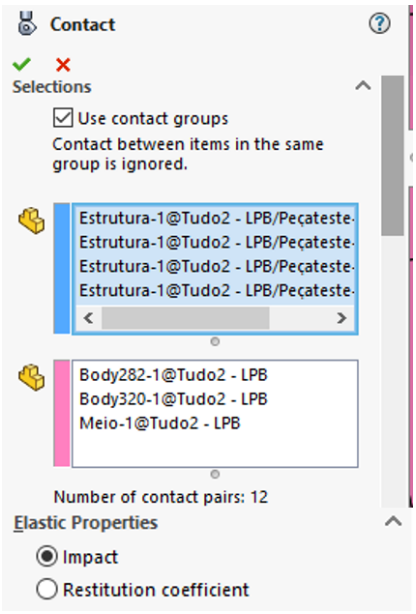

Figure 4.18: Contact parameters

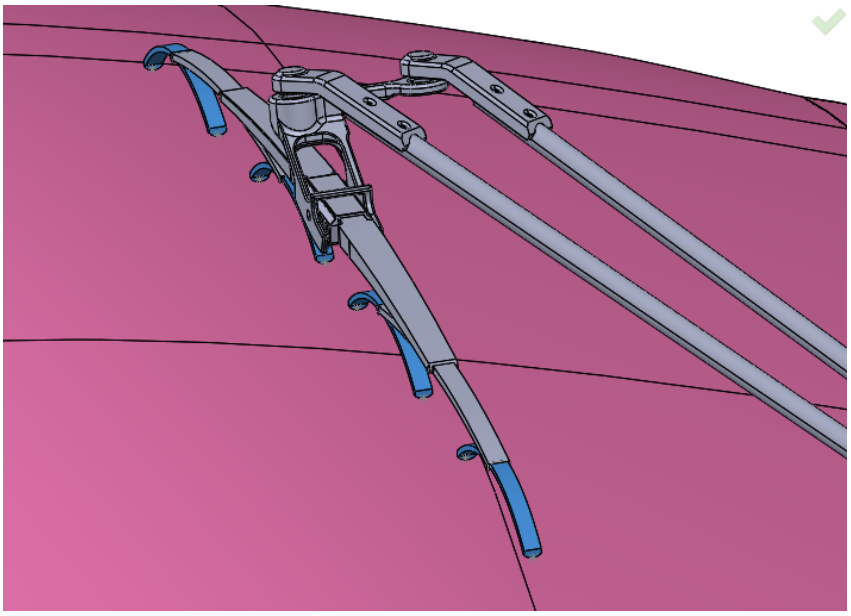

Figure 4.19: Contact groups

4.2.4 Motion Study

Up to this point all information regarding the kinematics of the model was obtained simply by moving its parts to see if it worked and how much. After having the model working as intended it was possible to move on to the kinematic analysis on the Motion Study Add-In.

Body Contact

A body contact between the selected groups in Figure 4.19 was created with the parameters shown in Figure 4.18. It was minded that two different groups should be distinguished to ease the simulation, since no other contact were to occur.

Also, at this point, there was still no need to add the materials for the animation process.

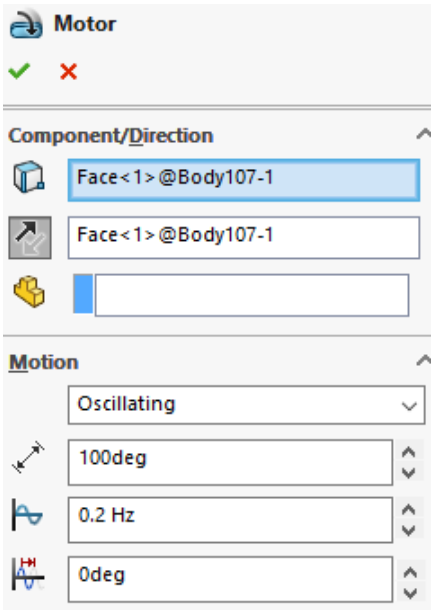

Figure 4.20: Motor parameters

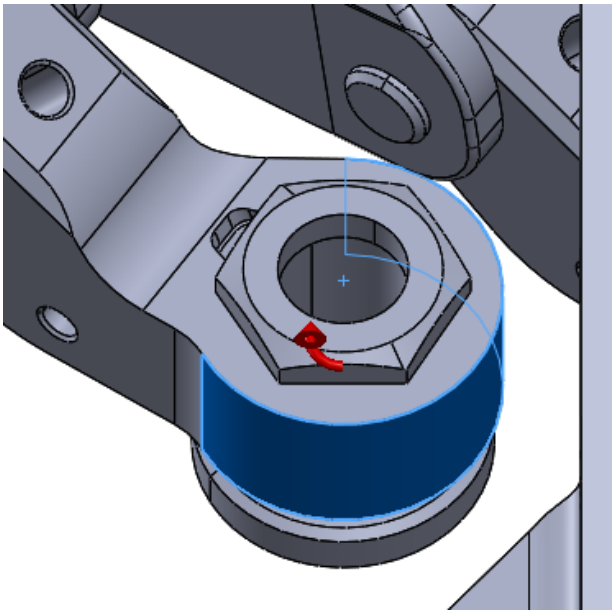

Figure 4.21: Motor location

Motor

In the motion study it was possible to replace the gear motor that was presented in the previous model for a rotary oscillating motor with the location as in Figure 4.21. Since it was found to be possible to have a total cleaning angle of approximately 108° but the AHD model rotates only 90°, the displacement angle used was 100°, as shown in Figure 4.20. The frequency was chosen arbitrarily yet regarding what seemed to be adequate with the reality, but it was not really important at this point. The phase shift was not used since the arms were positioned at the left maximum position (50°), as the starting point of the animation.

Springs

Again, at this point it was also not crucial to have final values to the springs. The minimum center distance between the holes (l_{sp}) where the springs were to be coupled, as seen in Figure 4.23, was previously measured during the motion with the value of 152 mm. This meant that 140 mm of relaxed position (x_{sp}), as in Figure 4.22, should be enough in order to keep the contact between the blade and the windshield. The other parameters were kept as they were originally and an equal spring was added to the second arm.

Gravitational acceleration

The gravity effect was added by choosing the motion element that applies the exact value of 1G of acceleration on the chosen direction (z).

The simulation was then run.

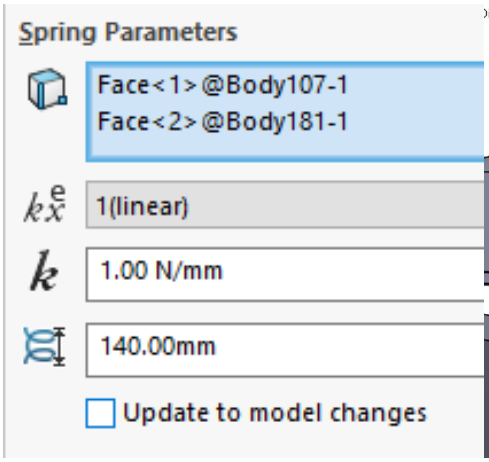

Figure 4.22: Spring parameters

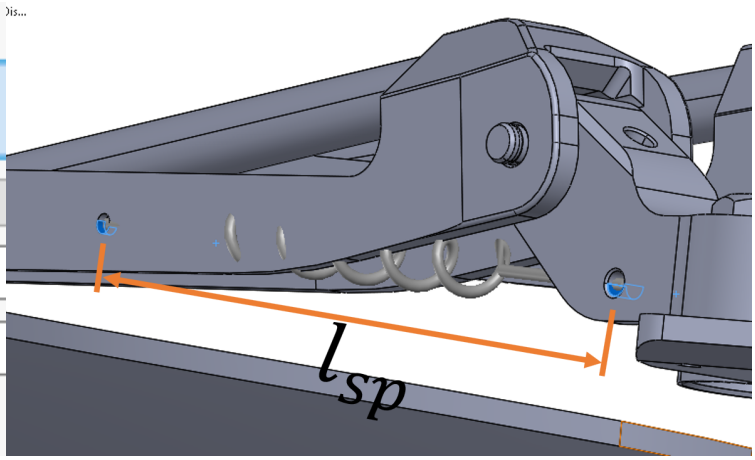

Figure 4.23: Spring location

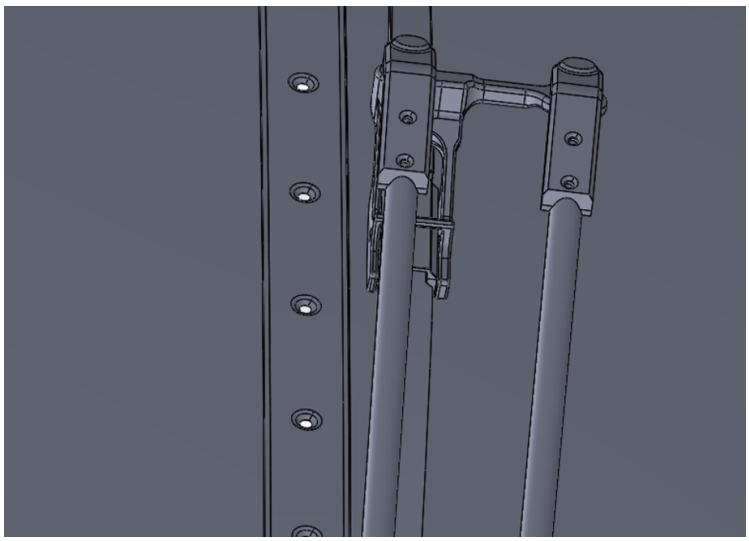

Figure 4.24: Plate joining both windshields

Problem and solution

It was noted that, with the parts provided by AHD, when the WWS passed through the middle plate the little contact arms would conflict with the holes shown in Figure 4.24 and penetrated them.

This problem was solved by deleting the middle plate and designing a new part from on assembly. The windshields had complex geometries and were not tangent to each other, so it was not possible to create a parts that transitioned smoothly from one side to the other. As seen in Figure 4.25, the found solution was creating a part from 53 arcs drawn along the windshield hight, with 300 mm radius, being almost planar but with a little curvature. This would ideally prevent bumps during the simulation when the arms in contact passed through.

Results

It was possible to represent the real model faithfully in this simulation making use of the add-in motion study. The main goal of understanding the kinematics behind the WWS, its

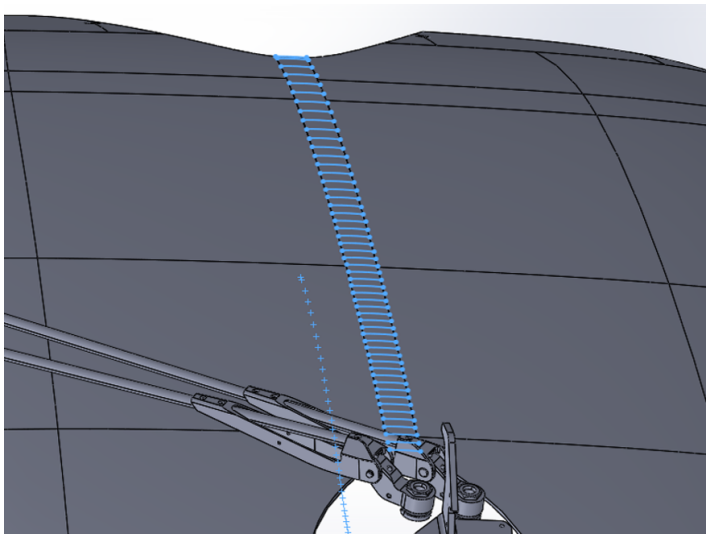

Figure 4.25: New middle part

specific characteristics and features was successfully achieved, obtaining a covered cleaning area of 100° as shown in Figure 4.26. This granted the covered area observed in the real model and measured by AHD, whom were satisfied with the outcome of the simulation, regarding its well representation of the H135 model.

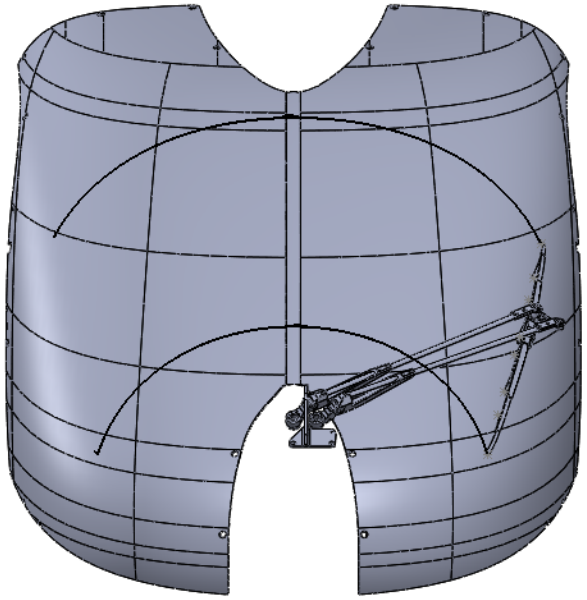

Figure 4.26: Covered area by the WWS

Chapter 5

H130 Windshield Wiper System Adjustment

In this chapter it will be described in detail the phases of design and development of new parts that allow the H135 WWS' adaptation into the H130's body frame. It will be presented some improvements made based on ideas and expertise of the Airbus' engineering crew, after some meetings were attended. It will also be presented and justified the progress made in the models, supported by software simulations and studies.

5.1 Direct adaptation

The H130 helicopter model presents a different challenge, in regards to the windshield, when compared to the H135. This aircraft has 3 surfaces, a middle smaller one and two bigger side ones, one in each side of the pilots. Besides the more demanding task of adapting a pantographic WWS to a 3 surface windshield, the means of connection of the WWS was also different than the one in the previous helicopter. The H130 was design to house a simple wiping system, which means that some adaptation method will have to be used to make it compatible with this aircraft.

After having a CAD model that resembled the real H135's WWS and presenting it to AHD, it was told by the company that the next step should be trying to adapt the previous studied pantographic system to an one axis fixation only helicopter. In order to study its adaptation a H130's frame and some parts were provided by AHD as seen in Figure 5.1. This was a smaller and more curved helicopter model which brought some other problems to care during the WWS's design and development.

It was also mentioned by the company that an effort should be made to keep the least number of modifications possible to the helicopter (such as internal parts and mechanisms, drilling, etc.), since these would have to be submitted again to specification and testing for approval, bringing undesirable extra costs and work to the process.

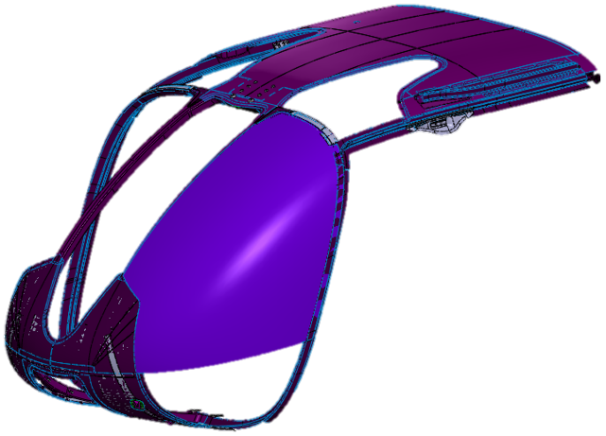

Figure 5.1: H130's body and window surface

5.1.1 Pantographic concept

As this helicopter model only had one axis of connection (the motor shaft), in order to figure out the desired position for the second axis of the pantographic system, the WWS was added directly to the body's model, as seen in Figure 5.2.

In this case, the pantographic movement won't be symmetric nor the cleaning area will be equal, which means that the relative position between the two axis will not be the same as on the H135.

The motor axis position was already settled since this helicopter has a single arm WWS in each side. This means that no further study needs to be made to position the first arm's connection.

Motor axis

Even though its place was already defined, in order to track the position desired for the second axis, firstly it's required to position the blade on the resting spot. Since the helicopter was symmetrical, the pilot side will be studied alone, not only because it would be redundant to study both sides but also because it eliminates a lot of extra parts that are not required to be in the model in order to carry the WWS' study. This simplifies the simulations, making it a lot faster.

The base of the left arm was placed concentric with the motor shaft, by adding the correspondent mate. To fully define the base of the arm's position, it was also added a coincidence mate between the part that acts as an isolation and the helicopter's surface, as seen in Figure 5.3 section view as number 1.

Second axis

After the motor axis was placed, the second axis' position was yet to be found. The first thing to be done was to pick the part that isolates the spindle and which contacts the helicopter surface on the bottom of the arm and placed it roughly where it should be, somewhat by trial

Figure 5.2: Direct adaptation on the H130 model

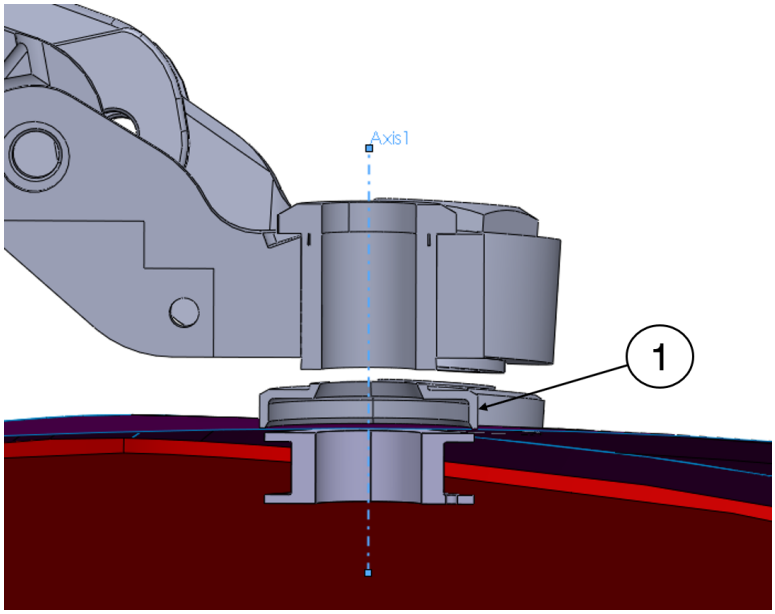

Figure 5.3: Bottom left arm's section view

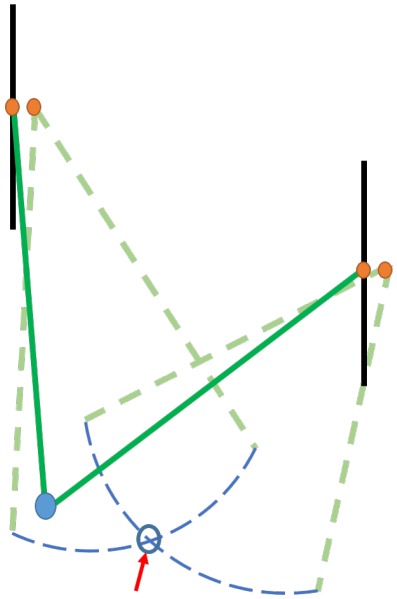

Figure 5.4: Second axis positioning scheme

and error. The area about where the second axis was to be placed was then found using the described method.

At this point the movement done by the WWS (by dragging, not by animation) was almost the intended but the final position of the blade was still not the proper one (Figure 5.5). It was also noticed that a slight change in the bottom position would heavily affect the blade's inclination and rotation, which meant that the second axis desired spot on the helicopter's surface would not be possible to be found simply by trial and error.

To be noted that the desired final position of the blade has a limitation imposed by AHD which was that the arms were never to be closer than 20mm of the surface of the windows at any point [15].

As illustrated in Figure 5.4, to ascertain where the second axis should be placed a simple study was done. Firstly the blade was located in the resting position and fixed. Secondly, by moving the second arm, an arc with the bottom part of it was marked on the surface. The same was done with the blade on the desired final position, which allowed to find the location of the point where the second axis would meet the surface. This new placement originated a better covered area as seen in Figure 5.6, which gives the pilot a cleaner view to the top left side.

5.1.2 Motion Study

Because this was still only an initial study to figure out the axis positioning, the motion study was done simply with a solid body contact, a rotary motor with an maximum angle and two springs, without care for values other than the correct direction and reach of the general movement.

Two studies were carried, as described in Section 5.1.1. The first still without the final position of the second axis, followed by the study with the desired position it. Both of them were performed with the exactly same properties.

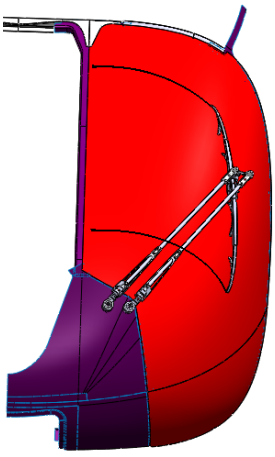

Figure 5.5: WWS covered area before second axis placement

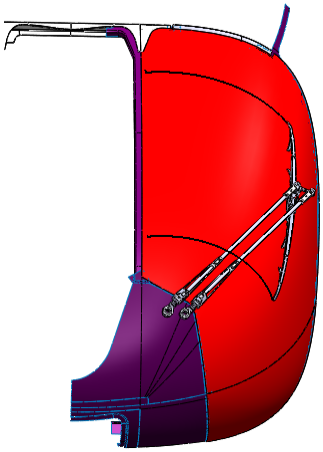

Figure 5.6: WWS covered area after second axis placement

Before axis replacement

Again, using the motion analysis model in the SolidWorks Motion Add-In, a solid body contact between the windows surface and the blade's structure rotational arms was added. No indication of the materials or the friction were given because it's not equated in this study. The elastic properties selected were Impact because that's the most similar option with the real situation. The Impact settings use standard stiffness, dumping and penetration values corresponding to the observed boundary interaction between the two parts in collision.

After having defined the contact, a rotary motor was selected, as previously, on the bottom part of the arm that connects to the motor shaft. The motion of the motor was defined as oscillating, with a frequency of $1Hz$, 0° of phase shift and 43° of reach (γ). Only the reach was modified due to the limitation of proximity of the arms to the glass.

Finally, the springs were added with no particular defined values, just what seemed to work well which was a $k = 1N/mm$ and $x_{sp} = 140mm$

After axis replacement

The same features and parameters were added to the second study, except the cleaning angle (that translates in the motor reach angle), which was possible to add 5°, arriving at 48°. The WWS reach was allowed to be greater in this iteration due to the imposed limitation of the 20 mm of distance from the arm to the windshield, that this time would occur later.

5.1.3 Results

The first and second studies cleaning areas are possible to observe and compare on Figures 5.5 and 5.6. The cleaning angle (γ) and the minimum distance between the arm and the window (h_{min}) are presented in the Table 5.1.

As the movement was done to the right, the closest arm to the wind shield had to be the left one. The fact that, in the before study, the closest arm to the surface was the right arm indicated

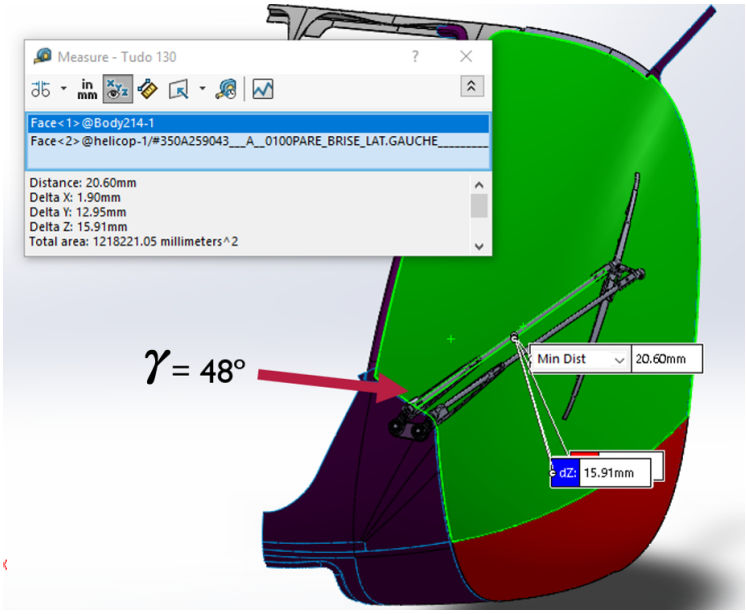

Figure 5.7: Maximum cleaning angle measurement

Table 5.1: Results comparison

Before	γ=43°	h_{min}=21.0mm (right arm)
After	γ=48°	h_{min}=20.6mm (left arm)

that the top connection had an excessive rotation. This was corrected in the after study which allowed a better reach, as seen in Figure 5.7.

When the results were presented to AHD, it was received as very satisfactory given that the simple WWS used in the H130 had a cleaning angle of only 40°.

5.2 Fixation part design

After much brain storming and considerations were done with the help of the advisors about different possibilities and less invasive solutions of adaptation, regarding the constraints of the pantographic system, it was agreed that it was not possible to have a pantographic system with only one axis. The one-axis only solution would have to be a complex gear mechanism with counter rotation on the second arm's base. This, though, was not intended as a viable solution when presented to AHD due to the difficulty of implementation that a complex system like this would inevitably carry.

5.2.1 No surface drilling design

The solution would have to be an extra part attached on the surface of the helicopter that would add the second axis. Since it was said by the company that, ideally, no changes should be made on the helicopter, a no drilling concept, reproduced in Figure 5.8, was made in order to be presented to AHD. This was still a simple model with no curvature, just to present the

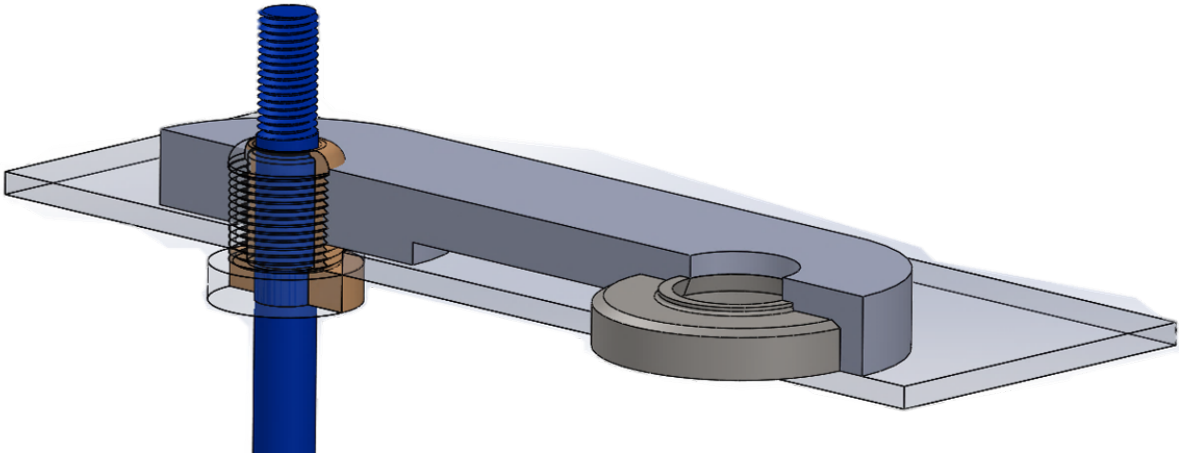

Figure 5.8: Section view of the concept model presented to AHD

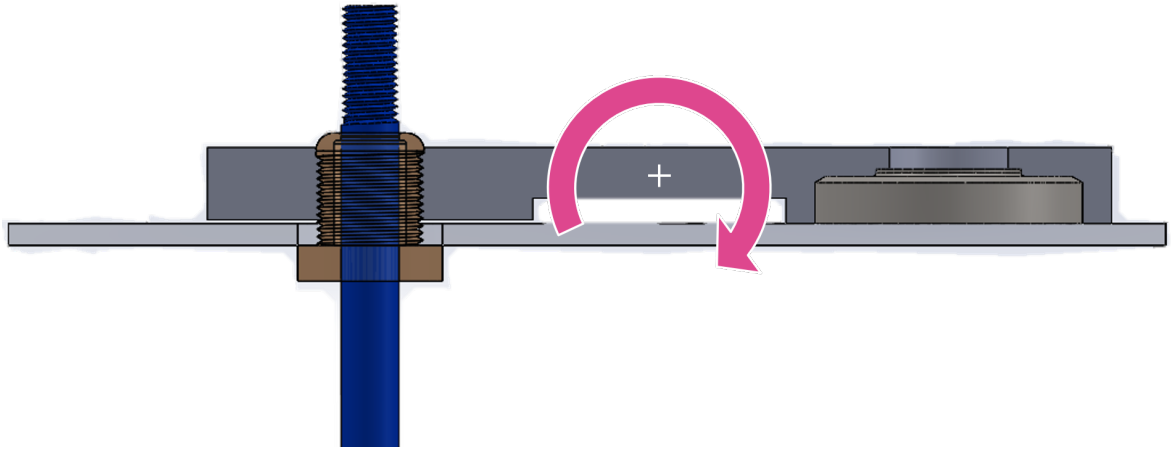

Figure 5.9: Torque scheme representation

general idea.

This model consisted in a part with two holes, one for the motor shaft (Figure 5.10) and a second one to accommodate the rotational spindle. The motor hole was threaded in order to accommodate an hollow screw with the motor shaft inside. This would allow to create a traction force, which would result in the fixation part to be pushed against the helicopter surface.

The rotational spindle would stay fixed on the defined place by the torque applied by the part's bending against the surface when the screw was tightened, as pictured in Figure 5.9. The gap seen in Figure 5.10 represents the space that would exist in the motor side of the fixation part that, when tightened, would achieve the torque necessary to keep a force applied against the helicopter's surface, making it impossible for the spindle to move from its place.

5.2.2 Design with curvature

After the previously mentioned design was presented to AHD and approved, a model with the fixation part following the surface curvature (Figure 5.11), along with a spindle (Figure 5.12) were made.

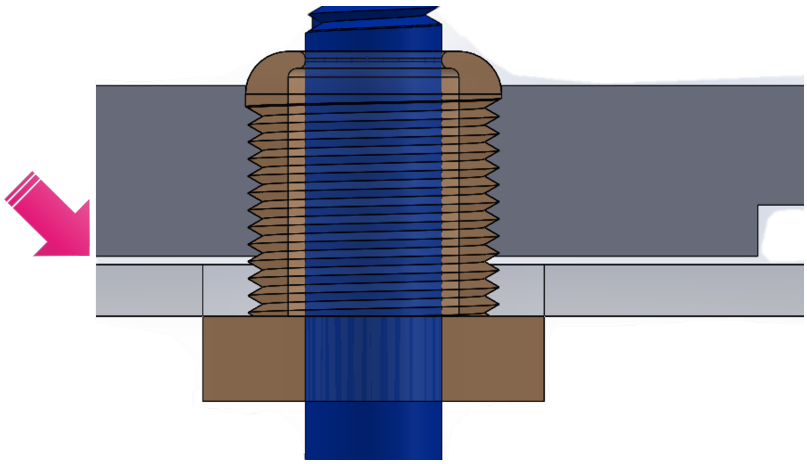

Figure 5.10: Section view of the motor axis

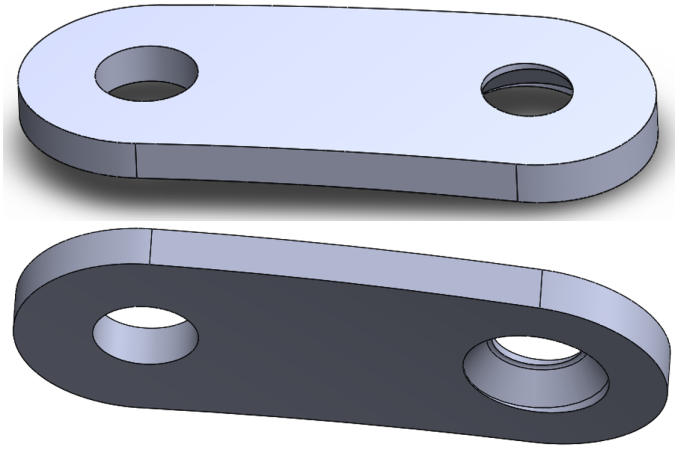

Figure 5.11: Curved fixation part

During the conference, it was mention to the company that, in order to adapt it to a variety of helicopter models, the parts involved needed to be projected specifically to that model, due to the different curvatures from each particular helicopter. It was mentioned by the AHD that there would be no problem since the entire WWS differs in every model, that would still be an improvement.

The new design was pretty much the same as the concept, except it was created along side the H130 model's surface, with a $7mm$ constant high. The spindle also had a base with the surface's curvature, in order to prevent its rotation, and $16mm$ diameter, matching the inside of the part that it would connect to.

Design problems

Despite the designed and planed, when this parts were to be assembled to the helicopter, it was noticed that motor's drive shaft and the shaft were separated by $1mm$ only. This meant that it would be impossible to have a bolt pushing the fixation part from inside the helicopter's surface without changing the drive shaft's geometry, as in Figure 5.13 . All this would involve the same certification requirements as to have any change in the surface of the aircraft, spe-

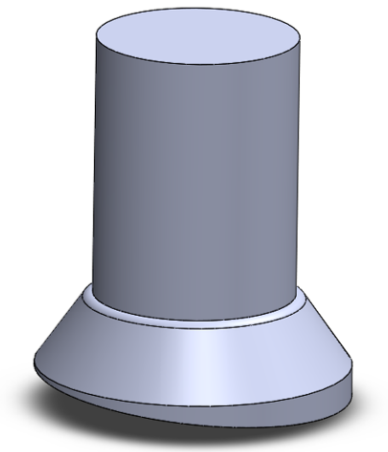

Figure 5.12: Spindle design for the second axis

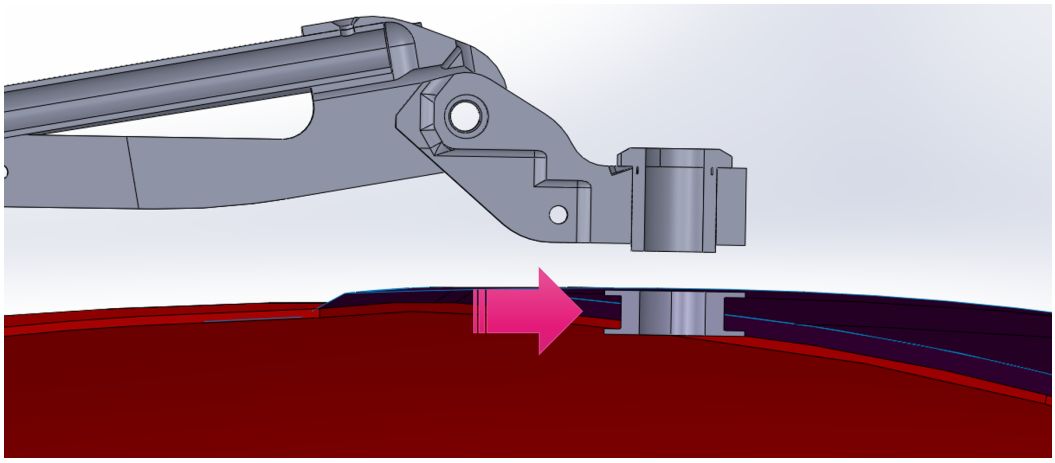

Figure 5.13: Section view of the motor drive shaft

cially since it would involve changes in the motor (that would even make the process more complicated).

5.2.3 One body design with four bolts

Since, to redesign the drive shaft would involve another project, which would also require new standards and specifications to be met and approved, consequently involving more costs, it was agreed upon with AHD that, as something needed to be changed, it would be more suitable to add bolts on the fixation part. This would be achieved by drilling the surface rather than changing parts on the interior in order to add a screw.

This way, the best approach was thought to be the piercing of the helicopter's surface. It was also said during the meeting that it was not necessary to have a separated body for the second axis, that it could all be one part, to be added four bolts to help with the fixation and stabilization of the second axis, being able to produce it all in one part.

Therefore three models with different locations of the threaded holes were shown in another web conference to AHD, as seen in Figure 5.14. It was then said that there was no need to fur-

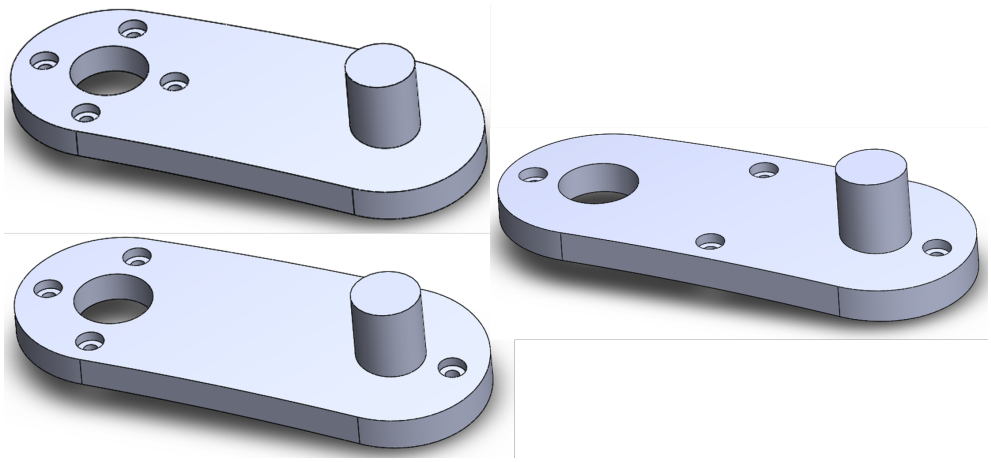

Figure 5.14: Three different bolted models

ther test the different models since the bolts should be spread out, in order to grant stabilization, thus the model on the right of Figure 5.14 should be the one chosen. Four M3 threaded holes were then made on the part, to allocate the bolts. The dimensions of the bolts were chosen based on what seemed to make sense, which is not important for the kinematic analysis but should be further verified if their use is fit for the purpose intended.

In order to simulate the fixation part it was first necessary to figure out the mechanical load that affects it. This would greatly depend on the forces transmitted by the action of the springs and also the contact between the blade and the surface.

Due to the fact that the WWS is a dynamic system, the forces affecting the part will fluctuate with time, so it was again necessary to use the Motion Analysis tool from SW in order to know when the reaction forces would be greater.

Motion Study

The limitations imposed by AHD were relative to the maximum torque that the motor would be able generate (62 $N \cdot m$ [15]) and this value depends directly on the friction force between the window and the blade. In its turn, the friction force depends on the contact force (normal to the surface) on the blade that is a consequence of the force produced by the springs' compression.

This means that in order to reproduce the real system faithfully, the force generated by the springs should keep the motor torque bellow 62 $N \cdot m$.

For the purpose of using the optimization tool in Design Study Add-In from SW, it was necessary to set up the Motion Study with sensors first.

An oscillating motor was created with the same characteristics as previously, a 48° displacement angle, $1Hz$ frequency and 0° phase shift, but this time a Result Plot was generated. The referred plot was to present the motor torque's magnitude, but also to create a sensor. This sensor was defined like seen in Figure 5.15, which meant that during the operation of the WWS a plot was to be generated and the maximum value of the torque was to be saved in order to be used in the optimization process.

After the motor was defined it was necessary to define the springs. Firstly the distance

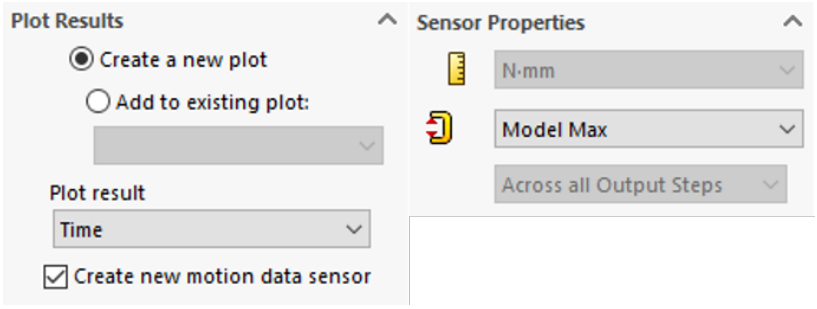

Figure 5.15: Creating a new plot and sensor

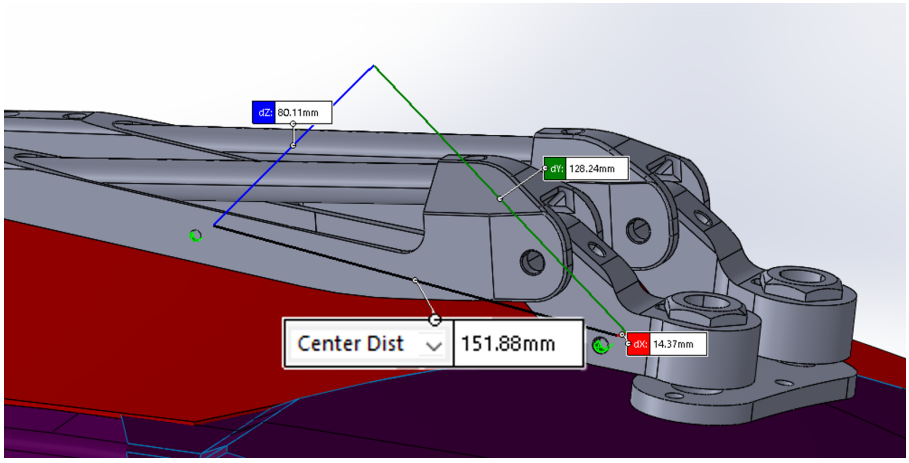

Figure 5.16: Spring measurement in the first contact

between the points of connection were to be measured, as seen in Figure 5.16, the first position, when the WWS was resting, the l_{sp} distance was $151.88mm$. It was also measured in the final position, at 48°, with the value of $148.62mm$ in the right arm (the one with the greater flexion). The chosen value for the free length of the spring was then $120mm$ (Figure 5.17) in order to ensure the contact and give a certain tightness trough out all the movement.

The most important parameter was the spring constant (k), that was to be used in the Design Study, in order to alternate the produced contact force. Since the value was to be optimized, it was not important to define it yet, so it was left the previous value, as the rest of the parameters were too.

All of the mentioned parameters were used in both springs, one in the bottom of each arm.

It was also added the gravitational acceleration effect in the Motion Analysis, as observed in Figure 5.18.

At that point it was only missing to define the solid body contact. As seen in Figure 5.19 two different groups were created in order to simplify the simulation. The first group was defined as the four small rotating arms and the second as the windshield body, as also shown in Figure 5.20. Back in Figure 5.19, it's possible to note that materials were added, both of them chosen from the small list of standard materials on this tool, as the most similar to the reality. In the Elastic Properties it was chosen Impact since the software uses automatically the properties (stiffness, exponent, etc.) relative to the chosen materials.

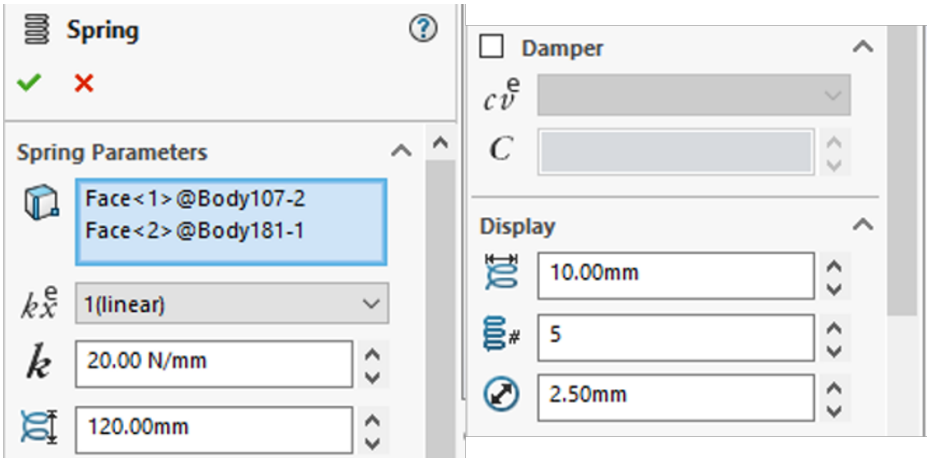

Figure 5.17: Spring parameters

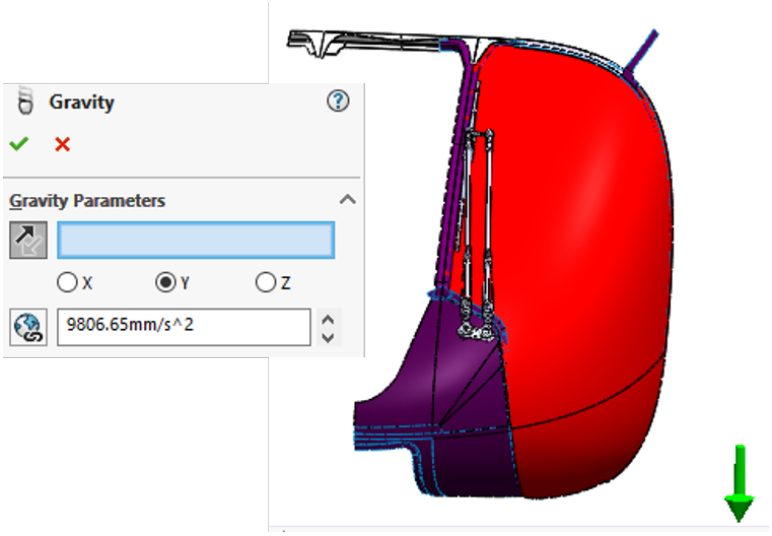

Figure 5.18: Gravity addition

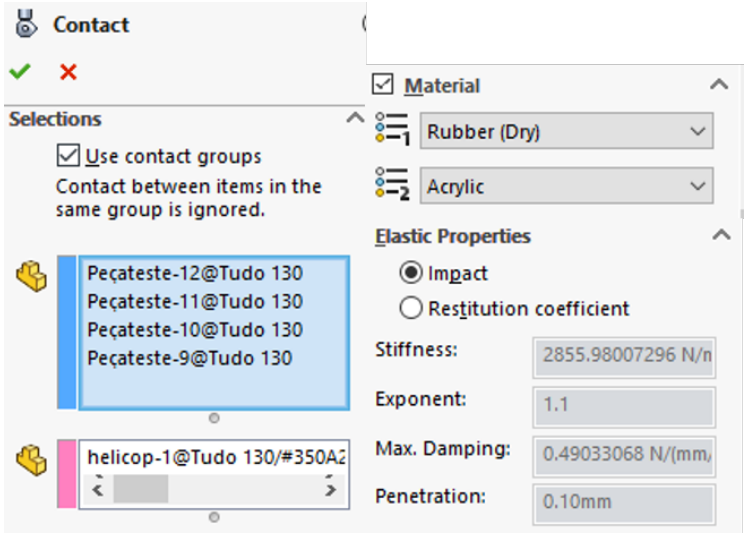

Figure 5.19: Contact parameters

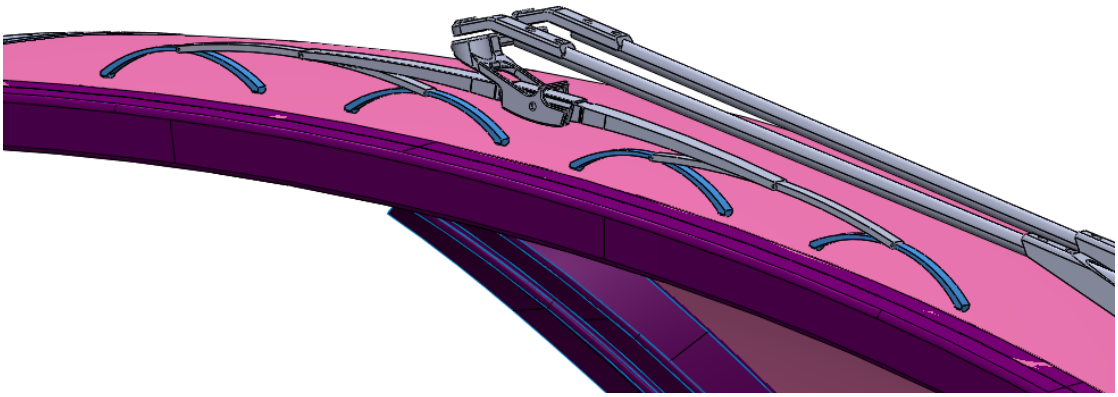

Figure 5.20: Contact groups

Design Study

Associated with the Motion Study in 5.2.3, a new Design Study was made considering the variables, as previously mentioned, the spring constants, being one per spring.

Step Firstly, before the optimization a $10N/mm$ step instead of a range was used, in order to understand between which values the k should be. This method was used since there was no idea of how big or small the values should be, and using the range between, e.g. $0N/mm$ and $100N/mm$, would take a lot of iterations, which meant a very long time to compute and calculate them all. The constrain was set as "is less than" the maximum of $62N \cdot m$ in the motor torque sensor and the goal as "is exactly" $62N \cdot m$. This may seem a redundancy but it made the value of the motor torque stay immediately below $62N \cdot m$ instead of slightly above, since the exact value was impossible to obtain by just resorting to the iteration process. The study was then run.

Range The k values from the previous study stayed between $60N/mm$ and $70N/mm$, so it was then proceeded to the range study with the same constrains and goals, but with the range of the spring constant between the referred values, as shown in the Figure 5.21 and the study was run. As seen in Figure 5.22, the optimal results were found to be between $65N/mm$ and $70N/mm$, in order to keep the the springs equal, the value was set as $66N/mm$

Optimized Motion Study

With the purpose of finding the resultant forces applied in the fixation part spindle a result plot was created from the concentric mate, producing a plot of the magnitude of the affecting forces. In addition to the magnitude plot shown in Figure 5.23, also three more result plots were created, each one with a reaction force component.

The four plots were created, as in Figure 5.24. In the last plot it was possible to observe and mark the time when the magnitude of the reaction force was greater (see the red line). The

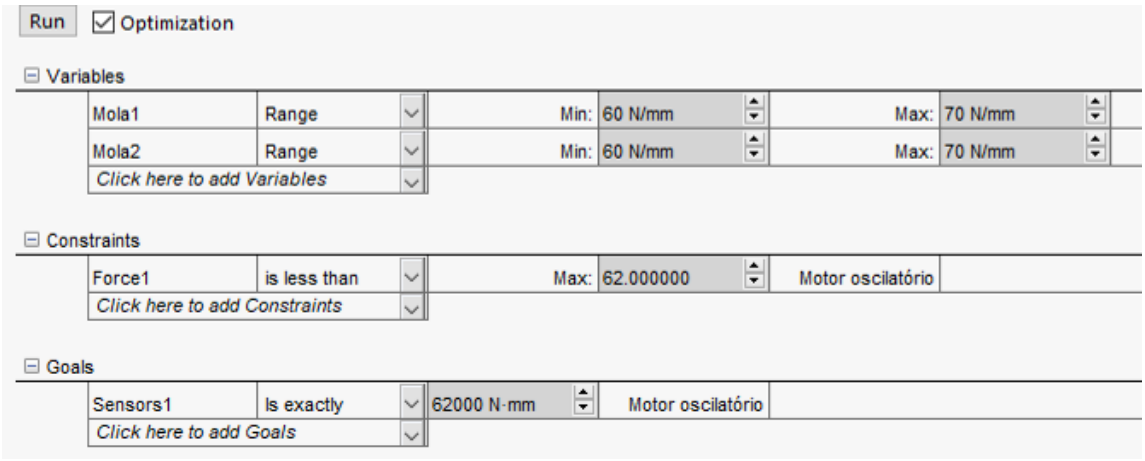

Figure 5.21: Variable view of the Design Study

		Current	Initial	Optimal	Iteration 1	Iteration 2	Iteration 3
Mola1		65.39238 N/mm	70 N/mm	65.39238 N/mm	70 N/mm	60 N/mm	70 N/mm
Mola2		69.99474 N/mm	70 N/mm	69.99474 N/mm	70 N/mm	70 N/mm	60 N/mm
Force1	< 62.000000	61.997501	63.870964	61.997501	63.870964	59.822666	59.214417
Sensors1	Is exactly 62	61.997501	63.870964	61.997501	63.870964	59.822666	59.214417

Iteration 4	Iteration 5	Iteration 6	Iteration 7	Iteration 8	Iteration 9
60 N/mm	70 N/mm	60 N/mm	65 N/mm	65 N/mm	65 N/mm
60 N/mm	65 N/mm	65 N/mm	70 N/mm	60 N/mm	65 N/mm
55.198921	61.560623	57.477581	61.841297	57.173374	59.518700
55.198921	61.560623	57.477581	61.841297	57.173374	59.518700

Figure 5.22: Optimization table results

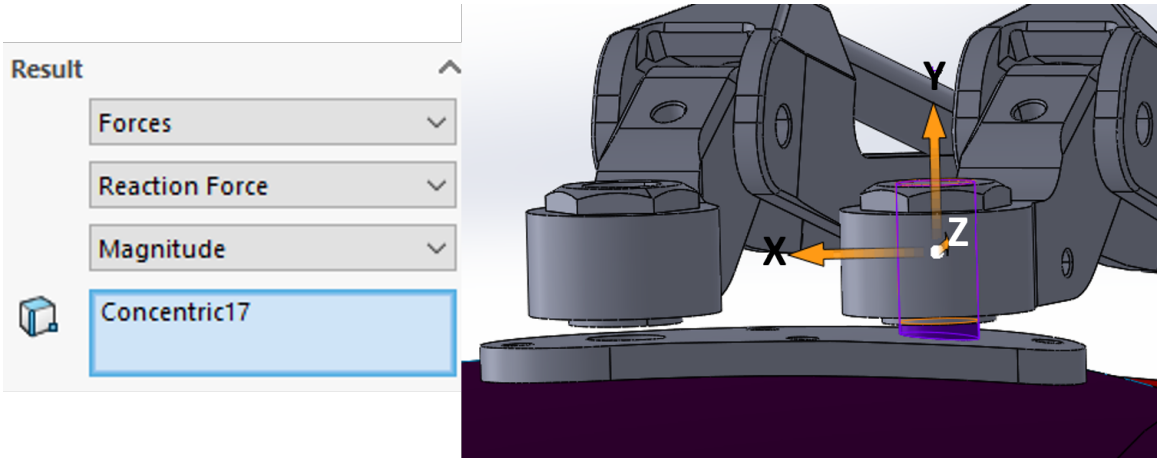

Figure 5.23: Reaction magnitude result plot creation

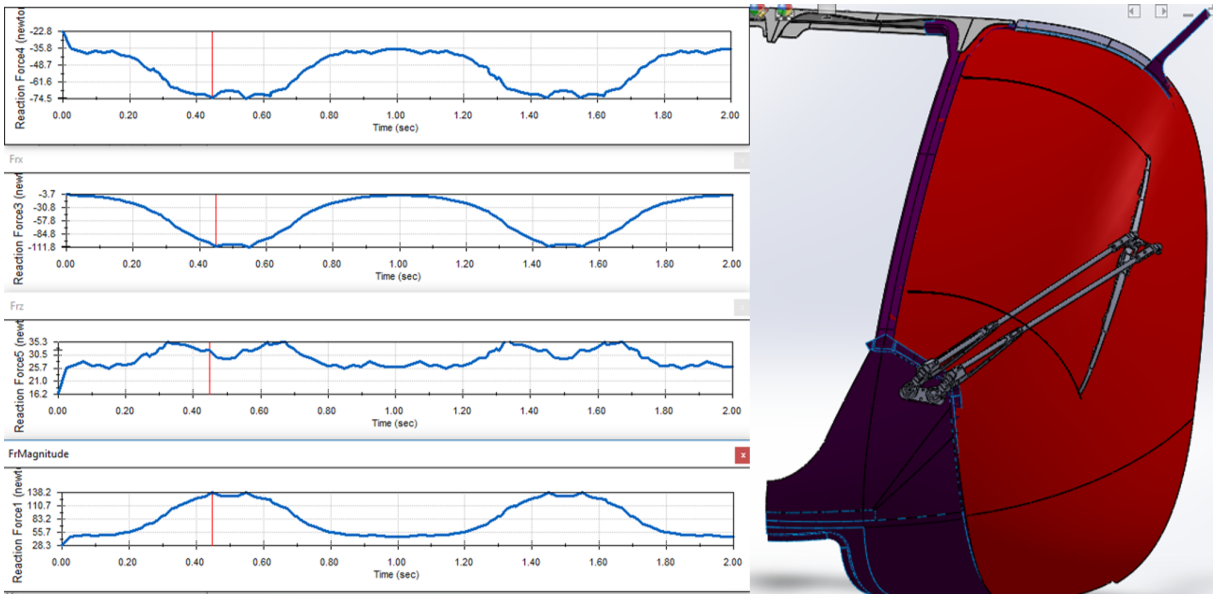

Figure 5.24: Force plot results and graphic representation of the WWS' position

Table 5.2: Maximum values of reaction forces from Figure 5.24

Magnitude	Rx	Ry	Rz
138.2N	-111.8N	-74.5N	32.2N

maximum value coincided with the final position of the blade, right when it started to go back to the starting position as it can be seen on the right of Figure 5.24.

After knowing when the magnitude was greater, the three component forces were to be recorded, from the plots above, to then be used in the fixation part's static simulation. The magnitude and the component values can be consulted in the Table 5.2.

Static Study

A static analysis was carried with the purpose of validating the fixation part with the static load obtained in the Motion Study.

Regarding the study's properties, the material used in this simulation was the 7075-T6 Aluminium Alloy (the mechanical properties can be seen in the annexes), which was indicated by the AHD as the standard aluminium alloy used by the aeronautical industry.

Using a FoS of 1.5 [3], the allowable stress for this material was given by

$$\frac{\sigma_{ys}}{FoS} > \sigma_{al} \Leftrightarrow \frac{505}{1.5} > \sigma_{al} \Leftrightarrow \sigma_{al} < 336.7MPa$$

This meant that at no time the maximum stress result on this part should surpass the value above.

The boundary conditions were then added to the part. The threaded cylindrical part of the four bolt holes were restrained on the three axis, as shown in Figure 5.25, simulating the bolts holding the part in place.

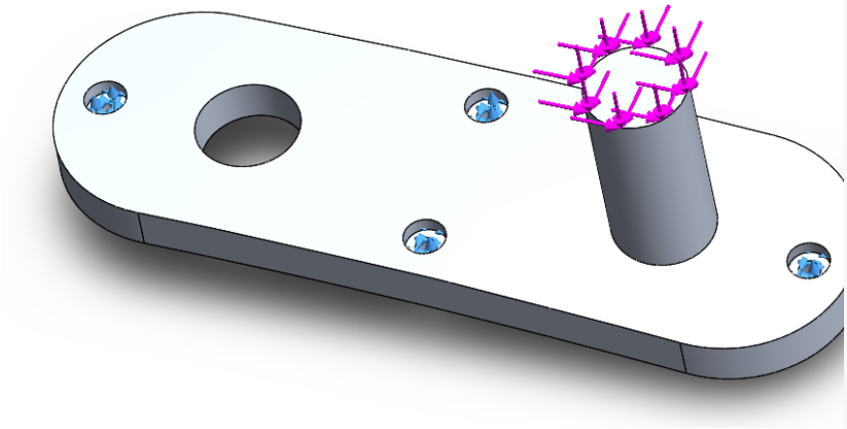

Figure 5.25: Simulation's properties

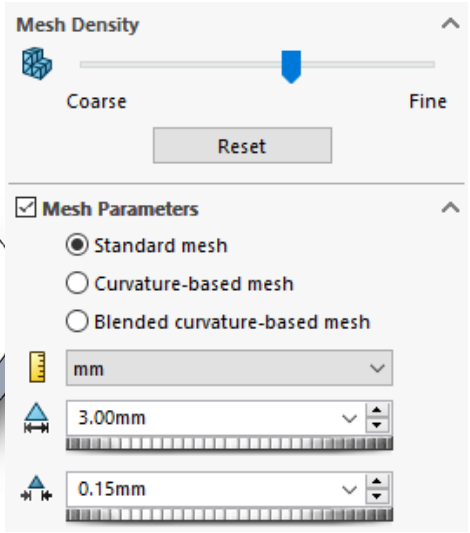

Figure 5.26: Mesh size

As also seen in Figure 5.25, three external loads were added. Each with the direction and value corresponding to the reaction forces observed in Table 5.2. Since it was not possible to locate these loads on a point inside the spindle, as the one where the reaction forces were located, as shown on the right of Figure 5.23, in the origin of the axis, it had to be set on top of the spindle's surface. This won't produce much different results, however it will engender a bigger torque, resulting in a greater mechanical stress, making this a more conservative approach. A mesh with the parameters as in Figure 5.26 was created and the study was run.

Bottom free The stress results presented were, as in Figure 5.27, using the von Mises yield criterion, with the goal of equating the equivalent stress across the part to be shown, particularly to find the location of the maximum value. The results shown are presented at the nodes and not in the elements, in coherence with Section 2.2.2

As shown in Figure 5.28 the referred maximum stress on the fixation part was in the bolt hole, the one located closest to the spindle, with a value of approximately 34 MPa, still very far from the 336.7 MPa of allowable stress (in about 10 times). The problem detected considering the mention results in this simulation was that the part was twisting to inside, in the direction of the helicopter's surface, what would be impossible to happen in the real life model, since there was a contact on the bottom.

Bottom restrained In order to correct the previously observed problem, the same model with a vertical restriction on the bottom of the fixation part, shown in Figure 5.29, was then simulated. No parameters were changed besides the added restriction. As seen in Figure 5.30, the maximum stress was then located in the back of the spindle. The rotation that previously should not exist in the side that promotes penetration, due to the existing surface contact, was corrected in this simulation, except that the opposite should be able to occur: the unscrewed portion of the bottom of the fixation part should be allowed to be lifted, what would relax the constrains resulting in smaller values of stress in the tension side of the spindle. It was

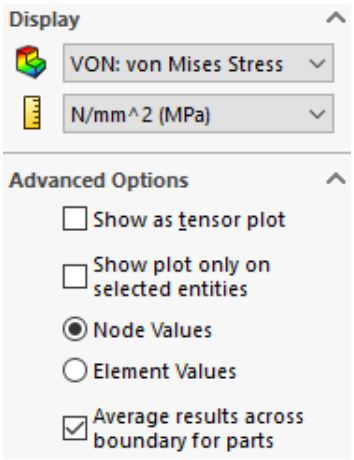

Figure 5.27: Stress plot definition

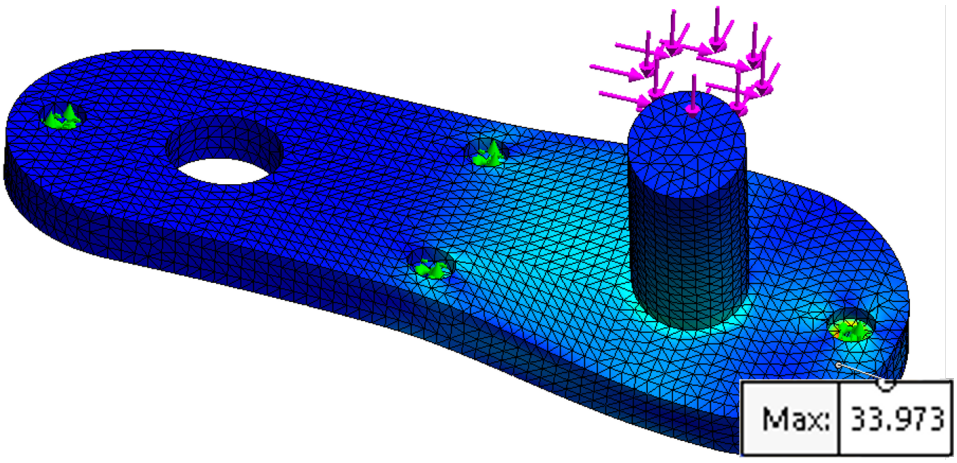

Figure 5.28: Stress results in MPa

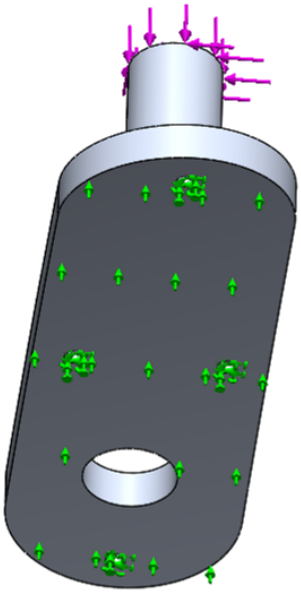

Figure 5.29: Bottom restrain addition

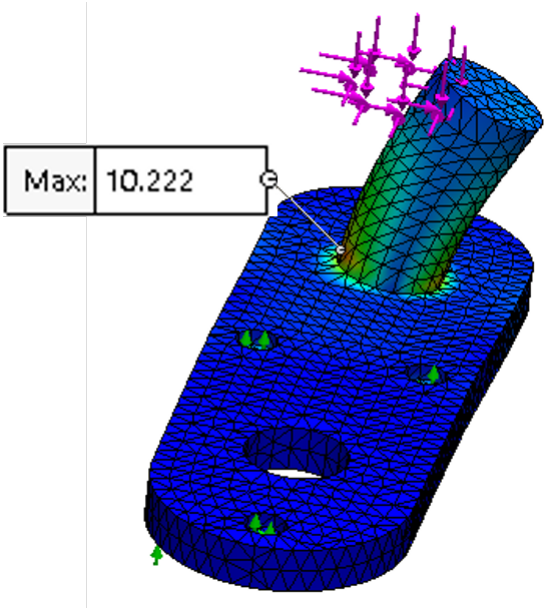

Figure 5.30: Bottom restrain stress results in MPa

also possible to change the maximum stress location from the threaded hole, that was under compression due to the free torsion of the part, to the bottom of spindle itself. This, however, was still not right since the stress should probably be located in the bottom of the spindle, but not on that side (since it should have lifted when loaded).

Multi-body Static Study

After the need of improving the model's similarity with reality, the solution was thought to be the addition of the helicopter's body to the study. This way the two bodies would not be able to penetrate each other, but on the other hand, it would make possible that the unattached sections to be separated from the surface.

As seen in Figure 5.31, the surface where the fixation part was to be connected to was included in the study. After a few attempts to run the study, it was inferred that too much computing processing power was required to mesh and calculate the contact interferences of the all body of the helicopter's front panel. Therefore, a few cutting operations were conducted, as shown in Figure 5.32, and only the needed portion of the panel was left out, with a very reduced thickness. This allowed a much quicker simulation run.

The components contact was defined as in Figure 5.33, allowing no penetration and with global contact, since there was only two bodies. Also no friction was added since there was no relative movement between the parts.

Relatively to the previous study, and since the helicopter's body was added to the this one, a fixture was added to the top and bottom surfaces, in order to prevent it from move even slightly when under the influence of the loads from the fixation part.

Regarding the previous study's parameters, nothing else was changed except for the fixation part's fixtures that went back to only the threaded sections of the four holes, remaining defined

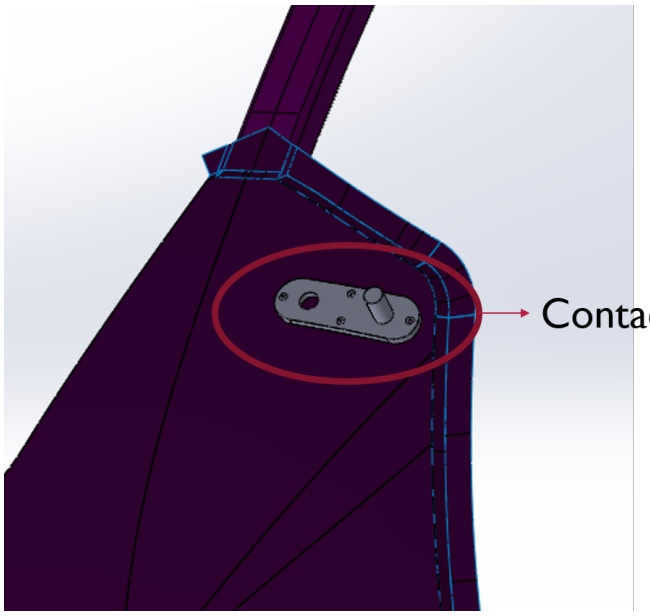

Figure 5.31: Contact location

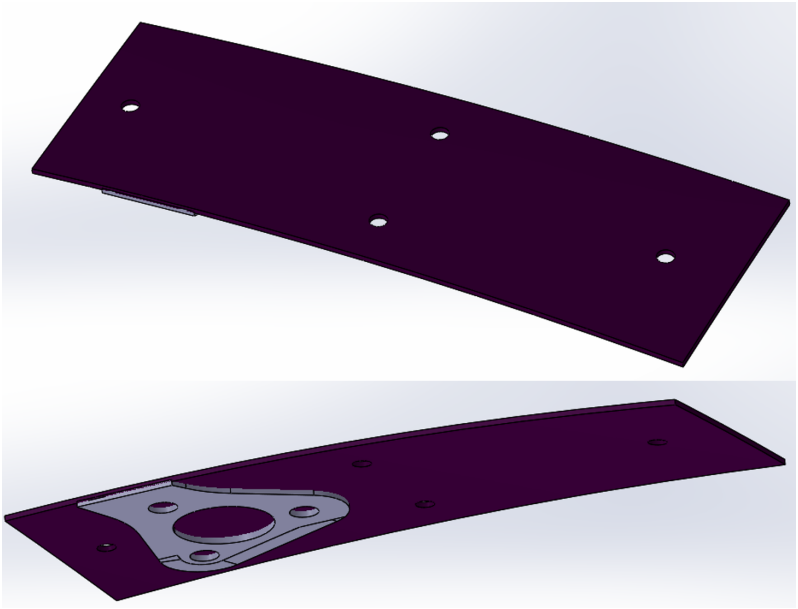

Figure 5.32: Surface thickness reduction

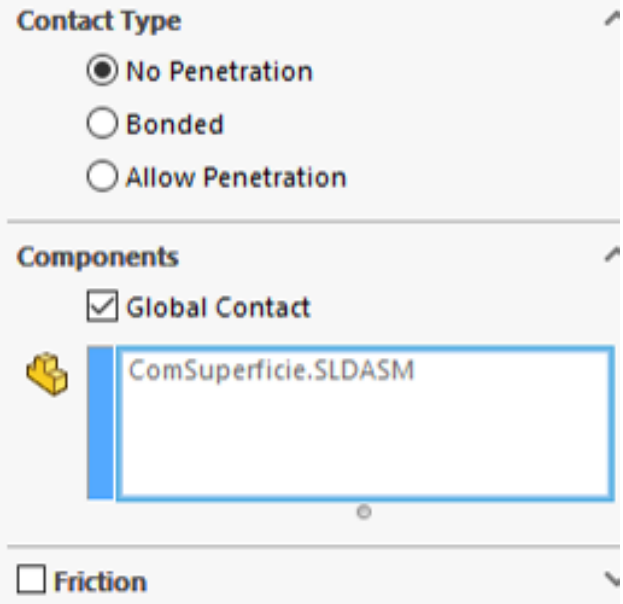

Figure 5.33: Contact parameters

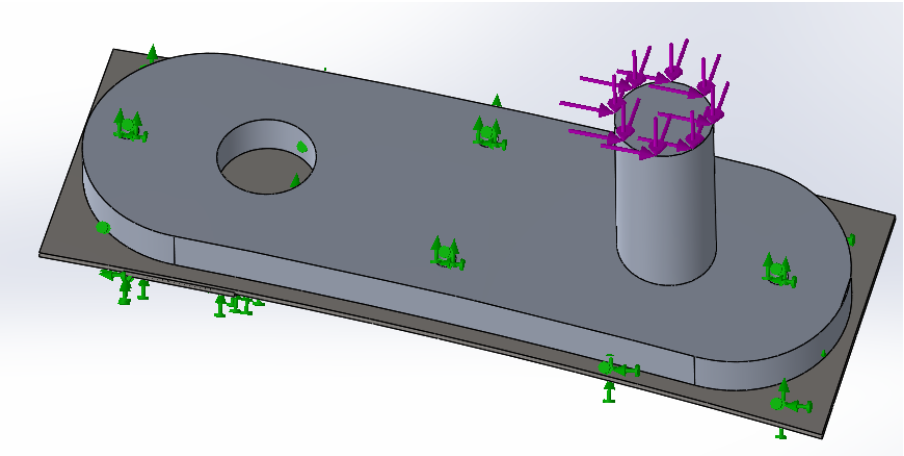

Figure 5.34: Defined multi-body static study

as shown in Figure 5.34.

Results Since, as previously mentioned, the yield criterion that was being used was the von Mises, the chosen FoS plot in this part was the correspondent one, as can be seen in Figure 5.35. In this study the displacement, as shown on the bottom right area of Figure 5.36, was more similar with what would be expected in a real life situation, since it can be noticed the section between the holes to be lifted up, but there was no penetration of the opposite side. The location of the maximum stress also became located in the compressed side of the spindle with the maximum value of 15.9 MPa, still very far from the allowable stress, which in Figure 5.37 can be noted the 31.8 FoS (relatively to the yield stress and not the allowable stress).

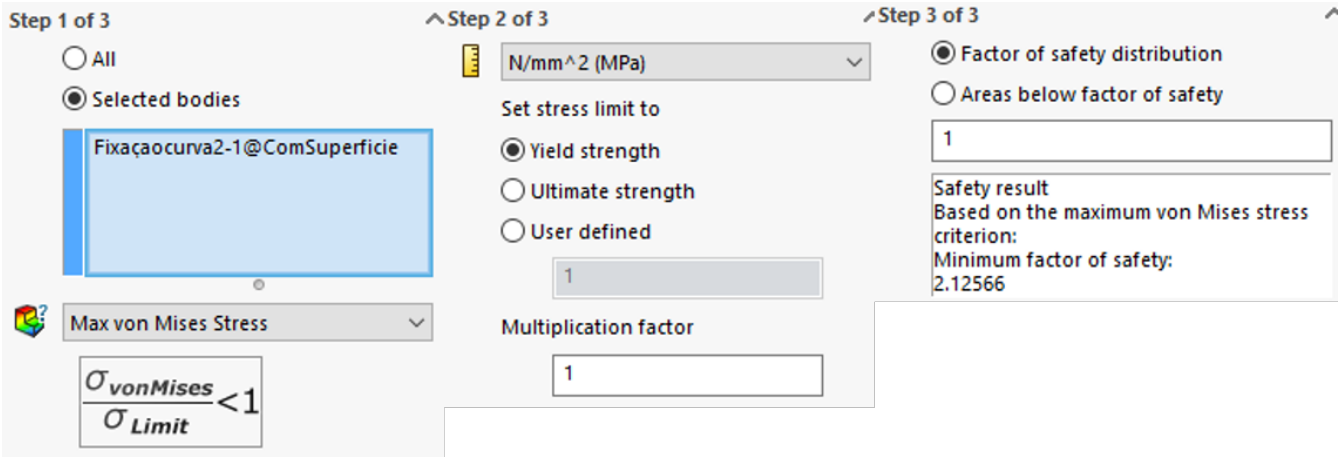

Figure 5.35: von Mises FoS definition

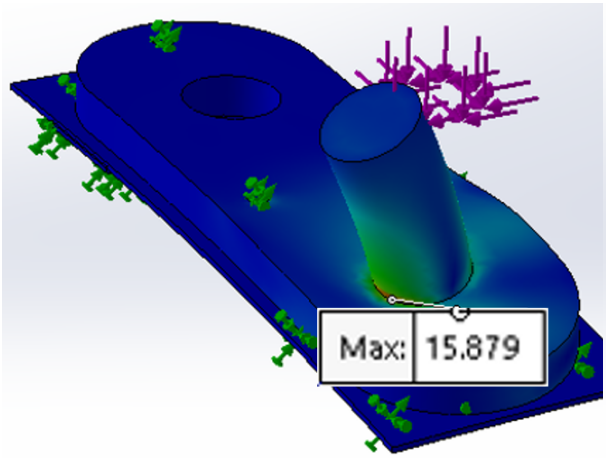

Figure 5.36: Multi-body stress results in MPa

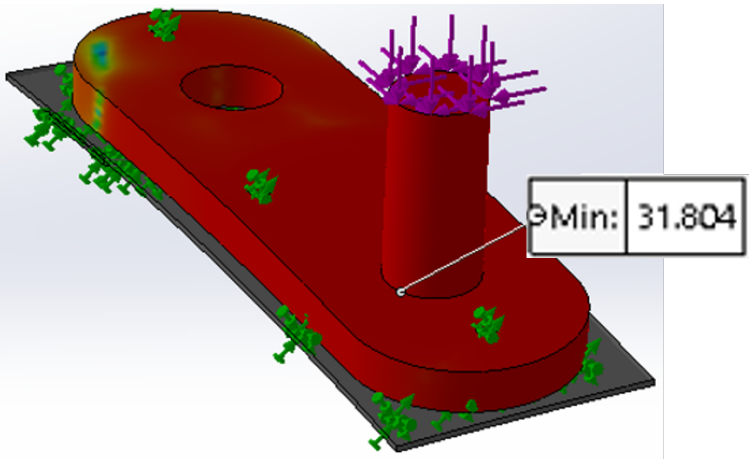

Figure 5.37: Multi-body FoS

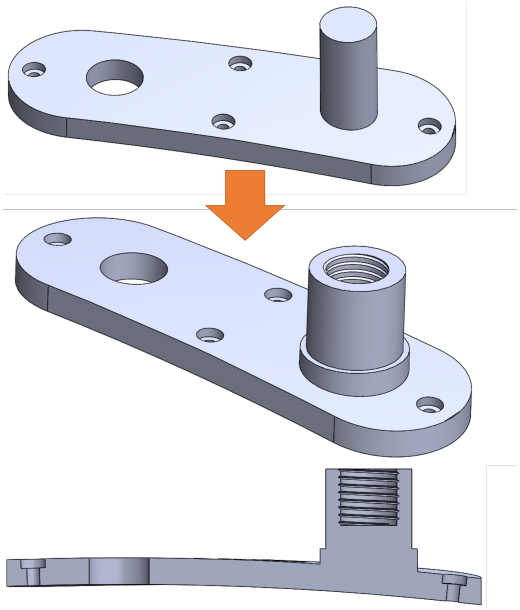

Figure 5.38: Model progress

5.3 Threaded pin design

Having the fixation part generally validated on stress wise, it was time to care for the spindle attachment to the arm, regarding the arm's rotation. Some web conferences where again held with AHD in order to figure out the mechanics behind the non-motored axis in the H135. Understanding how the coupling was created was important to keep as much as the original parts, and behaviour of the mechanism.

Surprisingly, it was mentioned in one of the conferences, that both the arms were connected to the motor. This was against the initial directions regarding this WWS model, which meant that further adaptations would have to be made, since in order to use only one motor axis, the second one could only be a "driver" axis.

The proposed way of adaptation suggested to AHD can be seen in Figure 5.38, which eliminated the bottom part of the arm seen with reduced transparency in Figure 5.39 (a big hollow screw that connected to the motor shaft). In the referred model the spindle had an threaded interior, in order to couple a screw that prevented vertical movement of the connected part of the arm, and an exterior that directly contacted this part, acting as a dry bearing.

It was also noted by the AHD engineers during the meeting that the value of maximum torque of the motor should never be used. The 62 $N \cdot m$ in the internal specification was a value extremely out of the range of regular functioning of the motor [15]. The values that should be taken into consideration were a normal functioning at 25 $N \cdot m$, with the possibility of reaching a maximum of 32 $N \cdot m$, but 62 $N \cdot m$ was meant for extremely exceptional cases only.

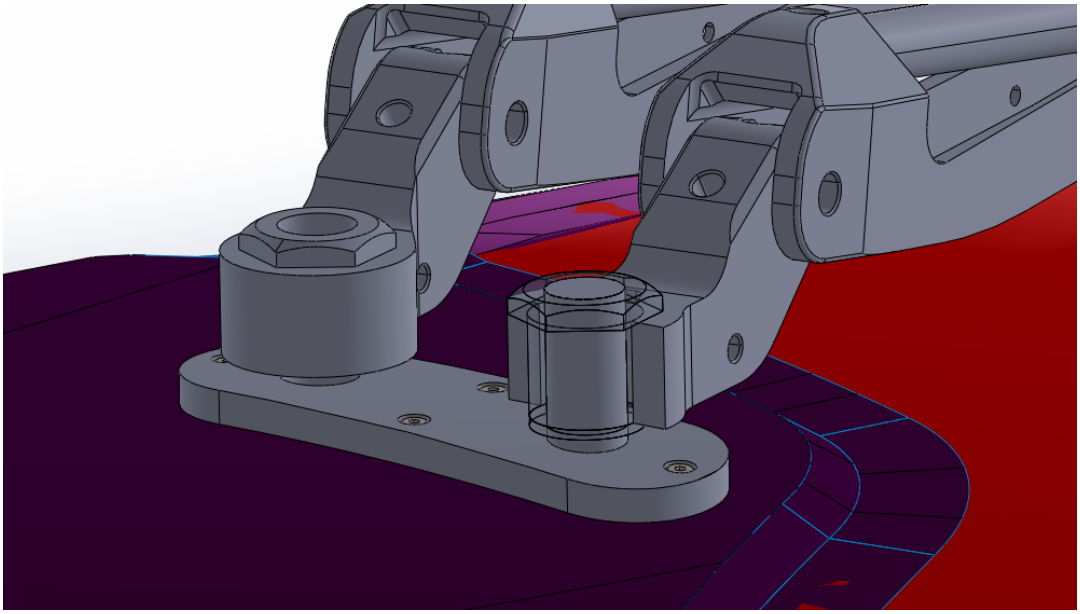

Figure 5.39: Previous model

		Current	Initial	Optimal	Iteration 1	Iteration 2
Mola2		24.5 N/mm	17 N/mm	24.5 N/mm	27 N/mm	22 N/mm
Mola1		27 N/mm	26 N/mm	27 N/mm	27 N/mm	27 N/mm
Force1	> 25.000000	25.236546	21.374420	25.236546	26.381227	24.113283
Sensors1	< 32.000000	25.236546	21.374420	25.236546	26.381227	24.113283
Force2	Is exactly 25	25.236546	21.374420	25.236546	26.381227	24.113283

Iteration 3	Iteration 4	Iteration 5	Iteration 6	Iteration 7	Iteration 8	Iteration 9
27 N/mm	22 N/mm	27 N/mm	22 N/mm	24.5 N/mm	24.5 N/mm	24.5 N/mm
20 N/mm	20 N/mm	23.5 N/mm	23.5 N/mm	27 N/mm	20 N/mm	23.5 N/mm
23.619429	21.312632	24.996635	22.712086	25.236546	22.463556	23.830423
23.619429	21.312632	24.996635	22.712086	25.236546	22.463556	23.830423
23.619429	21.312632	24.996635	22.712086	25.236546	22.463556	23.830423

Figure 5.40: Design Study results

5.3.1 Springs

Design Study

There was a need to redesign the springs since it was previously projected from the optimization in the Design Study, with the goals depending on what was thought to be the maximum value reached during the flight. As in the previous study, and shown in Figure 5.40, the springs variables were kept the same but the sensors were produced three times in order to have two constrains and one goal.

As it's possible to be noticed in the referred figure, the two constrains added were "is more than" 25 $N \cdot m$ and "is less than" 32 $N \cdot m$, in order to keep the optimization values between this range. A goal was also added as "is exactly" 25 $N \cdot m$, and the Design Study run.

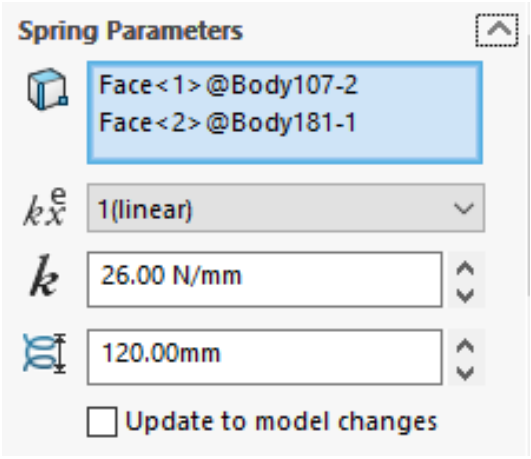

Figure 5.41: Springs parameters

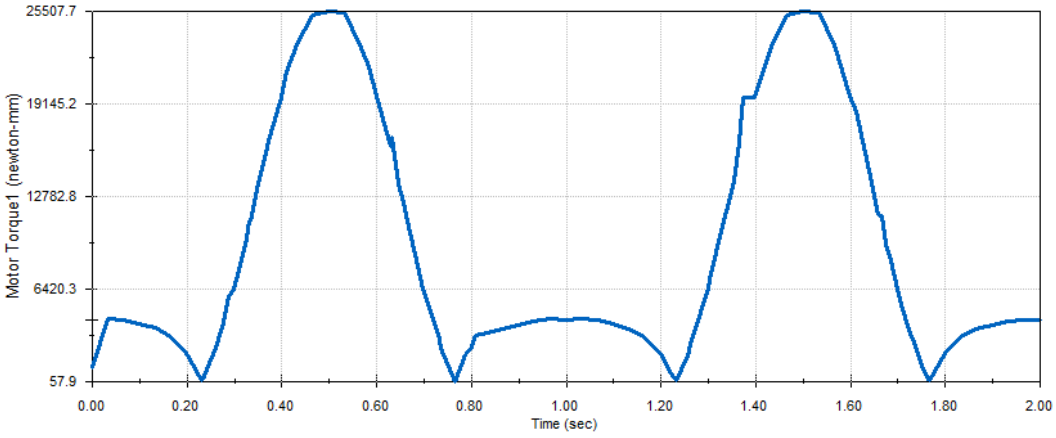

Figure 5.42: Motor torque plot during WWS' motion

Results The optimal values for the springs constant in the study were found to be between 24.5 N/mm and 27 N/mm, so the value selected for both the springs constant was 26 N/mm as in Figure 5.41. The model with the referred spring parameters was run and a motor torque plot created in order to check and validate its range. As seen in Figure 5.42 the maximum value of the motor torque was 25.5 $N \cdot m$, which was about the goal value and where it should work in normal conditions, but still far from the 32 $N \cdot m$ maximum torque. When the results were presented to AHD it was recognized as a good representation of the real system.

5.3.2 Motion Study

Again it was necessary to repeat the steps taken before, but the JAR specifications [4] were consulted, in which some particular loaded cases were directed. The mentioned cases to be considered were about relevant emergency landing conditions in six directions which were mentioned in Section 2.1.1 and are represented in Table 2.1. The application of the cases in the mentioned table, for this specific model, are illustrated in Figure 5.43.

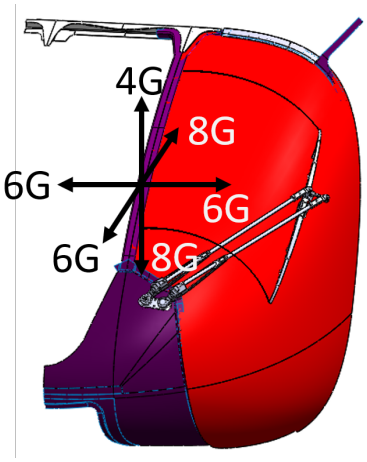

Figure 5.43: Load cases in emergency landing conditions

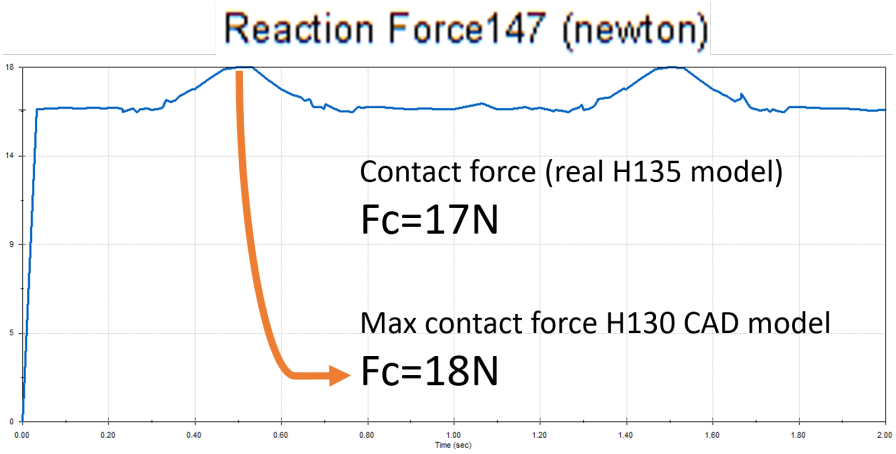

Figure 5.44: Contact force plot

Gravitational acceleration

It is worth mentioning that in the Motion Study with the regular gravitational acceleration, the contact force between the blade and the window was registered, the corresponding plot is shown in Figure 5.44. The measurement stated by AHD that was made experimentally by a dynamometer on this WWS, on the H135 helicopter model, was $17N$ wherein the simulation result was between $16N$ and $18N$, a 5.7% increase considering the maximum value, what showed that this computational model is equivalent to the real one with a great degree of trust.

Emergency cases

The load cases shown previously in Table 2.1 had to be taking into account in this study, which was a quick addition to the Motion Analysis configuration, since a gravitational acceleration downward was already in the recent previous studies. The only change that was necessary to be made was to adjust the direction of the acceleration to each case, and then multiply by the value required by the specification.

Six different simulations were then made wherein the results were reproduced in Table 5.3.

Table 5.3: Maximum values of motor torque and magnitude of the reaction force of the different simulations

					Lateral	
	Downward	Forward	Upward	Rearward	Left	Right
Max Torque ($N \cdot m$)	**35.5**	21.3	18.5	26.1	19.4	**28.8**
R Magnitude (N)	54.6	**69.5**	54.8	44.5	45.1	**65.6**

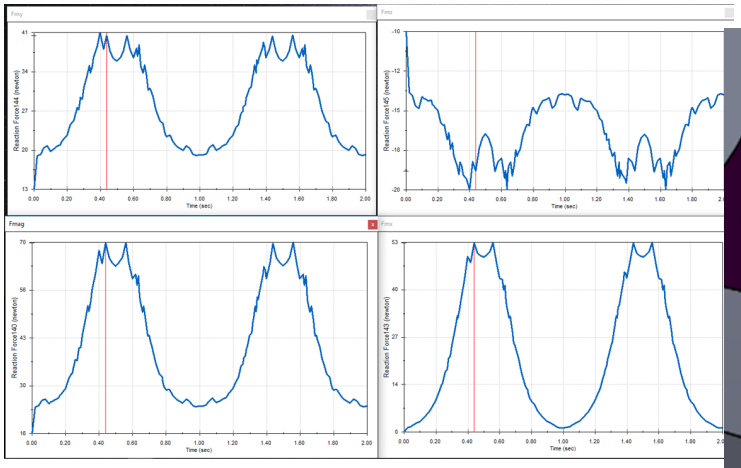

Figure 5.45: Reaction force magnitude and components plots

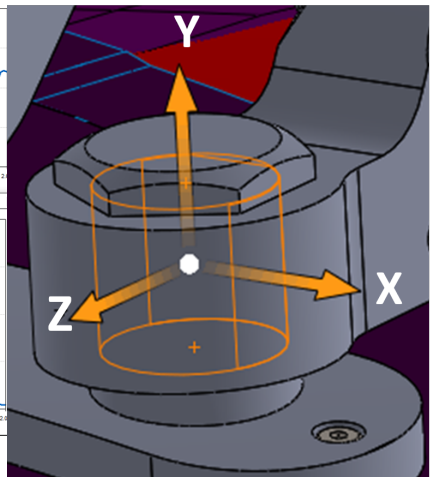

Figure 5.46: Reaction force referential

Observed in red are the maximum results, followed by the second greatest values in yellow.

It can be determined that the overall more demanding situation for the WWS was the lateral right load, which represented the second biggest values of both parameters, that conforms with the situation of a load against the movement of the blade, creating resistance on the motor and a bigger torque on the fixation part, this is, it could show less impact on the WWS' fixation part. The downward load was the most demanding situation for the motor, which is coherent with a bigger contact force and also a big load (8G), but would not necessarily transfer the biggest load to the fixation part. What would do that would be a load against the window, that would have to be compensated by the referred part, as it is in the forward load, with also 8G.

Taking into account the above mentioned, the maximum reaction force magnitude plot from the forward load case and the correspondent component forces plots were recorded, following the same procedure as before, as shown in Figure 5.45, with the referential of Figure 5.46. Their maximum values can be consulted in Table 5.4.

Table 5.4: Maximum values of reaction forces from Figure 5.24

Magnitude	Rx	Ry	Rz
69.5N	53N	41N	-19N

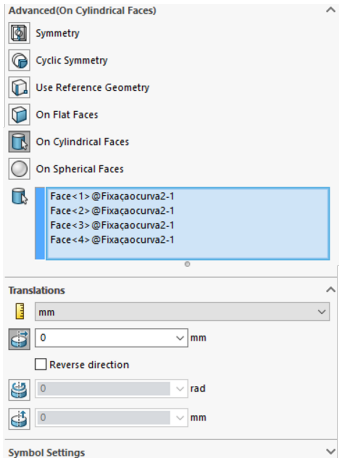

Figure 5.47: Cylindrical faces parameters

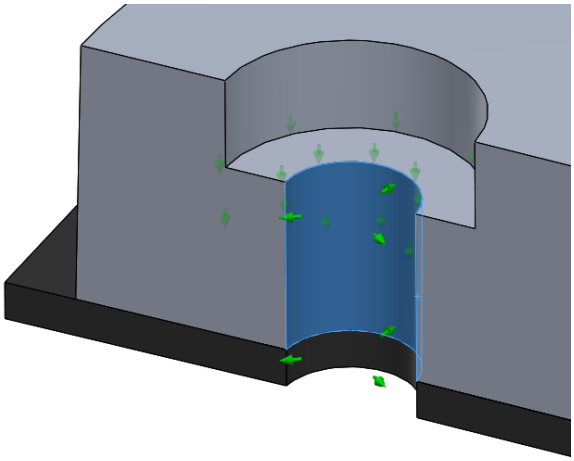

Figure 5.48: Cylindrical faces fixture

5.3.3 Static Study

In order to test this part for the maximum load previously obtained, a Static Study was conducted, as in Section 5.2.3. The material indicated for the part was the same as before, such as the contact type and mesh parameters used in the following study.

Bolts fixtures

Reviewing the model with the advisors, it was derived that the fixtures of the bolt holes could be changed to improve the model's similarity to a real life situation. Only the threaded cylindrical faces were made use of by fixing in all three directions, which was a more demanding fixture and consequently was increasing the stress values in that section, but, in order to replicate the real action of the bolts, the cylindrical faces and the top flat faces of the four holes were fixed in one direction only. This would restrict less the part's displacement in the bolt area.

As seen in Figures 5.47 and 5.48, the interior face of the hole was restricted in one direction only, normal to the axis using the cylindrical faces fixture, reproducing the screw tightening.

Also the top of the hole, where the bolt's head would rest was restricted, as in Figures 5.49 and 5.50, prevented the vertical displacement, normal to the face, using the flat faces fixture.

External loads

Following the results obtained on the Motion Study, and reproduced in Table 5.4, the three component forces were placed on the spindle of the referred part.

Since the current described model has two flat faces and the reaction force referential shown in Figure 5.46 is about between both of them, two cases of the same simulation were conducted. One with the load located in the top surface and one in the internal surface, as in Figure 5.51, in order to find the worst case scenario. Intuitively it would be the model with the load further

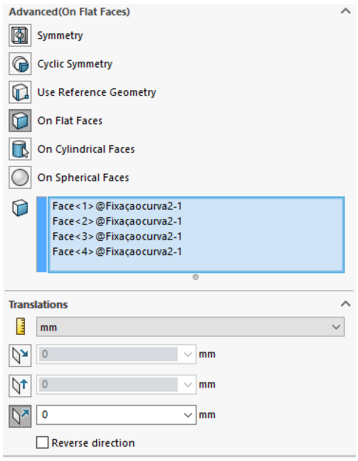

Figure 5.49: Flat faces parameters

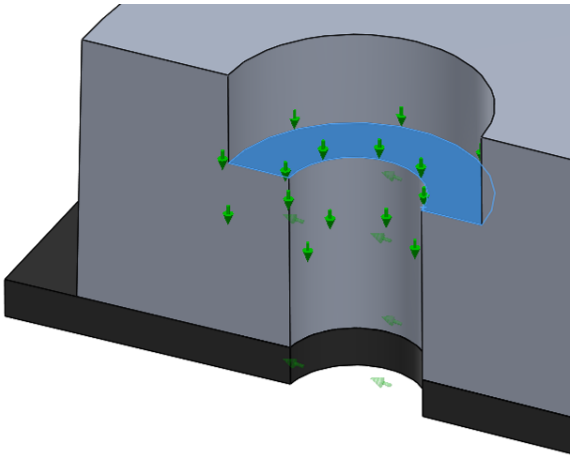

Figure 5.50: Flat face fixture

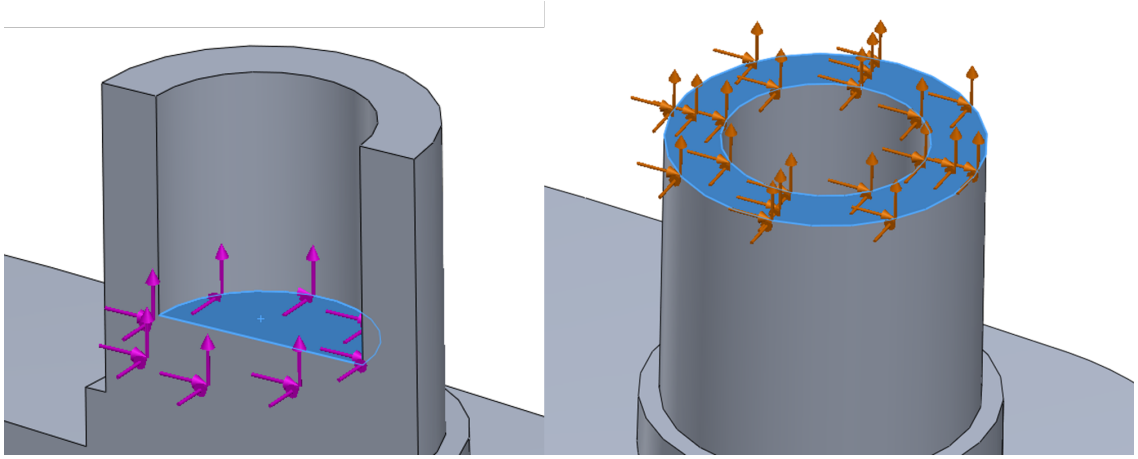

Figure 5.51: External load location

from the fixtures, but in any way both the situations were tested to insure that the intuition was correct.

Results The stress results of both studies can be seen in Figure 5.52. As predicted, the maximum value of stress was found on the model with the external load located higher due to the torque created. It can also be noted that, since the direction of the applied force is not the same, the part's displacement wasn't the same direction as the previous study, tilting this time to the upper right side. With this geometry the maximum stress wasn't verified on the spindle due to the increase of the outer diameter, which makes this section of the fixation part more prone to stand a bigger load without bending, but on the middle inferior bolt hole.

The maximum displacement value was also presented on the referred model, with the maximum value occurring on the top of the spindle, where the load was directed at. Shown in Figure 5.53, that value was 0.003 mm which was an extremely low value regarding the worst case scenario, justifying that way the minimum FoS value of approximately 74.3 in the hole, as in Figure 5.54.

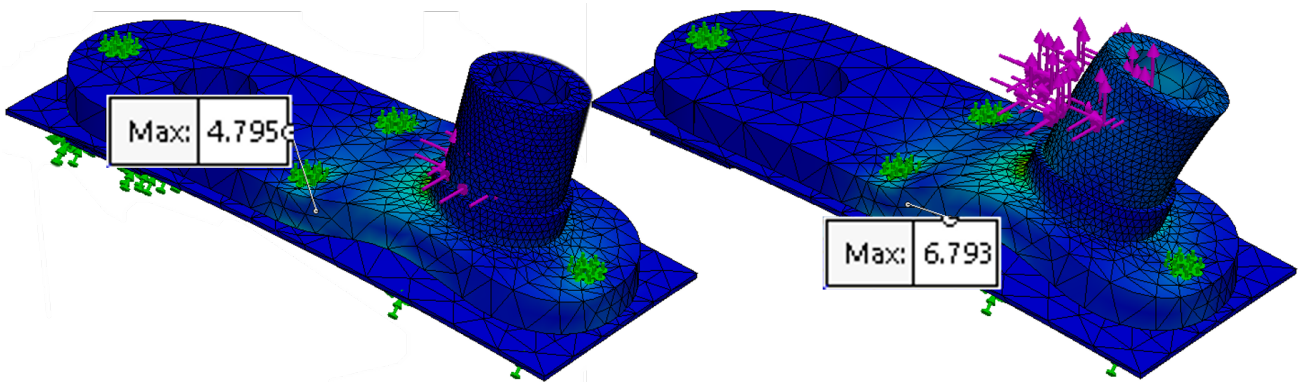

Figure 5.52: Stress comparison in MPa

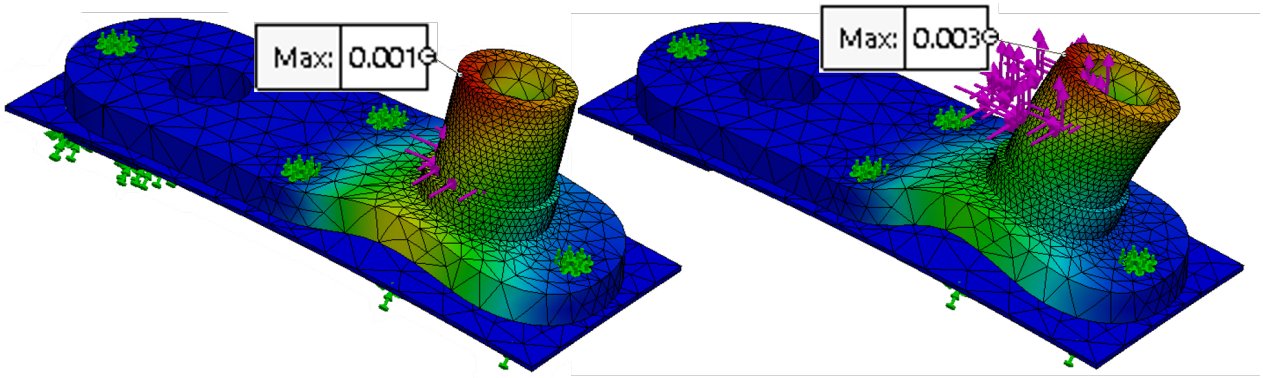

Figure 5.53: Displacement comparison in mm

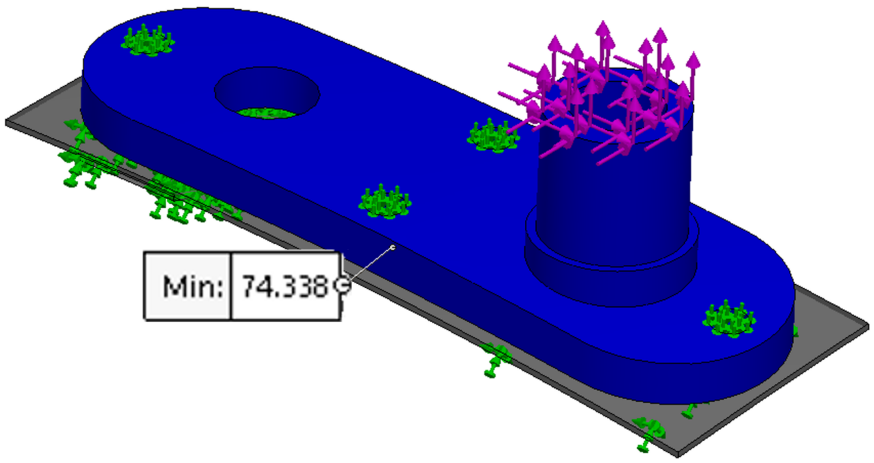

Figure 5.54: 7075-T6 Aluminium FoS

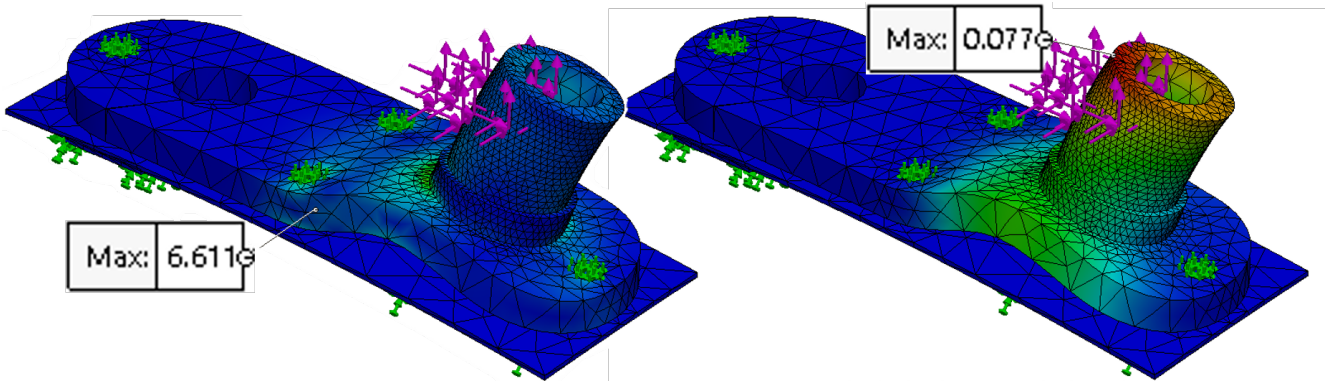

Figure 5.55: PVC Stress in MPa and Displacement in mm

PVC model

Since the results for the maximum stress and displacement were so low, it was thought that this part could be made in a cheaper material, such as a PVC polymer.

It was thought that this could be a good option regarding its low density and material cost, when compared with aluminium.

This material has an yield strength ten times lower than the 7075-T6 Aluminium Alloy previously used (50 MPa), which makes sense being a polymer, meaning that $\sigma_{al} < 33.3MPa$, still much higher than the maximum stress determined in the last simulation.

Static Study The same exact parameters were used as in 5.3.3 for this study, except for the material which was defined as a Rigid PVC with the mechanical properties in the Annex C, and the study was run.

Results The results seen in Figure 5.55 indicate a maximum stress result approximately the same as before, which made sense taking into account it doesn't depend on the material properties but on the part's geometry and load, and the displacement which grew by 185%, even though the value was still very low: less than 0.1 mm of maximum displacement.
Since the yield strength was lower this time, the FoS should also be lower, which was verified in Figure 5.56, with a minimum value of about 7.5 (10 times lower than the previous used material). A red area around the base of the spindle can also be noted which meant that the area between the holes in the middle and the spindle should have lower FoS due to a bigger mechanical stress demand, but never greater than 7.5. This was still a very large number, specially taking into account the 1.5 FoS recommended by the specification.

5.3.4 Fatigue

Understanding the fact that the WWS was a cyclical mechanism, the main concern after the static studies were done and validated, was with the fracture mechanics of the part due to fatigue.

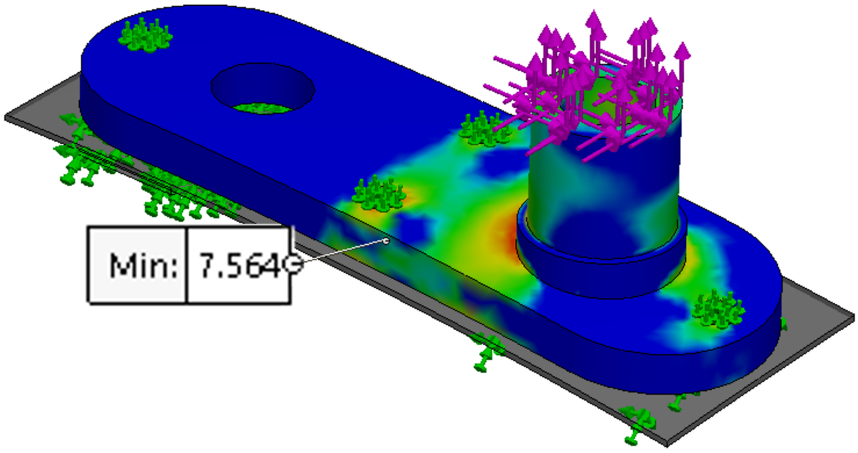

Figure 5.56: PVC FoS

Therefore, a fatigue study was conducted with the previous studied aluminium but also with two more. PVC was excluded from the fatigue study since it was a polymeric material, presenting plastic, meaning that the crack propagation and failure cannot be easily predicted. Consulting the SW materials database, the aluminium with the lowest price per kilo was chosen (Aluminium 518.0, die cast, F) and another was chosen considering the lowest density on the database (Aluminium 3105, wrought, H18). The mechanical properties of all the mentioned materials can be can be consulted in Annex C.

Static Studies

In order to proceed with the fatigue study, firstly, all the static studies had to be completed. Since the referred study had been carried out with the 7075-T6 Aluminium, it was only necessary to duplicate it twice and then change the material in each separate study without any further changes.

The results were, as expected, bellow those obtained with the 7075-T6 Aluminium, as these two other materials don't have such high mechanical characteristics as the 7075-T6. The maximum stress value was approximately the same as previously, since the stress doesn't depend on the material. It was, although, expected a slight variation since the values are so low, small difference between models might result in a discrepancy in the final figures. Also, in complex forms like these, the changes in the material's stiffness will, sometimes, result in a variation of the stress results.

As seen in Figure 5.57 and 5.58 the FoS minimum value has been reduced, both with the material cost and the weight cutback, but since the results obtained were above 20 it was very much above the minimum admissible (1.5).

Regarding the maximum displacement results, there was no changes with any of the three alloys, being $0.003mm$ in all cases. This was probably due to being a small value that such insignificant changes in the simulation will not have a big enough influence to be noticed.

Not much else could be concluded from the results of the static simulation since the only difference was the materials, everything else was kept unchanged. Hereupon, the fatigue studies

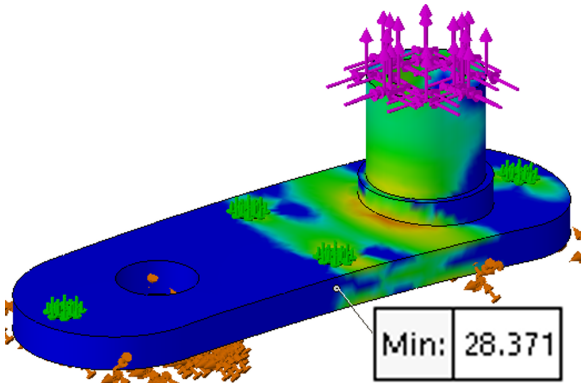

Figure 5.57: Minimum FoS in 3105 Aluminium

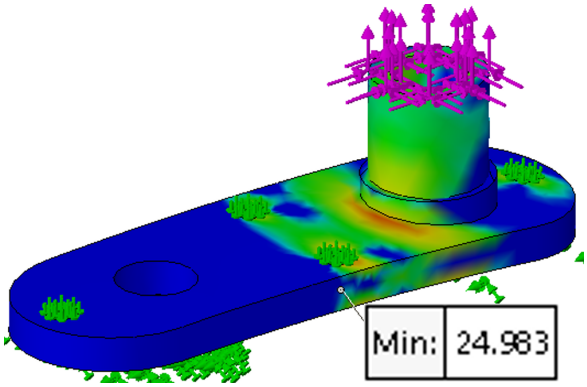

Figure 5.58: Minimum FoS in 518.0 Aluminium

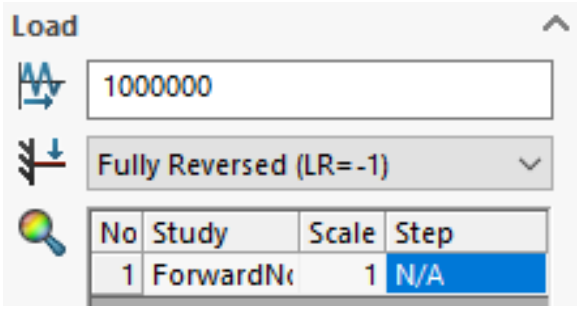

Figure 5.59: Adding constant event in Fatigue Study

had to be conducted to analyse it further.

Fatigue Studies

Three fatigue studies were created, each associated with one of the three static studies. An constant event was added, as shown in Figure 5.59, with a million cycles in order to ensure infinite life, fully reversed loading type, representing the eventual possibility of the wiping cycles applying an inverse force to the fixation part, and a scale of 1. There was no point of adding a greater value because in the fatigue study results there's a chance of generate a plot of Fatigue Load Factor (FLF).

The fatigue study options were considered as in Figure 5.60. Firstly, it was kept selected the Random interaction function, which was the more conservative by considering the sequence of events that result in the largest stress variation between them. In this case however, there's only one event so this is not an important option to consider. As previously was used, in this case again the von Mises equivalent stress was maintained to the detriment of the other options. The used method was Soderberg, again, for being the most conservative one, as stated in Section 2.4.3. The fatigue strength reduction factor (kf) was also not changed since it's intended for a multiplication of the alternating stress by a chosen value simulating a rough environment and, that way, reduce the number of cycles until failure. Finally, the infinite life was designate as a million cycles.

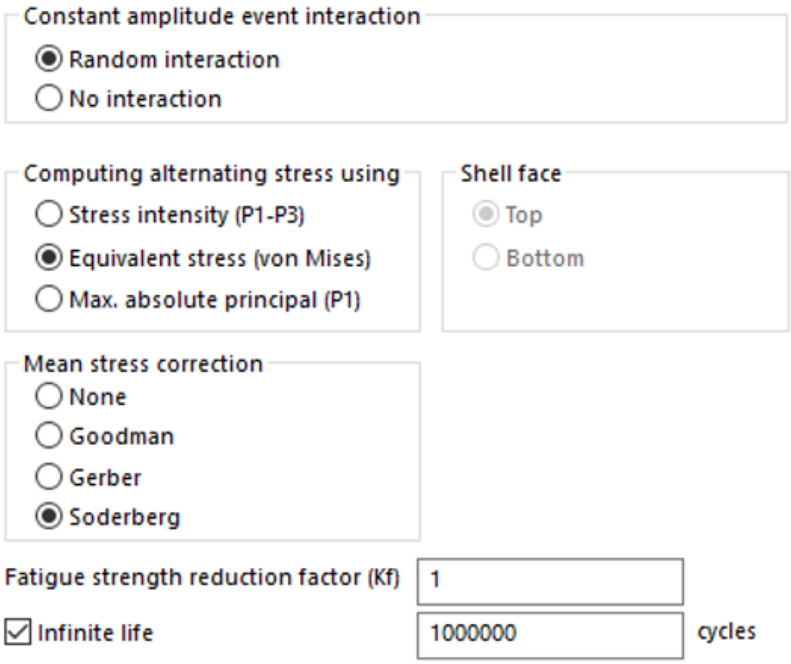

Figure 5.60: selection of fatigue study options

The S-N curves were updated independently to each of the material's mechanical properties from SW's fatigue database and the three studies were run.

Results

None of the models reached failure, which meant that by the millionth cycle the weakest area of the part still could carry out the same alternating stress until reaching failure, or the part could be subjected to a higher alternating tension to reach failure by the millionth cycle.

In order to learn quantitatively how much more of a load the fixation part could endure for the same number of cycles, a FLF plot was made in every study and a comparison table was built. As expected, both FLF values of the newly used materials shown in Figure 5.62 and 5.63 were inferior to those of the 7075-T6 Aluminium seen in Figure 5.61.

When looking at the fatigue limit stress column, in Table 5.5, the reason for the obtained results can easily be determined. Unlike in the yield stress field, where the 518.0 Aluminium had the lowest value, in the fatigue limit was the 3105 that had the lowest. This meant that the 518.0 should in principle have a better behaviour at fatigue than the 3105 Aluminium, when compared to the static behaviour. The 3105's FLF result, was 7.7 and, while being the lowest of the three, was still an high value.

The other two plots (damage and total life) didn't had much purpose on being analysed because, since the part didn't reach failure, there was no gradient or any variation along the part's plot, as shown in Figure 5.64, and the minimum σ_{fl} value was 1 million in every area on all the studies, precisely for the mentioned reason (infinite life).

Using the Iso Clipping tool, as shown in Figure 5.65, it was possible to identify the area where the problems due to fatigue where to happen. In the bottom of the previously identified

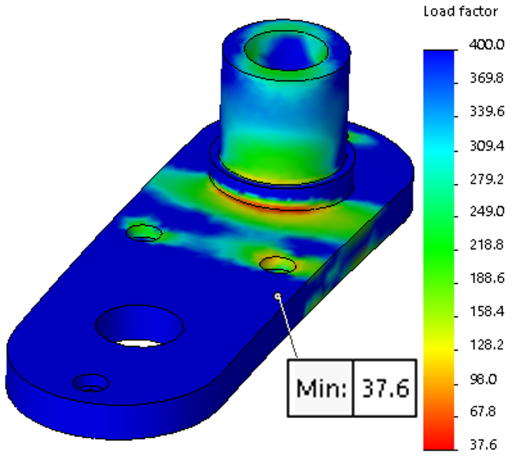

Figure 5.61: 7075-T6 Aluminium FLF

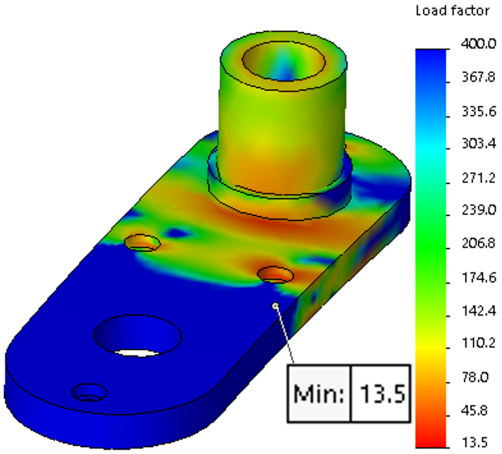

Figure 5.62: 518.0 Aluminium FLF

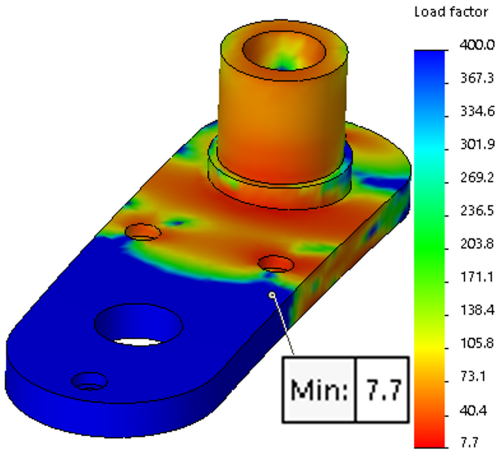

Figure 5.63: 3105 Aluminium FLF

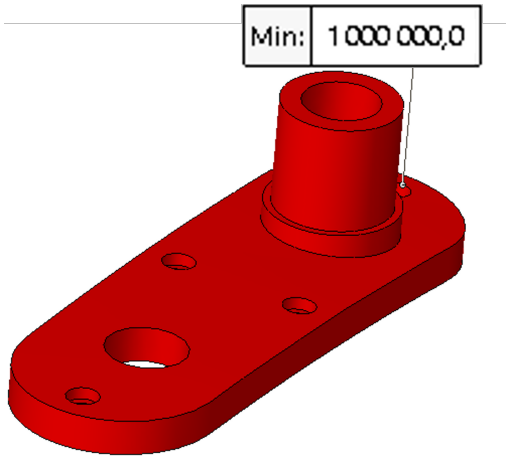

Figure 5.64: Total life in cycles

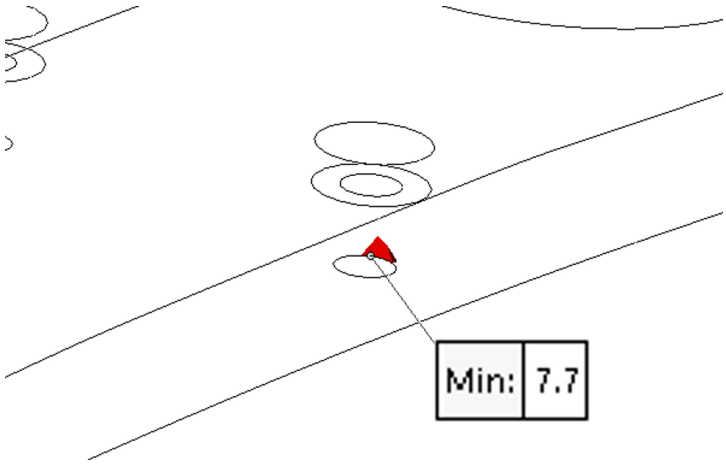

Figure 5.65: 3105 Aluminium Iso Clipping with FLF bellow 10

Table 5.5: Material properties comparison

Aluminium	€/kg	Density (kg/m^3)	Material cost (€)	σ_{ys} (MPa)	σ_{fl} (MPa)	Part's weight (g)	FoS	FLF
518.0	2.04	**2515**	1.62	**177**	96	**100.75**	**24.98**	13.5
3105	**1.865**	2700	**1.59**	185	**60**	108.17	28.37	**7.7**
7075-T6	**2.07**	**2800**	**1.83**	**505**	**255**	**112.17**	**74.3**	**37.6**

as the potentially more problematic hole, there could be found a small area in red where the FLF values were between 7.7 and 10. In the rest of the fixation part there was no other element where its values were in the mentioned range, which means that the load factor was always greater than 10, except for that very specific region.

This was very likely due to the constrains that were applied directly in the hole, which meant that, even acknowledging that the minimum FLF value was low, in real life the part should have an even better fatigue behaviour.

Besides the mentioned mechanical properties and studies results in Table 5.5 analysed above, and since the chosen materials respected a cost and weight criterion, the cost of the material by volume was calculated such as the part's total weight.

The cost per kilogram was an information already provided in the SW software, in the Financial Impact table, in custom tab of the material's properties. The material cost only considers the total raw material needed to produce the part, and not any other factor such as machining operations or the additional need for a certification of a new material that's not usually used by the company, which would have to be bought in a smaller quantity than a material used regularly, being already certified. This meant that, even though the price per kilo of a certain chosen material was eventually below the more expensive one, the final cost of making the part could be superior than using a more expensive one. Yet, just in order to compare them, it was an useful analysis since the machining operations with any of the chosen Aluminiums would be the same.

The part's volume was 40.06cm^3 (consulting the mass properties of the part on SW), con-

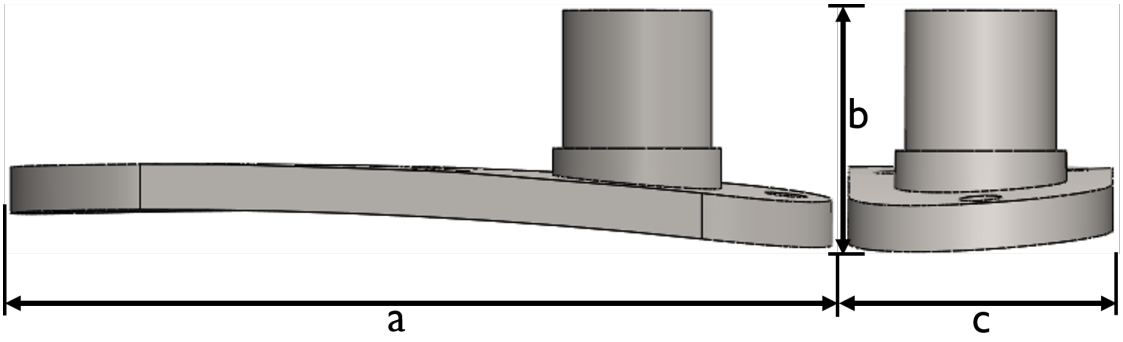

Figure 5.66: Part's measures

sidering a material block of $315cm^3$ obtained from the measures represented in Figure 5.66 by a·b·c with some allowances. The block's volume was taken into consideration to calculate the total cost and the part's volume to estimate its weight.

In Table 5.5, when comparing the material cost it's possible to notice that the biggest difference is between the most expensive Aluminium (in red) and the one with the value in the middle (in black), by 21 cents per part. At first this is maybe a small difference but if enough parts are to be produced, it might have a big impact in the final cost.

The next variable to be taken into consideration was the weight. Any weight reduction in the helicopter is welcome, and, in this case only 4 grams were spared between the heaviest and the second heaviest model, but the lightest one, presented in the table in green, with about 100 grams, saves almost 12 grams from the Aluminium used previously.

The lightest, the 518.0 Aluminium, however, had the lowest FoS which represents the worst performance at a static level but it was not a worrying result since it was 16.5 times higher than the minimum needed. Nevertheless, this Aluminium, when subjected to the fatigue study it presented a better FLF than the 3105. Taking into account that the cost reduction between the two referred materials is only 3 cents per part, but the weight could be cut in more than 7 grams, leading to the decision of the best Aluminium to be used in this part being the 518.0.

Chapter 6

Connectors and Torque Effect

6.1 Bolts verification

Up to this point the used bolt connections presented on the fixation part were M3 chosen by convenience in geometric terms, which also needed to undergo a verification under the stress that they were subjected to.

Following the calculations in Appendix B, it was found that for the M3 nonpermanent connections, it could be used class 4.8 or 9.8 bolts (table 8-11) [10].

It was chosen the 4.8 class bolt, with the applied 1169.5N, as shown in Figure 6.1, pre load stress (Fi) since the cyclical forces affecting to the fixation part are too low, that value should be enough for the part not to loose the bolts. In the following simulations, if it is found that the pre load stress is not enough to keep the part in place, the 9.8 bolt with 2452.1N pre load stress should be used instead.

Every bolt was placed choosing the upper and the lower circular edges as in Figure 6.2 repeating the same described process, with the standard parameters except the pre load stress which was changed to the calculated values, as mentioned before.

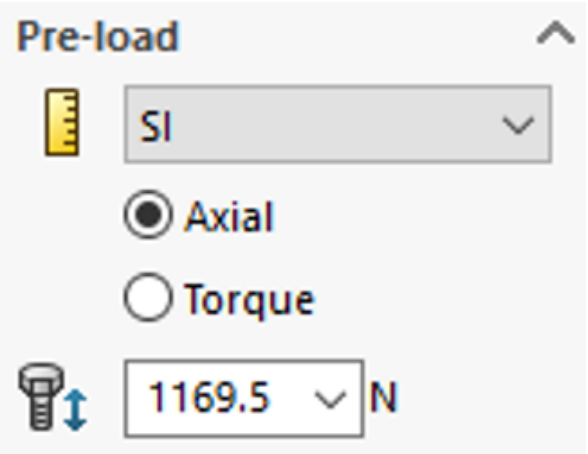

Figure 6.1: Bolts pre load parameters

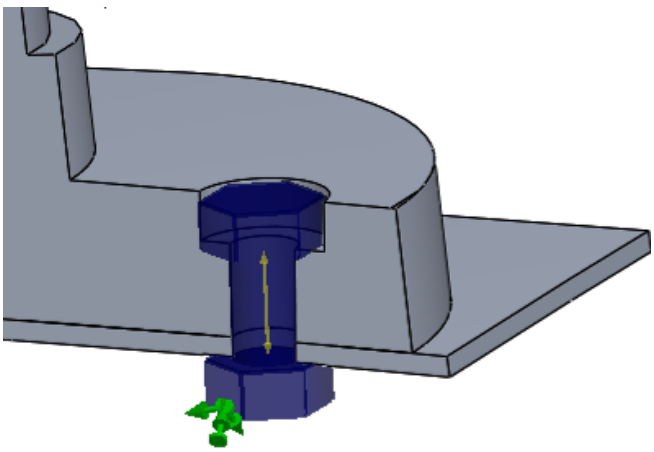

Figure 6.2: Section view of one bolt placement

Table 6.1: Mechanical properties for dry bearings and bearings with imperfect contact [16]

Material	Max Stress (MPa)	Max Temperature ($°C$)	Max Velocity (m/s)	Max $P \cdot v$ ($kPa \cdot m/s$)
PTFE (Teflon)	3.5	260	0.5	35

6.2 Dry bearing

At this point, with the kinematic and motion analysis between fixation part and the WWS already simulated, it was possible to check the parameters necessary do validate the contact type between them. Since the spindle is already sized and adjusted to couple the bottom part of the arm it was necessary to validate it.

It was firstly considered a contact with lubricating grease to be the ideal solution to minimize the friction between both faces. After a meeting with AHD it was indicated that a dry bearing solution should be pursued in order to reduce the need for maintenance, such as a Polytetrafluoroethylene (PTFE) tape/coating.

Therefore a verification of a dry bearing made of PTFE was conducted in order to understand if it could withstand the loading that it was subjected to by the action of the WWS and the environment. If a tape/coating was to be used, the real mechanical properties of the spindle would refer to the aluminium, which would have better mechanical strength than an PTFE spindle. This meant that if a PTFE dry bearing was found to pass all mechanical verification, the tape/coating solution should have an even better mechanical behaviour. All intermediate calculations are specified in the Appendix A

6.2.1 Velocity verification

The Table 6.1, regarding the mechanical properties of PTFE dry bearings, was consulted in order to know, firstly, the maximum velocity possible to operate that type of bearings. After checking the maximum functioning value allowed, it was necessary to calculate the service velocity, determined from the product of the angular velocity with the radius and cycles per minute as in Equation 6.1.

$$v_s < v_{max} \Leftrightarrow \frac{2 \cdot \pi \cdot n \cdot r}{60} < v_{max} \tag{6.1}$$

6.2.2 Stress verification

The same process was carried for the stress, taking into account the previously calculated forces that affect the spindle laterally, the Fx and Fz radial forces and the projected area of it. The service stress was then calculated and had to be lower than the maximum allowed stress seen in Table 6.1 in order to pass the verification.

$$\sigma_s < \sigma_{max} \Leftrightarrow \frac{F}{A} < \sigma_{max} \tag{6.2}$$

6.2.3 Temperature verification

Lastly, the spindle was checked for temperature. The calculations were made in two steps, firstly the specific heat for the worst case scenario was determined using the values from Table 6.1 and the minimum mixed-film friction coefficient (fm=0.02), in order to solve the service temperature equation which was the second step. The ambient temperature generally used in bearing verifications is $25°C$ but in the current case, and because the helicopters are sometimes used in more extreme situations, the ambient temperature considered was $100°C$. Also, the PTFE friction coefficient of 0.04 and the pressure and velocity previously determined were used to calculate the service temperature.

$$T_s < T_{max} \Leftrightarrow T_a + \frac{f \cdot P \cdot v}{ce} < T_{max} \tag{6.3}$$

Results

The calculated value of service velocity in Equation 6.1 was $0.0722m/s$, which was lower than the $0.5m/s$ of its maximum velocity, stated on the Table 6.1. This meant that the requirements for the maximum velocity of this dry bearing were met. Regarding the requirements for stress in Equation 6.2 results were $115.6kPa < 3.5MPa$ which validates it on stress. In respect of the temperature requirements, following Equation 6.3, the service temperature was calculated to be $212.1°C$ which is lower than $260°C$ for the maximum permissible temperature.

Since all verifications were passed, this PTFE dry bearing will have no problem working under the indicated conditions.

6.3 Torque addition

Something that was not been taking into consideration up until now, and at this point was thought if it should or not have been, was the torque reaction (or reaction moment) in the fixation part. When the reaction forces where determined in Section 5.3.2 the reaction moments were not contemplate because it was thought that, since the fixation part allows rotation along the Y axis of the spindle and also the WWS' arm allows its flexion by the rotation countered with the spring, the torque reaction shouldn't affect the spindle, and consequently the fixation part, due to the degrees of freedom mention.

Nevertheless, when the results were presented to the advisors it was acknowledge that the influence of all reactions should be studied because it was not being considered the impossibility of twisting on the bearing area in two axes, on the arm's base.

If it was concluded that no considerable differences were noted (or small enough to be ignored), the model with the reaction forces only could be used as a simpler model that represents faithfully the one with all reactions. Otherwise the moments had to be taking into consideration and the studies had to be redone.

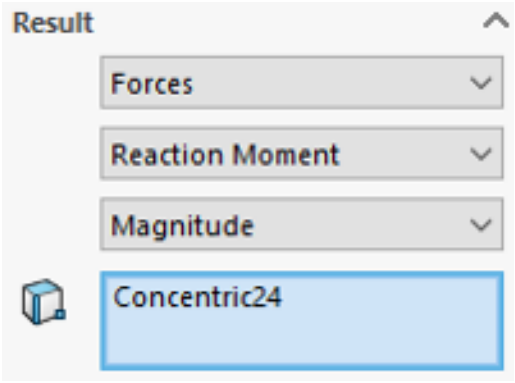

Figure 6.3: Reaction moment magnitude plot creation

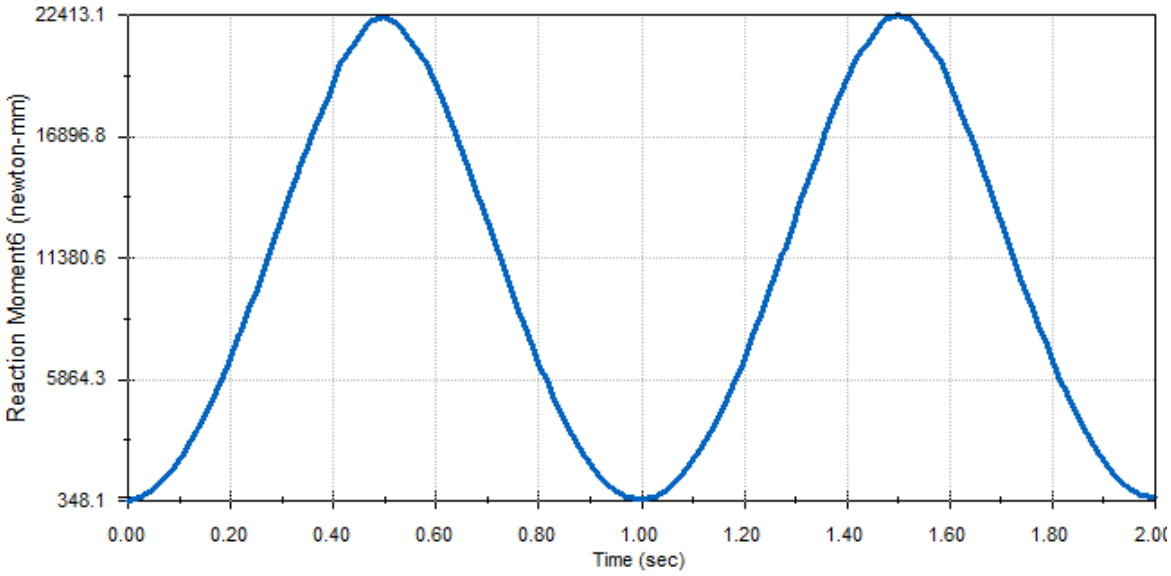

Figure 6.4: Reaction moment magnitude result plot in $N \cdot mm$

6.3.1 Motion Study

Consulting the Motion Analysis results of the previously produced motion study, it was only necessary to add another four plots, as in Figure 5.23, only this time with the reaction moment's magnitude, as shown in Figure 6.3. This was made in the model with the gravitational acceleration in order to understand the effect of the torque reaction in the regular case.

Results

As shown in Figure 6.4, the highest value of torque happens at half a cycle, where the WWS's blade is all the way to the right, before coming back to the rest position, and its value is approximately $22.4 N \cdot m$.

This is a value that was not possible to ignore because it will very likely have a great effect on the mechanical behaviour of the fixation part, making it necessary to be further considered in a new iteration.

Knowing the magnitude value of the gravitational acceleration study it was fundamental to

Table 6.2: Maximum values of motor torque and reaction's force and torque magnitude of the different simulations

						Lateral	
	1G	Downward	Forward	Upward	Rearward	Left	Right
Motor Torque ($N \cdot m$)	25.4	**35.2**	21.3	18.5	26.1	19.4	**28.8**
R Magnitude (N)	55.0	57.0	**70.0**	54.6	44.5	46.0	**65.6**
M Magnitude ($N \cdot m$)	22.4	22.6	21.7	22.6	**23.0**	**23.1**	21.8

produce the three component plots (x,y,z) in order to apply them on the static study. After this was done, it had to be repeated in every other motion study (downward, forward, rearward and the laterals).

The motor torque in Table 6.2 matters mainly to make sure the value was never superior to 62 $N \cdot m$ which, as previously mentioned, is the absolute maximum torque allowed. The motor torque should stay between 25 $N \cdot m$ and 32 $N \cdot m$ in its normal functioning but, since this is an extreme case, the maximum value being 35.2 $N \cdot m$ was not a problem.

Unlike in Table 5.3, each study has now two parameters results (force and torque reactions) to be considered, which means it's not straightforward which was the worst case scenario, if the more problematic would be the one with the biggest value of force or the one with the biggest torque. Having that in consideration, both studies with the reactions represented in red were chosen to proceed to the static study.

Worst case scenario reaction components

A doubt that arose and was not regarded before was, if the reaction forces were being considered in the right direction, since only the concentric mate was chosen, the given reaction components results could be the inverse of what should be considered.

The reaction plots were remade adding the parameter shown in Figure 6.5 which was ignored before, forcing the results to be regarded as about the chosen part, being then highlighted in light blue in Figure 6.6 instead of grey.

It was noted that with this new configuration of coordinates the Y component became zero in all simulations, which is what should have happened before, since the plot was generated after the concentric mate, allowing movement in the Y direction. In order to understand the forces involved in this direction another plot had to be made involving another mate. As seen in Figure 6.8, the coincidence on the bottom of the screw with the interior of the spindle was chosen in order to assess the Y components of the forces affecting the fixation part. The parameters, as in Figure 6.7 don't differ from the previous shown plot except for the mate from which the reactions are analysed.

Besides the reaction forces, the moment plots were also created in order to know the components that affect the fixation part, and then to include them on the static study. As shown in Table 6.3 the forward emergency landing case (which is the worst case scenario for the force) had those component forces and moments and, in Table 6.4, are shown the reactions for the

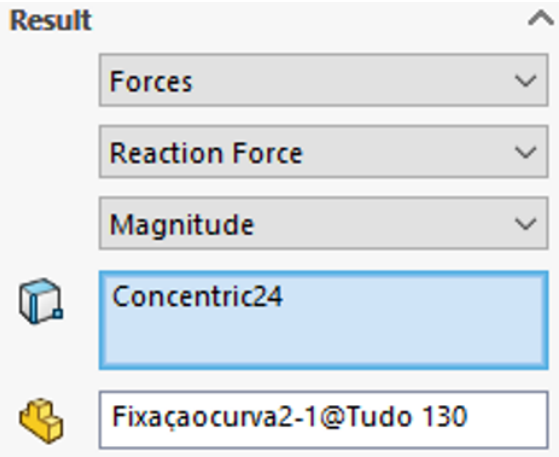

Figure 6.5: Reaction force magnitude parameters

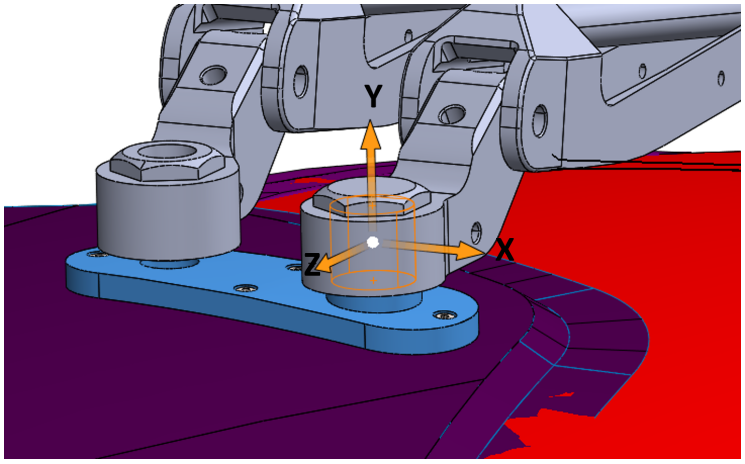

Figure 6.6: Reaction coordinates

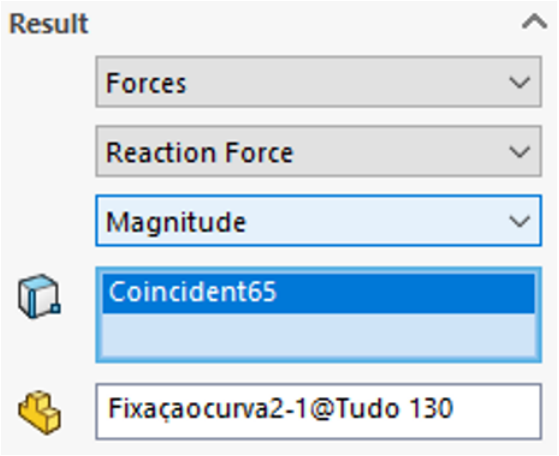

Figure 6.7: Reaction force magnitude parameters

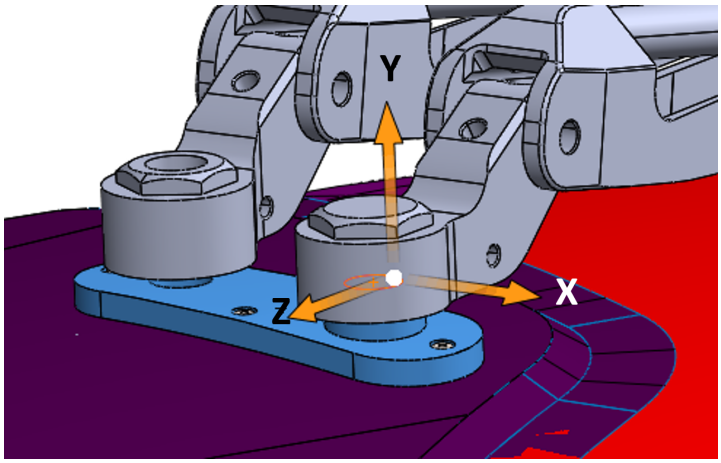

Figure 6.8: Reaction coordinates

Table 6.3: Reaction forces and moments of the forward emergency case

Fmag	70.0 N	Mmag	21.7 $N \cdot m$		
Fx	46.0 N	Mx	-15.4 $N \cdot m$	Fybolt	18.0 N
Fy	0 N	My	0 $N \cdot m$	Mybolt	0 $N \cdot m$
Fz	-52.0 N	Mz	15.25 $N \cdot m$		

Table 6.4: Reaction forces and moments of the lateral left emergency case

Fmag	46.0 N	Mmag	23.1 $N \cdot m$		
Fx	30.0 N	Mx	16.4 $N \cdot m$	Fybolt	27.0 N
Fy	0 N	My	0 $N \cdot m$	Mybolt	0 $N \cdot m$
Fz	-34.0 N	Mz	16.3 $N \cdot m$		

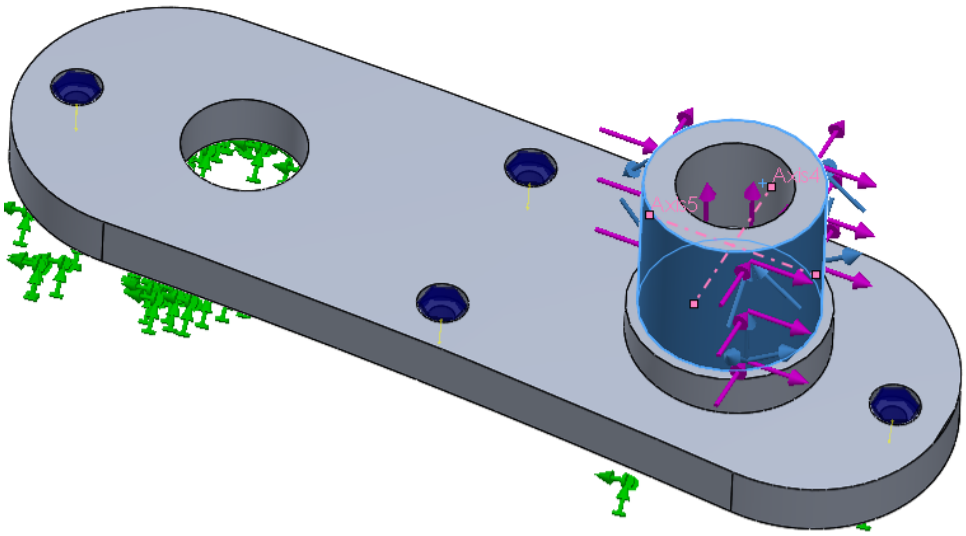

Figure 6.9: Applied forces and moments

lateral left case (worst case for the moment).

It's possible to observe that, in both cases, as described before, the y forces are null so the reactions in that direction were consulted from the mate in the bottom of the bolt (represented by Fybolt in the Tables) and the magnitude as equal to the Fy reaction, as expected.

Also, by allowing the WWS's cylindrical connection to the dry bearing in the fixation part, it was expected not to exist any moment reaction in the y axis, which can be attested in both Tables.

6.3.2 Static Study

Repeating the process in Section 5.3.3, the static studies were conducted with changes regarding the component force's values and adding the moments. As shown in Figure 6.9 two axes were added on the reactions coordinates origin, corresponding to the x and z axes. The correspondent moments were then applied in the outer surface of the spindle, which is where the contact exists.

Differently from the previous static study, the forces instead of being located on the top surface of the spindle were also located on the cylindrical surface, highlighted in blue. This was done in order to keep the coherence, since the torque was applied to that surface, the forces should be too. Previously, the forces were located on the top surface because it wasn't found a better way to locate them on what would correspond to the center of the axis, but, after searching for a way to apply them in a non planar surface it was found that, in alternative, as seen in Figure 6.10, the cylindrical face could be selected as long as the used direction reference was a plan. The lateral face seen in pink in Figure 6.12 was then selected and both forces could be produced relatively to the plan as shown in Figure 6.11.

Only the vertical force on the interior of the hole was missing, which could be inserted simply by adding a force in the y direction, in the interior of the spindle as in Figure 6.12 represented in vertical purple arrows.

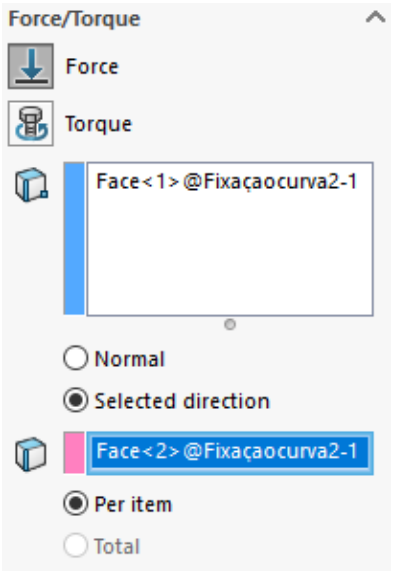

Figure 6.10: Force location parameters

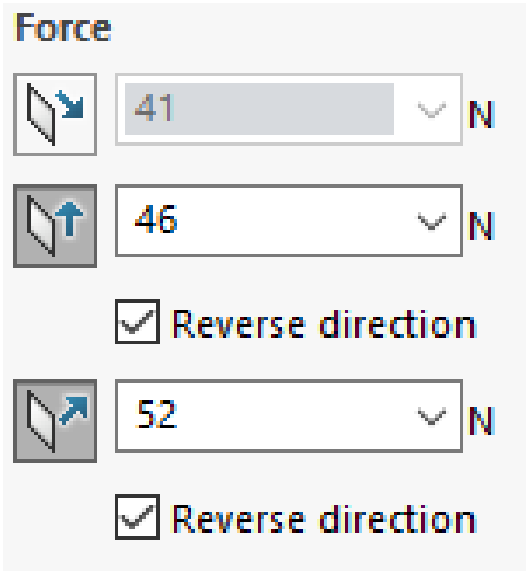

Figure 6.11: Force direction parameters

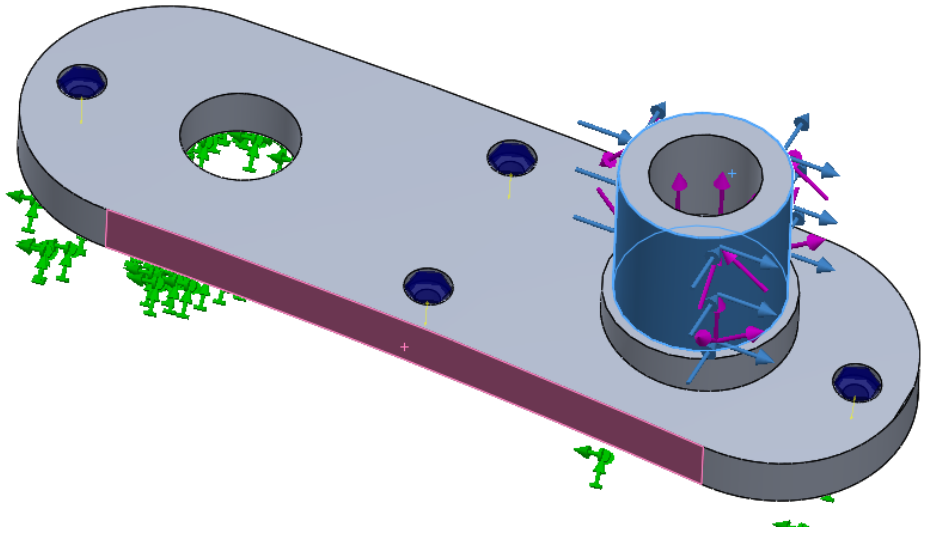

Figure 6.12: Graphic representation of the applied forces

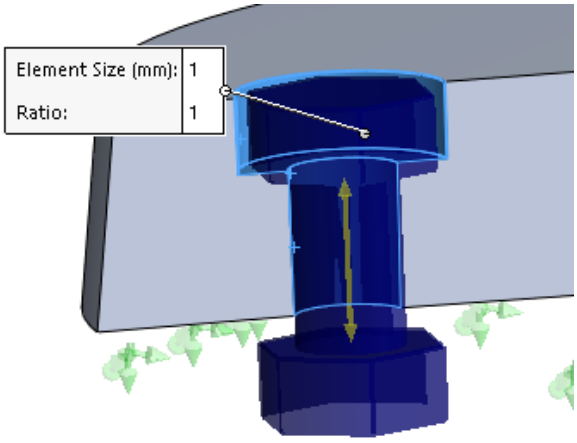

Figure 6.13: Graphic representation of the applied mesh control

The study was duplicated and the two were carried for both emergency landing cases, changing only the component values for the moment and force reactions applied in the part respecting the values in Table 6.3 and Table 6.4.

It's possible to notice that the helicopter's surface was suppressed. This was done because its suppression would not change the contact type between the parts but would allow a better view to the one that was being study. Also, in case the values studies in the assembly (e.g. maximum stress, minimum FoS) were located in the part corresponding to the helicopter's surface, by suppressing it, it was possible to consider only values in the parts shown. What sometimes could also happen would be that, a small section in the fixed part would not be affected by the constrains applied to it, but all the area around it would be. This'd result in great tension values in that small area due to being the only zone allowing some strain. This way, showing only results in the fixation part was most desirable since only the referred part was being study and not the helicopter's surface.

The mesh was also considered, using mesh control in the most problematic bolt hole (it was the same hole in all simulations) seen in Figure 6.14, applying the parameters of $1mm$ elements with a ratio of 1 in the area of the thread and also in the head hole as in Figure 6.13. This was important in order to have a considerable number of elements in the part's depth.

Boundary Conditions simplification

When the simulation was run with the described model, it was found that it was requiring too much computing power, which was expressed in a much longer time to finish the static study.

Since it was not feasible to take that long per simulation, taking into consideration that several static studies were to be made, and even worse (regarding computing power), fatigue studies were also needed to be done, it was decided to analyse how much the results would differ if a simpler fixture was to be used.

As in Section 5.3.3, a simulation with normal boundary restrains (normal to the cylindrical part and to the top face) was added as well as one with fixed restrains. This was done with the

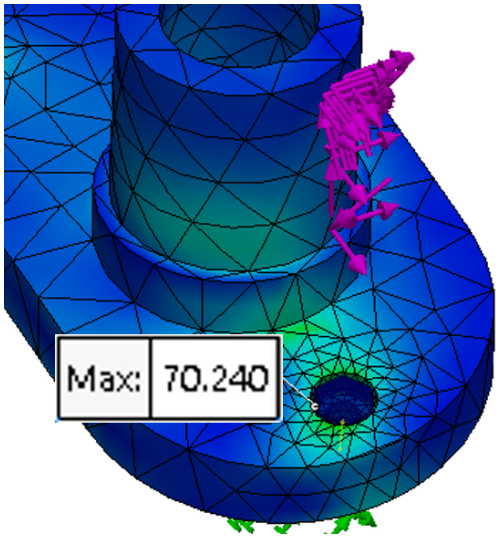

Figure 6.14: Maximum stress plot for the forward simulation

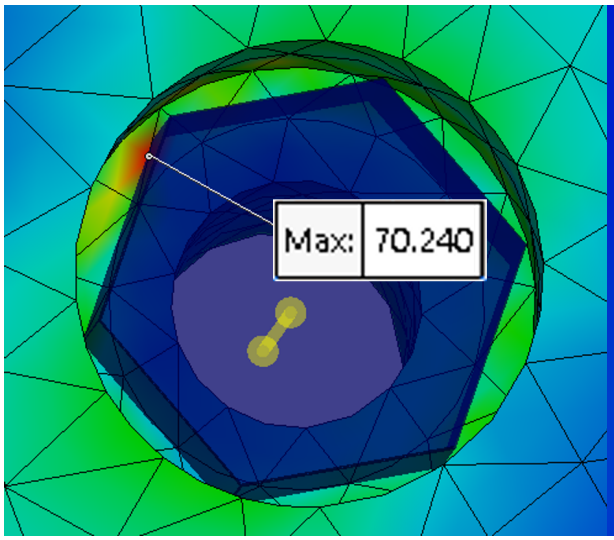

Figure 6.15: Maximum stress hotspots detail for the forward simulation

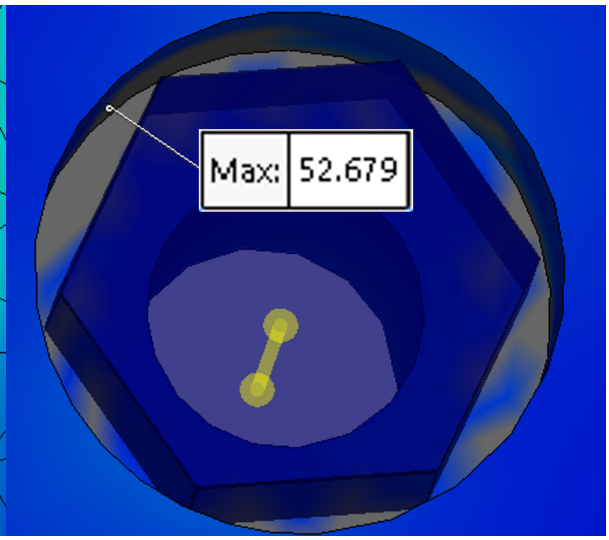

Figure 6.16: Maximum stress using hotspot detection for the forward simulation

intent of making a comparison and see how much the results would differ.

As stated before, in all cases the maximum stress was located in the bolt hole nearest the spindle, as shown in Figure 6.14. What was observed, stress wise, between the models, was a lowest value in the bolt case, followed by the normal case and, with the greatest values, the fixed constrains case.

This was expected due to the gradual increase of restrictions for each case, not reflecting the possibility of having some looseness as in the real life model due to the presence of bolt connections.

It was also observed that in the bolt case, the corners of the head, when in contact with the part, generated small points of stress concentration as in Figure 6.15. In order to appraise if it was something not worth taking into account because it wouldn't happen in real life, the Hotspot Detection tool was used.

Table 6.5: Results of the static studies with different boundary restrains

		Smax (MPa)	FOS	Hotspot (MPa)
Normal	Forward	77,2	6,5	77,2
	Left	97,2	5,2	94,1
Fixed	Forward	115,4	4,4	115,4
	Left	203,3	2,5	203,3
Bolts	Forward	70,2	7,2	52,7
	Left	103,8	4,9	86,2

This tool evaluates abrupt rise of values in the nodes by comparing it with its adjacent nodes, deciding then if it can be considered a stress concentration point and, thus, be ignored. In the mentioned case it was the reality. The Hotspot Detection tool identified the contact areas under the corners of the head as a stress concentration, ignoring those areas and lowering the maximum stress value of the simulation, as explained in more detail in Section 2.2.3.

This process was done again for all cases and the values were put together and compiled in Table 6.5. The FoS and the Hotspot column are sub-products of the stress analysis, which means that the FoS column concerns the maximum stress one, not the Hotspot.

Looking at the table it's possible to determine that, in all different boundary condition cases, the lateral left emergency landing case was the one with the highest value of maximum stress and lowest FoS.

As previously observed, the model with loosest restrains showed bigger FoS values, followed by the one with two normal boundary conditions and, ultimately and with more problematic results, the fixed restrains.

Also, regarding the stress concentration, the SW's tool Hotspot Detection was unable to identify any in the fixed model, producing equal results between the maximum stress value in the stress plot and the Hotspot plot as seen in Table 6.5. In the normal fixtures simulation, it's only possible to acknowledge differences in the results of the lateral left case of about 3%, which is pretty much negligible. In the bolts simulation, however, it's clear that there was an stress concentration effect on the maximum stress values. As stated before, the head of the bolt creates points of high pressure, resulting in 25% increase in the maximum stress results of the forward simulation and 17% in the left one. The influence of the geometry of the bolts confirms the need previously stated in Chapter 5.3.3 to change from fixed boundary conditions to vertical constrains in the head rest of the bolt and in the threaded hole.

The ideal use of this analysis, with the Hotspot detection, would be to link it to the fatigue study in order to ignore the stress concentration points. This, however, was not possible since the fatigue study uses the information obtained from the general stress study, with all nodes being considered. Nevertheless, it was important to notice that this cases were observed and, possibly, the damage, maximum life and FLF obtained in the future fatigue studies will not consider the Hotspots, resulting in a greater damage than what would be expected in a real life

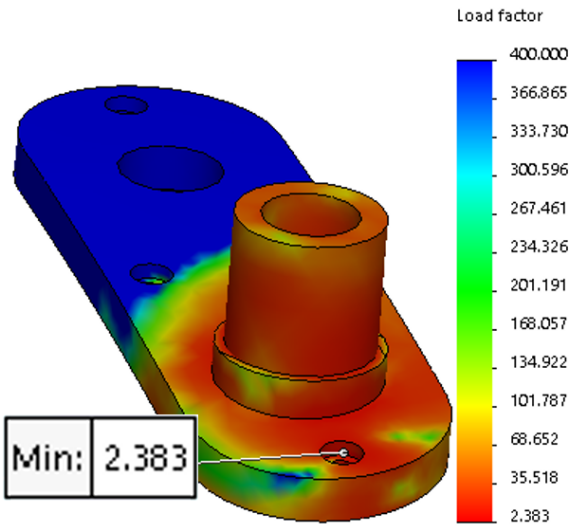

Figure 6.17: FLF plot for the left simulation

scenario, which is preferable to the opposite.

When comparing the differences between the bolts and normal simulations, both forward cases have a 9.5% variation, which is not a major value. In the left case, which is in both the greatest and potentially more problematic result, a difference of 6.6% was observed, being even smaller than before. Considering the proximity between the results of the bolt and the normal simulations, in their maximum values obtained from the stress plot, it can be assessed that it's a good simplification of the bolts model.

Therefore, the model with the normal restrains will be used for the fatigue simulation, which will be referenced to the worst case scenario, the lateral left.

6.3.3 Fatigue study

Using, again, the same parameter as the previously described in the fatigue study in Chapter 5.3.4, the study linked to the lateral left case was run.

Similarly as before, the fatigue failure was not reached showing no need to analyse the damage or life cycle plots, but the FLF shown in Figure 6.17 was quite important.

The most affected area this time, however, was around the bolt hole near the spindle. It's lowest value was 2.38, much lower than the 7.7 obtained before but still very satisfactory considering the CS-27 recommended safety coefficient value of 1.5.

Those results indicate that the fixation part in 7075-T6 Aluminium, and considering the applied forces and torques, will not fail neither by static load nor by fatigue when subjected to the worst emergency case.

6.4 Aluminium 518.0

The same process was carried through, again, changing the mechanical properties corresponding to the material that was previously found to be suitable for the intended use, the

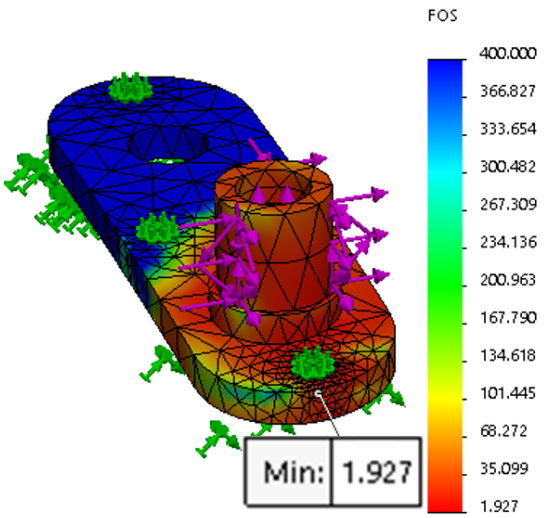

Figure 6.18: FoS plot results for the Aluminum 518.0

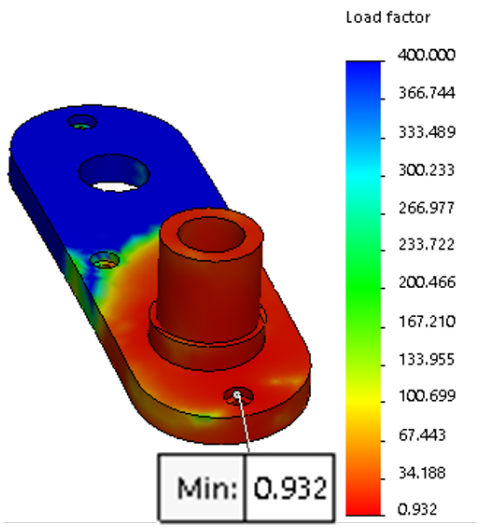

Figure 6.19: FLF plot results for the Aluminum 518.0

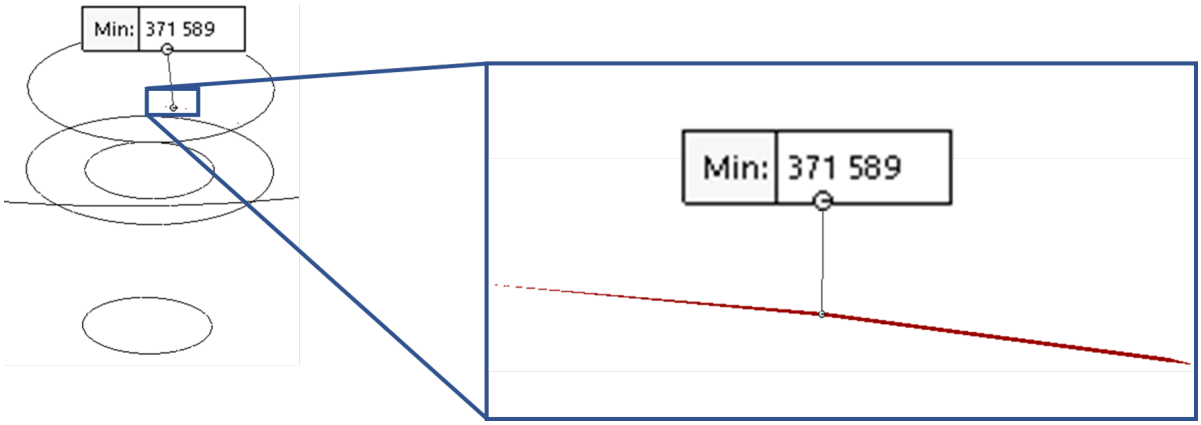

Figure 6.20: Iso Clipping detailed view of the total life in cycles

Aluminium 518.0, die cast, F. With this option the production of the part could eventually be less expensive, but having the addition of the moment affecting the part this time, the results would probably differ from the earlier case.

6.4.1 Results

Since the stress values in the part were the same, as the only change made in the simulation was the material properties, the analysed plots were the FoS and FLF.

As seen in Figure 6.18, the FoS results ware in agreement with the recommended safety coefficient, since it was always above 1.5. This meant that the aluminium 518.0 would be fit to use it in a static loading situation, but, when used in a cyclical load situation like the one in the current project, it showed not to be fit. As seen in Figure 6.19, in the right bolt hole there's a spot that presents a FLF lower than 1. This meant that, even before reaching a million cycles, the part has already failed.

The Iso Clipping tool was then used on the total life plot to analyse where the failure would

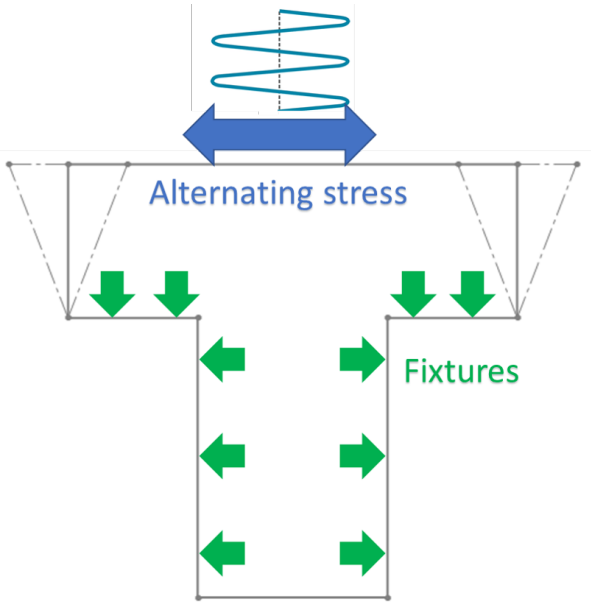

Figure 6.21: Normal fixtures and displacement scheme on the bolt hole connection

start to appear. The Figure 6.20 shows in detail the nodes with total life cycles between the minimum value and infinite life (one million cycles). It's possible to notice in the close up image the crack that begins to appear, in its origin at the 371 589^{th} cycle.

Due to the complexity of the geometry of this part, it's not possible to conclude if the presence of the crack is legitimate or if it's due to the simplification process carried from the bolts fixtures to a normal boundary condition. This could be the case because, as observed in the scheme in Figure 6.21, the threaded cylinder face and the top head rest face are unable to move in one axis. This makes the face immediately after to have to bear all the displacement that cold be distributed if bolts were to be simulated.

Observing the crack location it's possible to recognize similarities with hotspot presence in some of the static simulation, in the previous models. As stated before, in the static studies result plots it was possible to see the results ignoring the hotspots. However, this could not be done in the fatigue studies, which might indicate the presence of early cracks in less than 400 000 cycles.

The mentioned observations might be the reason why this material cannot be validated for the intended use, being chosen the Aluminium 7075-T6, which having the same flaws in the model, the safety coefficients are all above the minimum.

Chapter 7

Conclusions

This project was carried with the aeronautical industries standards in mind. It was a first approach with the certification of the adaptation of a modular windshield wiper system in view, regarding the design of a new part. All the CAD design and simulations of the new part were carried as an industry project would, in order to implement and produce the developed model.

After gathering information about the different types of wiping systems and its pros and cons for a more broad understanding of the concepts of the subject, a simple and general computational model of WWS was accessed. With that model, the kinematical information and procedures about the more generic system was attained, and the same was done with the Airbus' pantographic model. With the model developed buy AHD it was a more demanding task to overcome since problems regarding its kinematical functioning were identified in the simulation software. It was found that some material properties observed in a real life functioning of the system cannot be reproduced in a situation with the same correct constrains, which require an adaptation in terms of the used constrains: an hinge was replaced by a ball hinge. This allowed a full implementation of the wiping system to the H135's windshield, resulting in quantitative output about its performance in the H135 aircraft's windshield such as the full cleaning angle. That way, a reliable digital WWS was created, which made possible to carry further analysis knowing that the results would be trustworthy.

The adaptation to the H130 helicopter model, with only one motor axis connection was done by successfully adding a newly designed part in order to have a second axis that allowed the pantographic movement of the blade. This part had to be conceived by iterations of several models, having minimal changes in mind, in order to keep the aircraft as the original and make additions purely on the exterior. If possible, that would prevent further need for certifications of the helicopter, being treated as an external load, but those solutions were found not to be suitable for the studied case. The best solution was thought to be a new part with bolts keeping it attached to the surface in the motor axis area. The loadings affecting the part were attained from the forces dynamically acting on the driving axis. For this to be possible, the Motion Analysis hat to be set up but only after knowing the springs properties. In order to figure it out a Design Study with an optimization process was carried, providing the rightful information about the settings to be used, and, that way, allowing the new part to be further simulated

kinematically, statically and against the fatigue, in order to resist the cyclical loadings. In this simulations it was found that the design presented good safety coefficients. These studies included different materials that allowed the weight and cost to decrease while still keeping the part in the safety domain.

The bolts also had to be verified to the affecting loads that they were subjected to, considering the pre-loading, as well as the dry bearing, to the mentioned cyclical motion of the arms and the consequent contact endurance. This ensured that the designed part can work in an extreme situation as for instance, fire fighting and emergency landings. Everything was again calculated and the simulations reviewed after the torque from the motion study had been revealed quite influential in the total load, being added to the studies. All results came out still suitable for the chosen material.

The work on this document present a good proof of concept and a basis for future development of the modular WWS, although far from a finished document of the final product. Some progress will be required in order for it to be ready, but it gives a fair support base for future work development.

Chapter 8

Future Works

This project is not yet concluded, still needing to be further improved. As such, several aspects and details observed as important to regard in the future can be seen in the following chapter.

What was limiting the cleaning angle (γ) was noticed to be the distance between the arms and the windshield, represented in Figure 8.1 as h_{min}. In order to project a bigger value of γ in the future, three values can be taken into consideration:

1. The height of the base of the arms (d) - if it can be extended it will result in a bigger distance of the arms to the windscreen

2. The total height of the blade's structure (e) - each small curved arm can be enlarged in height, resulting in a total gain of a considerable distance from the windshield

3. The long straight arms can be instead curved (radius represented by r), having the arms themselves a greater distance from the windshield without any changes to the rest of the model

Since there are still perspectives and problems in this project that should be subjected to further considerations, some future work will have to be done by continuing the carried progress. The following points are considered to be subsequently the most important:

- Cleaning angle versus windshield curvature: A study considering the maximum cleaning angle versus the windshield curvature radius should be done in order to find to which degree this adaptation is conceivable and viable;

- Dry/Wet operation: Test the system for a wet and dry surface and understand the implications;

- Aerodynamics: Figure out the aerodynamics impact of the adaptation in the aircraft and quantify its losses;

- Environment Factors: Test it to aggressive environments like wind, rain, mud and snow.

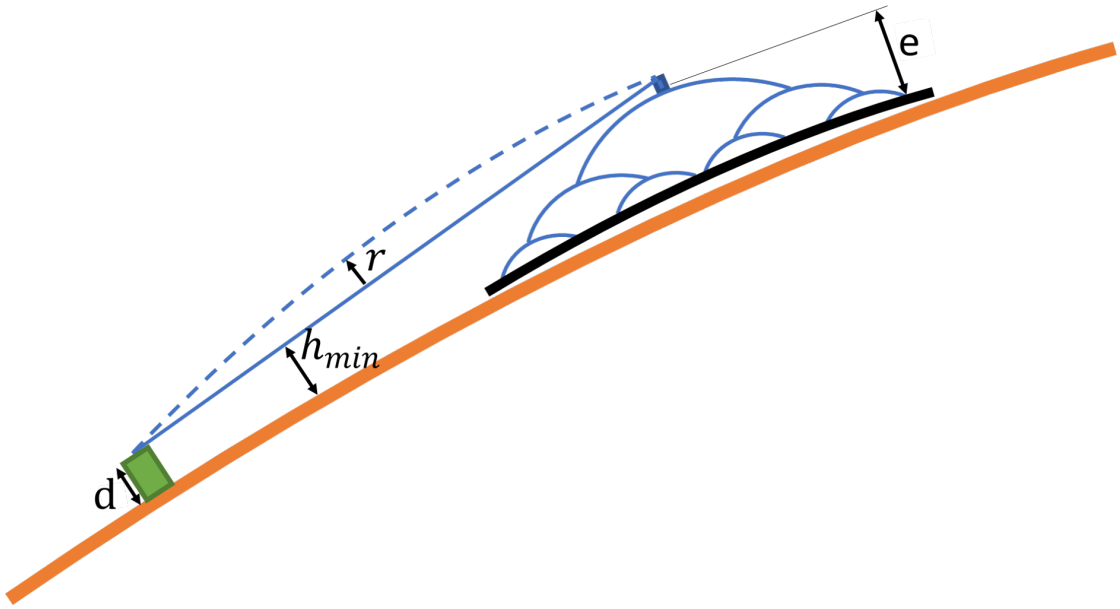

Figure 8.1: Schematic representation of the variables that influence the maximum cleaning angle

In order to adapt to more windshield geometries and means of connection, it will also have to be considered a redesign of the hollow bolt that connects to the motor spindle, for each case. Also, the length of the arms may have to be adjusted if the windscreen hight is too different from the standard for this WWS.

Bibliography

[1] *Regulations*. EASA, 2019. URL www.easa.europa.eu.

[2] *SKYbrary electronic repository*. SKYbrary, 2017. URL https://www.skybrary.aero/index.php/JAA.

[3] European Aviation Safety Agency. Certification Specifications and Acceptable Means of Compliance for Small Rotorcraft CS-27. Certification Specification Amendment 6, EASA, December 2019.

[4] Joint Aviation Authorities. Certification Specifications for Small Rotorcraft JAR-27. Certification Specification, JAA, January 2012.

[5] Jacob Fish and Ted Belytschko. *A First Course in Finite Elements*. Wiley, Chichester, England ; Hoboken, NJ, 1st edition edition, May 2007. ISBN 978-0-470-03580-1.

[6] Filipe Teixeira-Dias, A. Pinho da Cruz, Robertt Valente, and Ricardo J. Alves de Sousa. *Método dos Elementos Finitos - Técnicas de Simulação Numérica em Engenharia*. 2010. ISBN 978-972-8480-25-7.

[7] *SolidWorks Online Help*. SolidWorks, 2017. URL http://help.solidworks.com/2017/English/SolidWorks/sldworks/c_introduction_toplevel_topic.htm.

[8] Chaitanya Raj Goyal. *Uncertainty Quantification in non-linear seismic wave propagation*. Dissertation, Carleton University, 2017.

[9] Abdel Makhlouf and Mahmood Aliofkhazraei. *Handbook of Materials Failure Analysis*. Elsevier, 2015. ISBN 978-0-08-101928-3. doi: 10.1016/C2016-0-01329-3.

[10] Richard G. Budynas and Keith J. Nisbett. *Shigley's Mechanical Engineering Design*. McGraw-Hill Education, New York, NY, 10 edition edition, January 2014. ISBN 978-0-07-339820-4.

[11] Ferdinand Beer, E. Russel Johnston, John DeWolf, and David Mazurek. *Mechanics of Materials*. 3rd edition, 2003. ISBN 0-07-762525-0. URL https://www.mheducation.com/highered/product/mechanics-materials-beer-johnston-jr/M9780073398235.html.

[12] M. Janssen, J. Zuidema, and R. J. H. Wanhill. *Fracture Mechanics*. VSSD, Delft, 2 edition edition, February 2006. ISBN 978-90-407-2221-9.

[13] William D. Callister and David G. Rethwisch. *Materials Science and Engineering: An Introduction*. JOHN WILEY & SONS INC, Hoboken, NJ, 009 edition, December 2013. ISBN 978-1-118-32457-8.

[14] Norman E. Dowling. *Mechanical Behavior of Materials*. Pearson, Boston, 4 edition edition, March 2012. ISBN 978-0-13-139506-0.

[15] *Airbus industrie material specification*. Airbus, June 2018.

[16] A5 - Dry rubbing bearings. In M. J. Neale, editor, *Tribology Handbook (Second Edition)*, pages A5.1–A5.4. Butterworth-Heinemann, Oxford, January 1995. ISBN 978-0-7506-1198-5. doi: 10.1016/B978-075061198-5/50006-0.

Appendix A

Dry bearing intermediate calculations

```
restart

#Maximum Velocity:
vmax := 0.5 :#m/s
v := 2·π·n·r / 60 :#m/s
n := 60 :#rpm (1Hz)
r := 11.5e-3 : #m
vmax > v;
```

$$0.07225663103 < 0.5 \quad (1)$$

```
#Maximum Stress:
σmax := 3.5e6 :#Pa
    #Radial Forces
    Fx := 53 : Fz := -19 :#N
    #spindle projected area:
    l := 21.18e-3 :#m
    a := l·2·r :#m^2
F := evalf(sqrt(Fx^2 + (Fz)^2)) :
σs := F / a :#Pa
σmax > σs;
```

$$115578.1768 < 3.5\ 10^{6} \quad (2)$$

```
#Maximum Temperature:
Pvmax := 35e3 :#Pa·m/s
Tmax := 260 :#°C
Ta1 := 25 :#°C
Ta2 := 100 :#°C #in case of combating fire
fm1 := 0.02 :#worst case coefficient of friction
fmt := 0.04 :#Teflon coefficient of friction

ce := solve(Tmax = Ta1 + fm1·Pvmax / ce, ce) :
Ts := Ta2 + fmt·σs·v / ce :
Tmax > Ts;
```

$$212.1458899 < 260 \quad (3)$$

Appendix B

Bolt connectors intermediate calculations

> $Fi := 0.9 \cdot Fp$: #Pre load for nonpermanent connections (equation 8-31)

> $Fp := At \cdot Sp$: #Proof load (eq 8-32)

Nominal Major Diameter d mm	Coarse-Pitch Series Pitch p mm	Tensile-Stress Area A_t mm^2	Minor-Diameter Area A_r mm^2
1.6	0.35	1.27	1.07
2	0.40	2.07	1.79
2.5	0.45	3.39	2.98
3	0.5	5.03	4.47
3.5	0.6	6.78	6.00
4	0.7	8.78	7.75

> #Table 8-1

> $At := 5.03e{-}6$: #mm^2

> #Consulting table's 8-11 miniumum proof strength for M3

> $Sp_{4.8} := 310e6$:#Pa

> $Sp_{9.8} := 650e6$:#Pa

> $Fi_{4.8} := 0.75 \cdot At \cdot Sp_{4.8}$;#N

$$Fi_{4.8} := 1169.4750 \quad (1)$$

> $Fi_{9.8} := 0.75 \cdot At \cdot Sp_{9.8}$;#N

$$Fi_{9.8} := 2452.1250 \quad (2)$$

>

Appendix C

Mechanical Properties of the Materials

Aluminium 7075-T6

Property	Value	Units
Elastic Modulus	7.2e+010	N/m^2
Poisson's Ratio	0.33	N/A
Shear Modulus	2.69e+010	N/m^2
Mass Density	2810	kg/m^3
Tensile Strength	570000000	N/m^2
Compressive Strength		N/m^2
Yield Strength	505000000	N/m^2
Thermal Expansion Coefficient	2.36e-005	/K
Thermal Conductivity	130	W/(m·K)
Specific Heat	960	J/(kg·K)
Material Damping Ratio		N/A

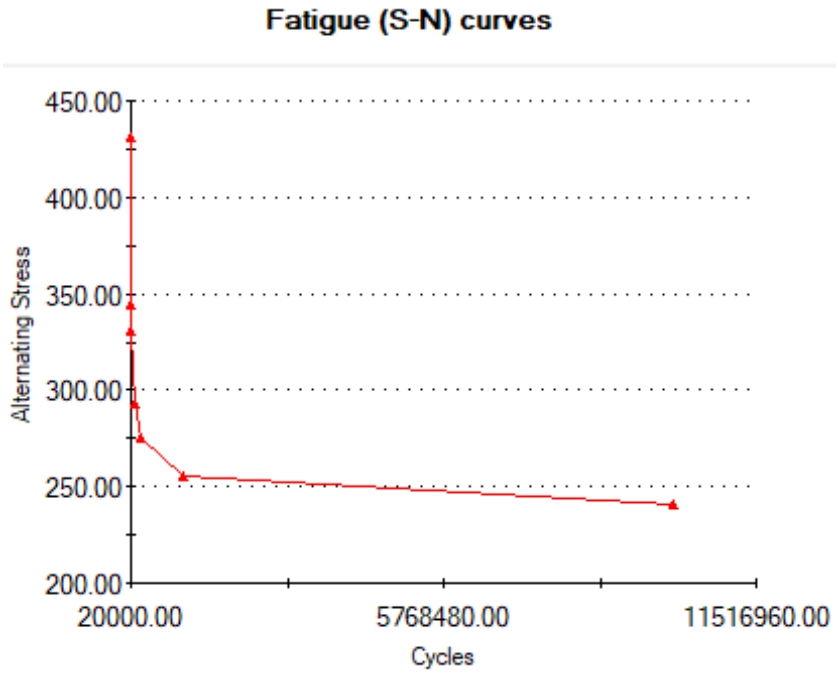

PVC Rigid

Property	Value	Units
Elastic Modulus	2410000000	N/m^2
Poisson's Ratio	0.3825	N/A
Shear Modulus	866700000	N/m^2
Mass Density	1300	kg/m^3
Tensile Strength	40700000	N/m^2
Compressive Strength		N/m^2
Yield Strength	50000000	N/m^2
Thermal Expansion Coefficient		/K
Thermal Conductivity	0.147	W/(m·K)
Specific Heat	1355	J/(kg·K)
Material Damping Ratio		N/A

Aluminium 518.0

Property	Value	Units
Elastic Modulus	6.96e+010	N/m^2
Poisson's Ratio	0.322	N/A
Shear Modulus	2.6e+010	N/m^2
Mass Density	2490	kg/m^3
Tensile Strength	310000000	N/m^2
Compressive Strength	177000000	N/m^2
Yield Strength	177000000	N/m^2
Thermal Expansion Coefficient	23.5	/K
Thermal Conductivity	0.2256	W/(m·K)
Specific Heat	1386	J/(kg·K)
Material Damping Ratio		N/A

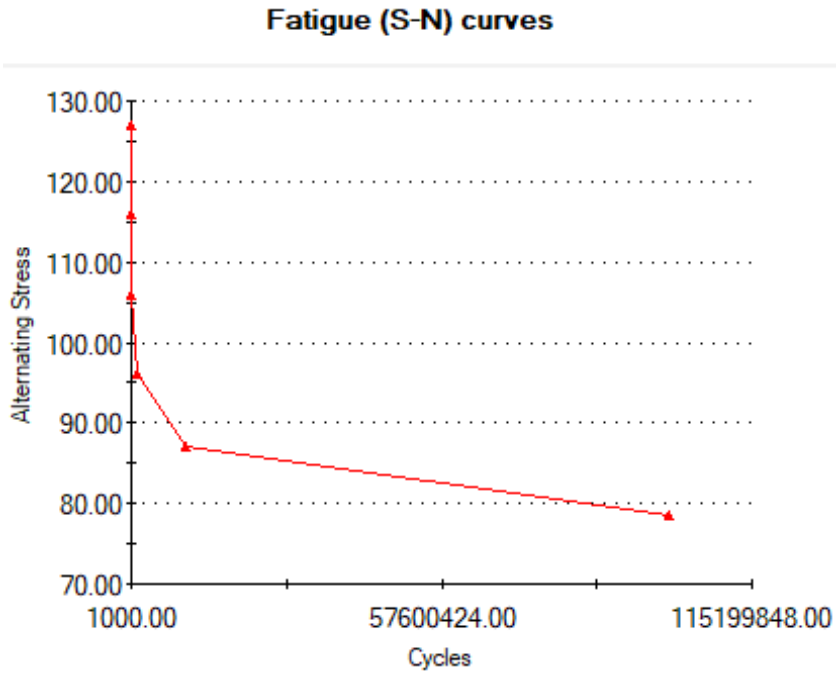

Aluminium 3105

Property	Value	Units
Elastic Modulus	6.9e+010	N/m^2
Poisson's Ratio	0.325	N/A
Shear Modulus	2.5e+010	N/m^2
Mass Density	2700	kg/m^3
Tensile Strength	214000000	N/m^2
Compressive Strength	185000000	N/m^2
Yield Strength	185000000	N/m^2
Thermal Expansion Coefficient		/K
Thermal Conductivity	0.2256	W/(m·K)
Specific Heat	1386	J/(kg·K)
Material Damping Ratio		N/A